Lehrstuhl für Statik

Fakultät für Bauingenieur- und Vermessungswesen

Technische Universität München

# Design and Analysis in Shape Optimization of Shells

## Natalia Camprubí Estebo

Vollständiger Abdruck der von der Fakultät für Bauingenieur- und Vermessungswesen der Technischen Universität München zur Erlangung des akademischen Grades eines

### Doktor-Ingenieurs

genehmigten Dissertation.

Vorsitzender:           Univ.-Prof. Dr.rer.nat. E. Rank

Prüfer der Dissertation:

    1. Univ.-Prof. Dr.-Ing. K.-U. Bletzinger

    2. Univ.-Prof. Dr.-Ing. W. A. Wall

# Abstract

Optimization has become nowadays an important discipline in the global design process of structures because it represents a systematic method to improve designs with respect to certain criteria. In design of shell structures, shape optimization is especially important because of the close and sensitive relation between shape and structural behaviour. However, this is a complex task due to the difficulties inherent to structural analysis of shells and geometrical definition of arbitrary surfaces.

In the present work, decisive aspects of design and analysis of shells in shape optimization are studied.

In the optimization loop, the optimization algorithm takes decisions about improving the actual design based on information provided by structural and sensitivity analysis. Therefore, the reliability of these analysis is crucial for the optimization result. In the structural analysis of thin structures, standard displacement elements suffer from locking phenomena, which yield inaccurate results. In an optimization process, these effects spread from structural analysis to sensitivity analysis and, as a consequence, to the optimization loop. Numerical experiments performed with standard displacement elements and with elements based on the DSG concept, avoiding locking, show the effects of locking in the optimization result both qualitatively and quantitatively. Final results obtained with standard displacement elements may have a wrong principal type of design or even may be unfeasible. The reliability of the sensitivity coefficients depends also strongly on the applied technique of sensitivity analysis. The need of more accurate results legitimates the use of analytical approaches, which require a higher mathematical effort but yield more accurate sensitivity coefficients than those computed with other approaches.

The importance of the design module in the optimization process lies in the fact, that it determines to a large extent the optimization result, insofar as it determines the set of admissible designs. A comparison between CAD- and FE-based parametrizations is done, with emphasis on the flexibility regarding shape description. The FE-based design parametrization allows more freedom in the design than the CAD-based parametrization, which makes it suitable for free formed shells or for a predesign phase. However, designs obtained with this parametrization may be wiggly shapes, which may affect the finite element formulation due to the high mesh distortion. A shape control technique aimed to achieve shape regularization using intrinsic surface curvature measures is pro-

posed. This approach facilitates obtaining smooth designs and avoiding wiggly shapes in optimization results obtained when using FE-based parametrization. A method to compute intrinsic curvature measures of a surface approximated by a polygonal mesh is shown. The method shows good performance, while sensitivities of these curvatures can be computed analytically. Moreover, it is applicable not only for smooth control of shells, but also for membranes or surface boundaries of 3D bodies.

# Zusammenfassung

Optimierungsmethoden gehören heute zu den entscheidenden Disziplinen beim Entwurf technischer Strukturen, weil man mit ihnen Designs systematisch und gezielt bezüglich bestimmter Kriterien verbessern kann. Aufgrund der ausgeprägten und empfindlichen Wechselwirkungen von Form und Strukturverhalten spielen Formoptimierungsmethoden beim Entwurf von Schalentragwerken eine besonders wichtige Rolle. Allerdings ist diese Aufgabe auch besonders anspruchsvoll, wobei die Strukturanalyse und die geometrische Definition von beliebigen Flächen aufgrund ihrer Komplexität die größten Schwierigkeiten bereiten.

In der vorliegenden Arbeit werden relevante Aspekte des Entwurfs und der Analyse im Rahmen der Formoptimierung von Schalentragwerken untersucht.

Innerhalb des Optimierungsalgorithmus werden Entscheidungen zur Verbesserung des Entwurfs auf der Basis von Informationen aus der Struktur- und Sensitivitätsanalyse getroffen. Deshalb ist die Zuverlässigkeit dieser Analysen entscheidend für das Optimierungsergebnis. Bei der Berechnung von dünnwandigen Strukturen mit verschiebungsbasierten finiten Elementen können Locking-Phänomene auftreten, die zu ungenauen Ergebnissen führen. In einem Optimierungsprozess überträgt sich diese Wirkung von der Strukturanalyse auf die Sensitivitätsanalyse, mithin auf die gesamte Optimierungsschleife und deshalb schließlich auf das Optimierungsergebnis. Numerische Experimente mit Standard-Verschiebungselementen und mit Elementen, die auf der Basis des DSG-Konzepts formuliert sind und Locking vermeiden, zeigen sowohl die qualitativen als auch die quantitativen Auswirkungen von Locking auf das Optimierungsergebnis. Die Entwürfe, die mit verschiebungsbasierten finiten Elementen erhalten werden, können eine prinzipiell falsche Form haben oder sogar außerhalb des zulässigen Bereiches liegen. Die Zuverlässigkeit der Sensitivitätskoeffizienten hängt auch von der Art der Sensitivitätsanalyse ab. Das Bedürfnis nach präziseren Ergebnissen berechtigt die Anwendung von analytischen Verfahren, die zwar mathematisch aufwendiger sind, dafür aber genauere Sensitivitätskoeffizienten als anderen Methoden liefern.

Die Bedeutung des Entwurfsmoduls im Optimierungsablauf ist darin begründet, dass es durch die Ermittlung des Bereichs der zulässigen Entwürfe einen wesentlichen Einfluss auf das Optimierungsergebnis hat. In Bezug auf das Entwurfswerkzeug wird ein Vergleich zwischen CAD- und FE-basiertem Design, mit speziellem Augenmerk auf der Flexibilität bei der Formbeschreibung, angestellt.

Die FE-basierte Parametrisierung erlaubt mehr Freiheit als die CAD-basierte, was sie insbesondere für den Entwurf von Freiformschalen und für die Vorentwurfsphase eignet. Allerdings können bei der Anwendung der FE-basierten Parametrisierung unerwünschte wellige Formen auftreten, die aufgrund der Netzverzerrung auch die Finite-Elemente-Approximation beeinträchtigen können. Es wird eine Formregelungsmethode vorgeschlagen, die die Fläche durch vorgegebene Krümmungsmaße regularisiert. Das Verfahren ermöglicht den Entwurf glatter Flächen und vermeidet wellige Ergebnisse bei der Verwendung einer FE-basierten Parametrisierung. In diesem Zusammenhang wird ein Verfahren zur Berechnung intrinsischer Krümmungsmaße einer mit finiten Elementen diskretisierten Fläche entwickelt. Die Methode liefert gute Ergebnisse und die Sensitivitäten dieser Krümmungen können analytisch berechnet werden. Die vorgeschlagenen Methoden sind nicht nur für die Kontrolle der Glattheit von Schalen, sondern auch bei Membranen oder Oberflächen von dreidimensionalen Körpern anwendbar.

# Acknowledgments

This Thesis is the result of my work at the Department of Structural Analysis (Lehrstuhl für Statik) of the Technische Universität München (Munich, Germany) between 2002 and 2004.

I would like to thank sincerely Prof. Dr.-Ing. K.-U. Bletzinger for giving me the opportunity of working in such an interesting field at the Department and for his engagement for providing good research conditions and facilities. I would also like to thank Prof. Dr.-Ing. W. Wall for his helpful comments and suggestions.

I would like to express my appreciation to my colleagues at the Department of Structural Analysis (Lehrstuhl für Statik) of the Technische Universität München. They received me with open arms and created a very nice and enriching atmosphere at the Department. I wish to thank specially Dr. Manfred Bischoff for his patience, engagement and constructive discussions, which were always a source of motivation for continuing the research.

I am most indebted with Dr. Ignasi Colominas, Prof. Fermín Navarrina and Prof. Manuel Casteleiro from the School of Civil Engineering of the University of A Coruña (Spain) for their supporting guidance. They introduced me in the field of Computational Mechanics and encouraged me to pursue the doctoral studies, giving me always very good advice. I am deeply grateful to them.

I would like to express my gratitude to the Fundación Pedro Barrié de la Maza (A Coruña, Spain) for the scholarship which brought me to Munich in 2000 to pursue a Master course in Computational Mechanics.

I would like to thank all those friends who have accompanied me during the completion of this work and gave me their support and love. I will always keep in my heart the moments we have shared.

Finally, I would like to thank my family, and specially my parents, for all the love, support and devotion they always show. In the last years, despite the distance, they were always there, sharing the small things, acting as link with my homeland, and letting me feel loved. Their love has always been an invaluable support. This thesis is dedicated to them.

# Contents

x

# Chapter 1

# Motivation and Objectives

## 1.1 Motivation and state of the art

Design is an activity inherent to the human being and closely related to his desire to excel. Its main objectives are to serve a functional purpose and to provide esthetical pleasure. From the beginning, the human being has designed for these two purposes: the functional one, to create tools in the most general sense of the word, and the esthetical one, to create art. Moreover, in many cases limits between both objectives are diffused and both of them are coupled into a single design process.

Design is a discipline which requires intuition, creativity, experience and knowledge. In addition to these factors, the available design tools are fundamental in the design process. The design activity implies the search for a certain design which serves the final purpose and simultaneously best satisfies certain criteria. The concept of 'best design' brings optimization onto the stage of design activity. It should be remarked that a design can only be considered as optimal in the global context of the formulation of the design problem and with respect to another initial design.

Several factors are involved in the formulation of the design problem. The designer has the control of the whole formulation and, therefore, the result is always subjected to the subjectivity of his decisions. He chooses the criteria to be considered and takes previous decisions about the final design, that is, prescribes its fundamental characteristics. A very important point of the optimization process is to translate these criteria into mathematical expressions to measure wheter a certain design is satisfactory or not. Typical examples of

quantifiable criteria are weight, cost or strength. However, not every criteria chosen by the designer can be quantifiable. Esthetics is a very determinant factor in many design processes, but there is no way to quantify it. Decisions with respect to this subjective criteria have to be taken directly by the designer, as they cannot be made by a mathematical expression.

The historical development of structural optimization is closely related to the evolution of experience and knowledge in engineering and the development of analysis tools. Navarrina (1987) gives a detailed review of the such historical development.

It is impossible to determine the first attempt of structural optimization. Probably this concept has always been incorporated in the structural design process, although until recently it has not been part of concious decision-making. Chronologically, the first stage of evolution of structural optimization is based mainly on experience and experiments. The historical progress in the use of different materials and structural typologies can be considered as one structural optimization process at a global scale.

The key idea in an intuitive and experimental structural optimization is to identify the relation between shape of the structure and flow of the forces. The interaction between shape and forces is especially important in the case of shells. These structures are a particular case of a three-dimensional solid, where one dimension (thickness) is very small compared with the other two. The shape and particularly the curvature of a shell are decisive in its mechanical behaviour. The optimal load-carrying behaviour of a shell is by membrane forces in absence of bending. By this, optimal utilization of material is achieved.

The Romans, excellent engineers, stand out because of their profuse use of circular arcs and cupolas made of masonry. The numerous arcs and cupolas of that and following periods, some of them impressive still today, were designed based on intuition, experience and basic rules of geometry and physics. These designs were guided mainly by esthetic and religious considerations.

In the Renaissance, there was a return to the nature as model of beauty and perfection and, thus, shapes suggested by natural laws are recognized as optimal. An important progress was made in 1675 by Robert Hooke with the identification of the relation between hanging models and optimal shape of arcs and shells. Through an anagram, he stated 'Ut pendet continuum flexile, sic stabit contiguum rigidum inversum', that is, 'As the flexible cable hangs, so the inverted arch stands'. The relation between natural shapes and structural design was also later studied by Antonio Gaudí, Frei Otto, Heinz Isler and Félix

Candela, among others. They successfully applied the method of hanging models to the design of construction projects with the final aim to attain beautiful structures through harmony in statics (see Ramm and Schunk (1986) and Otto and Rasch (1995), for instance).

Regarding structural analysis of thin structures, Kirchhoff (1850) formulated the present *thin plate* theory, based on the previous works of Bernoulli and Navier, among others. The key assumption of the theory, known as the Kirchhoff constraint, is that a straight line, normal to the mid surface, remains straight and normal to the deformed surface throughout deformation. The corresponding shell theory was formulated about fourty years later by Love (1888).

A *thick plate* theory was proposed by Reissner (1945) and Mindlin (1951) considering a relaxation of the Kirchhoff assumption. In this case, it was assumed that a straight line, normal to the mid surface, remains straight throughout deformation, but not necessarily normal to the deformed surface. As a consequence, transverse shear deformations can be taken into consideration. Naghdi (1972) was the first who applied *Reissner-Mindlin kinematics* to shells. Consideration of transverse shear deformations is an important feature for thick plates and shells. The advantage of this theory in the frame of finite element analysis relies on the low continuity requirements for the trial solutions.

Although these are the most important plate and shell theories in the context of the finite element analysis, they are not the only ones. A more detailed historical relation of the development of shell theories is given by Benbenuto (1991) and Bischoff (1999). It should be noted that, until the Finite Element Method was first used, the objective of most theories was the closed form analysis of the structure. The Finite Element Method was first applied to the study of plates and shells in the early 1960's. Shell elements can be based on a shell formulation derivated from the continuum theory, from the direct approach, or can be based on the degeneration concept. A detailed overview of modeling and discretization aspects in finite element analysis of thin-walled structures is given by Bischoff et al. (2004).

In the meantime, the first analytical works of structural optimization appeared gradually. These works are closely related to the evolution of structural analysis methods. Important contributions to structural optimization were done by Galilei (1638), Bernoulli (1687) and Lagrange (1770), who treated the optimal sections of beams and colums for some particular cases. The merit of these works was that they were the first to address the problem of structural optimization from an analytical point of view, although these attempts lack systematic and generality.

3

This generalization, at least for a certain structural typology, was first achieved by Michell (1904), based on the previous work of Maxwell (1890). He presented a methodology to obtain optimal two-dimensional truss-like structures with minimal weight and with the consideration of restrictions on the admissible stresses. The approach was based on the trajectories followed by the carried loads.

The modern concept of structural optimization is a result of the integration of modern numerical techniques into the optimization process. This achievement is mainly due to Klein, Pearson and Schmit. Klein (1955) formulated the general optimization problem as it is known today introducing inequality constraints. Later, Pearson (1958) complemented these ideas integrating structural analysis and optimization in a coherent process and presented a method to convert an inequality constrained problem into an equivalent unconstrained one. With this background, Schmit (1960) proposed the concept of *structural synthesis*. Schmit (1981) describes with enthusiasm the gestation of this idea and the experiences that influenced it. The idea of structural synthesis is to couple finite element structural analysis and nonlinear mathematical programming to create an *automated optimum design* process applicable to a broad class of structural systems. With these contributions a new philosophy of structural design was born. Later, structural optimization took shape as a synthesis of several disciplines which interact with each other in the resolution of an optimization problem. In addition to the structural analysis and mathematical programming modules, a design module and sensitivity analysis were considered. A control system organizes interactions and information transfers between modules.

The first optimization problems considered within this new structural design concept were concerned with size optimization of discrete structures. In size optimization, the shape and topology of the structure are already known, but certain parameters of the structural components have to be determined. In the case of discrete structures, a design variable is directly associated with a structural component and, therefore, the design parametrization is determined by the formulation of the structural problem. The most representative example of sizing in discrete structures is the optimization of cross sections of members in a truss structure.

In shape optimization, the geometry of the structure in a more general sense has to be determined, while connectivity and type of the structure are given. Strictly speaking, distinguishing between sizing and shape optimization is often unclear and it is related with how design variables affect the analysis rather than with the physical optimization problem itself. In shape optimization, design

variables are concerned with the nodal positions of the analysis mesh, while in sizing, they are related to properties of the mesh elements. Therefore, in shape optimization design variables affect structural analysis in a more complex manner. The first examples of shape optimization were also performed in discrete structural systems. The shape of truss structures was optimized considering nodal positions as design variables.

Continuous enhancement of numerical and analysis techniques together with improvement of computer capabilities permits the solution of more complex and general optimization problems. As a consequence, optimization of the structural shape of continuous structures is addressed. The performance of the structural analysis by the Finite Element Method is decisive to this point. Zienkiewicz and Campbell (1973) were the first to set a shape optimization problem in a general form, considering positions of finite element nodes as design variables. A fundamental difference between shape optimization of discrete and continuous structures is that in the second case design parametrization is not automatically given by the structural model. On the contrary, it has to be explicity defined by the designer in relation to the structural analysis model or to an underlying geometrical model. Design parametrization of continuum structures is a very important aspect in shape optimization, as it influences the optimization process and its result. These implications will be studied in the present work in the frame of shape optimization of shells.

Topology optimization is the most general type of structural optimization because the structural type is not prescribed. In the case of discrete structures, topology optimization is set as a combinatoric problem. Topology optimization of continuum structures is a material distribution problem and it is often used as a preprocessor of shape optimization. That is, first the topology of the structure is sought, and then, the final form of boundaries is searched with shape optimization (Bendsoe, 1989). Typical applications are for determining the optimal connectivity in a truss structure or the number and positions of holes in 2D or 3D structures. Nowadays, topology optimization is widely used in industry and academia. It was successfully applied to a wide range of problems in disciplines such as structural mechanics, electronics and acoustics.

In general, it can be stated that topology optimization is more complex than shape optimization. Nevertheless, complexity of shape optimization is closely related to that of the underlying finite element formulation and to the definition of the design model and its interactions with the mesh. These two aspects are in turn connected to the complexity of the geometrical model of the structure. For these reasons, the complexity of shape optimization of shells increases

significantly as compared to that of other structural types.

The most interesting applications of shape optimization of shells can be found in automotive and aeronautical industries, in the design of bodies of cars or fuselage and wings of planes. Other applications can be found in civil engineering in the design of roof structures. These applications are very important but unfortunately still not so numerous, due to the mentioned structural and geometrical complexities of shell structures, which affect the whole optimization process and especially the design module. However, nowadays there is a desire of increasing the use of shape optimization techniques in the design of shell structures.

A special discipline closely related to shape optimization of shells is form finding. Form finding methods have been developed in order to obtain the membrane geometry that satisfies the state of equilibrium of any prescribed membrane stress state. As a membrane stress state is statically determinate, there is a unique membrane geometry which matches with it, providing that boundaries are well defined (Bletzinger et al., 2002). From the mathematical point of view, it is an inverse problem. The final shape found in form finding is the deformed shape corresponding to the prescribed membrane stresses (see Bletzinger (1998)). It is important to note the essential difference between form finding and shape optimization. Figure 1.1 shows a scheme of the comparison between form finding and shape optimization methods. Form finding is a kind of particular case of shape optimization where the objective is the satisfaction of the equilibrium equation and the final form obtained is the deflected shape.

Optimal structural behavior of a shell is achieved when prerequisites and assumptions of the membrane theory are satisfied. The most relevant of these prerequisites are: $C^2$-continuity of the middle-surface of the shell, absence of thickness jumps and supports meeting the requirements of tangential forces (Bletzinger and Ramm, 1993). This allows the shell to resist the loads only by membrane forces, avoiding bending phenomena. But in real situations, membrane prerequisites are difficult to fulfill. It may also happen that the main objective of the structural problem is not to achieve a membrane stress state, but to minimize weight, displacements or stresses of the structure. In such cases, it is talk about shape optimization in a more general sense. The aim of shape optimization of shells is to play with the interaction between shape and structural response in order to achieve an optimal undeflected design satisfying certain objectives and fulfilling certain constraints.

FORM FINDING STRUCTURAL OPTIMIZATION

Given:

| Boundaries geometry |
| Stress state |
| Material properties |

Given:

| Initial design |
| Acting loads |
| Material properties |

Condition: equilibrium

Conditions: objective function
constraints
equilibrium

Obtained:

| Deflected shape |

Obtained:

| Optimal undeflected shape |

Structural analysis

| Deflected shape |
| Structural response |

Figure 1.1: Comparison between form finding and shape optimization

## 1.2   Objectives of the present work

In a general sense, there are two basic difficulties in shape optimization. First, it requires a deep control of the finite element analysis and an understanding of the mechanics behind the problem. In addition, selection of design variables and the relation between changes in the design and the updates of the mesh have to be determined. These difficulties become more pronounced when the structure to be optimized is a shell, because os the added complexities inherent to a shell finite element formulation and to its shape description.

This work studies certain aspects of shape optimization of shells related to the shell as structural type and as design model. Attention is paid to the modules of design and analysis (both structural and sensitivity) of the optimization loop. This is due to the fact that in these modules the nature of the shell is present either from the structural or geometrical point of view. In the mathematical programming module, the optimization problem is dealt with in its most abstract form, that is, more independently of the structural typology. Therefore, no interaction of the shell formulation or design is analyzed in this module. However, the solution strategies adopted in the mathematical programming module are also related with the modeling of the problem in a general sense.

This aspect is treated by Papalambros and Wilde (2000).

As design and analysis are components of the system of the optimization process, any factor affecting any of these components may have influence on the optimal result. In the present work, two key points are mainly studied: the influence of the reliability of the finite element formulation on the optimization result and the effects related to the techniques of shape description and control.

In an optimization process, the optimization algorithm makes decisions about the design based on information provided by structural and sensitivity analysis. Therefore, the quality of this information may affect the quality of the optimal design obtained. In particular, the influence of locking effects in the optimization result is studied. Under certain circumstances, displacement elements suffer from locking phenomena and, as a consequence, they yield inaccurate results. In the case of shear deformable thin elements based on the standard displacement formulation, locking effects appear when slenderness tends to zero. These effects have been studied in the frame of structural analysis and alternative formulations to avoid these problems have been proposed (see Bathe (1996) and Zienkiewicz and Taylor (2000a,b), for instance). In general, the influence of locking in structural optimization has been underestimated. Nevertheless, it should be noted that these phenomena may affect not only the structural analysis, but also the sensitivity analysis.

The sensitivity analysis technique used is also determinant in the quality of the information obtained from this analysis. For this reason, a review of the different sensitivity analysis techniques will be done and the sensitivity analysis for the shell element considered with the most suitable technique will be presented.

In relation to the design module, key aspects of shape description and control of surfaces are studied.

The technique of shape design parametrization is crucial insofar as it determines the set of admissible designs of the problem. That is, it determines the space in which the optimal solution is to be found. To this point, it is important to remark that the result of an optimization problem is optimal within the scope of the mathematical model describing it and subject to the subjective judgment of the designer.

In the recent history of structural optimization, it can be observed that there has been an evolution from simple techniques that allow to solve simple specific problems to approaches valid for a more general class of problems. There is, therefore, a trend toward generality and freedom of decision within the optimization problem. With this background, the most used parametrization techniques

in shape optimization of surfaces will be compared and advantages and disadvantages will be analyzed. Attention will be focused on how the selection of the parametrization technique conditions the optimization result.

A further way to influence the optimal result from the design module is through shape control techniques. In shape optimization not only the design that satisfies some structural requirements is desired, but often the designer wants it to satisfy some geometrical requirements. These are imposed through shape control techniques. The most troubled point related to shape control in shape optimization of shells is the smoothness control. A further objective of the present work is to develop a technique that allows the designer to control this smoothness, while attaining low modeling cost.

The premise of the present work is to study certain factors relative to design and analysis in shape optimization of shells, which have not received much attention until now, but are very important in the determination of the optimal result.

In Chapter 2, some fundamentals about shape optimization, Continuum Mechanics and the Finite Element Method are given. This does not pretend to be a detailed introduction, but more a brief review oriented to locate the work in the global context of structural optimization and to introduce the notation used in the following chapters.

Chapter 3 describes in detail the formulation of the shell element used. The shell element considered has Reissner-Mindlin kinematics, that is, it is shear deformable, and the director vectors at nodes are computed as the average of the normals to the adjacent elements. The different coordinate systems considered in the formulation are explained in detail. Two formulations of this shell element are considered. First, the standard displacement formulation, which suffers from the well-known locking phenomena is presented. Second, an alternative formulation based on the DSG concept, avoiding locking effects, is considered.

In Chapter 4, a review of the different sensitivity analysis techniques is presented. Attention is paid to the comparison between them and in their advantages and disadvantages for different problems. The sensitivity analysis by the discrete analytical approach for the considered shell element is presented in Chapter 5. Derivation of the element stiffness matrix both for the standard displacement and DSG formulation is explained in detail.

The influence of shear locking in shape optimization is studied in Chapter 6 by means of some numerical experiments. This influence will be analyzed both from the qualitative and quantitative point of view.

The most used shape description techniques for shape optimization of shells are briefly outlined in Chapter 7. A comparison is made between CAD- and FE-based design parametrizations. Attention is focused on the influence of parametrization techniques in the optimization result. A shape control technique to control surface smoothness is presented, based on the control of curvatures by regularization techniques emerging now in shape optimization for fluids. Moreover, a method to compute curvature measures on a surface described by a $C^0$ continuous mesh is proposed. The computation of the sensitivities of these curvature measures is also presented. Numerical experiments related to this control technique and to the comparison between CAD- and FE-based parametrizations are presented.

In Chapter 8, conclusions to this work are drawn and further lines of research are outlined.

The present shell element, its sensitivity analysis and the shape control technique proposed were implemented as a module in CARAT (Computer Aided Research Analysis Tool), a program first conceived by Bletzinger (1990), Kimmich (1990) and Reitinger (1994) (see also Bletzinger et al. (1993)) at the Department of Structural Analysis of the Universität Stuttgart in the nineties.

# Chapter 2

# Fundamentals

## 2.1 Structural optimization

In the present chapter, an introduction to the fundamentals of structural optimization is given. The aim of this chapter is to introduce some basic concepts, give an overview of the overall optimization process and show how the modules on which this work is focused fit in this global process. Each discipline taking part in structural optimization constitutes a line of research.

In a structural optimization process, the objective of designers may be to find the best design in terms of cost, weight, reliability, mechanical properties or esthetics, for example. A key point of the design process is to translate these objectives into criteria expressed mathematically to measure if a certain design is satisfactory or not.

The *objective function*, also called *cost function*, is the function to be minimized (or maximized) during the optimization process and constitutes the criteria by which a certain design is chosen among a group of alternatives. Typical objective functions are weight, cost or strain energy of the structure. These properties can be expressed by a mathematical function and, therefore, they are quantifiable.

The objective function is a function of the *design variables*. According to Tikhonov and Arsenin (1977), two types of minimization problems can be distinguished. First, there are problems where the minimum (or maximum) of a functional $f(\mathbf{s})$ has to be found and it is not important which variables $\mathbf{s}$ provide the minimum (or maximum). Second, there are minimization problems where the aim is to find which variables $\mathbf{s}$ minimize the functional $f(\mathbf{s})$. These

problems are called *minimization with respect to the argument*. Structural optimization problems belong to this second category, since the final aim is to find the structural design that minimizes the considered objective function. Therefore, structural configuration is a function of the chosen design variables and these are actually the unknowns of the optimization problem.

In addition to the objective function, in a general optimization problem *constraints* can be considered. These are restrictions to the problem to be satisfied in order for the design to be acceptable. That is, these constraints define the *feasible domain*. *Equality constraints* are those restrictions where a certain expression has to be equally satisfied. In *inequality constraints*, a certain expression has to be lower or higher than a certain prescribed value. In structural optimization inequality constraints are of major importance. Until 1960, equality constraints were used indiscriminately to obtain *fully stressed designs*. However, Schmit (1960) proved, with a simple but enlightening example, that those designs were not always optimal from the structural point of view and underlined the significance of inequality constraints.

Constraints can be an explicit or an implicit function of the design variables. In the first case, they are called *side constraints* and they limit the values of the design variables. They are a certain form of shape control. When constraints are a implicit function of the design variables, they are called *behavior constraints*. Typical examples are displacement or stress constraints.

In general, a structural optimization problem can be stated as

$$
\begin{aligned}
\text{minimize} \quad & f\left(\mathbf{s}, \mathbf{u}\left(\mathbf{s}\right)\right); \quad \mathbf{s} \in \mathbb{R}^{n_s} \\
\text{such that} \quad & g_j\left(\mathbf{s}, \mathbf{u}\left(\mathbf{s}\right)\right) \leq 0; \quad j = 1, ...p \\
& h_j\left(\mathbf{s}, \mathbf{u}\left(\mathbf{s}\right)\right) = 0; \quad j = 1, ...q
\end{aligned}
\tag{2.1}
$$

where $\mathbf{s}$ is the vector of design variables or optimization variables, which has a dimension of $n_s$, and $\mathbf{u}$ are the state variables, i.e. the displacements. According to the definitions given above, $f$ is the objective function, $g_j$ are the inequality constraints and $h_j$ are the equality constraints.

The formulation of the optimization problem can be divided into two tasks. On the one hand, the design model has to be set and the optimization variables have to be selected. On the other hand, objectives and constraints have to be formulated according to the general expression (2.1). Both tasks are crucial, insofar as they determine the scope in which the final design can be designed as optimal. However, they are determined to a large extent by the subjectivity of the designer's criteria. Therefore, it is very important that the designer realizes

the implications of the decisions taken in setting the problem and is aware of the available tools. Regarding the definition of objective functions, Maute and Raulli (2004) proposed an interactive method to assist the designer in selection of design criteria and formulation of optimization problems.

In the design model, the designer defines the initial design and the design variables which will be considered in the optimization process. The selection of the design variables determines strongly the structural optimization problem. First, it determines the kind of optimization problem, that is, whether it is a *sizing*, *shape optimization* or *topology optimization* problem. Second, the selection of the design variables for a certain problem determines the optimum, insofar as it determines the set of admissible designs, that is the set where the optimal design is searched during the optimization process.

In addition to this description of the shape, certain measures of shape control can be set. The aim is to control the geometry of the design as desired by the designer. Moreover, through shape parametrization and control, the designer can implicitly consider those criteria of the optimization problem which can not be directly translated into a mathematical expression. One can consider esthetics, for instance. This is a very subjective factor, which is impossible to translate into a mathematical expression, but it is often a decisive point in designing. The designer directly controls esthetics in the modeling phase, particularly in the selection of the design variables, and in the shape control during the optimization process. Decisions with this respect are taken based on the subjective criteria of the designer.

Some common techniques of shape control are variable linking, side constraints or regularization techniques. In Chapter 7, the two most used techniques of design parametrization in shape optimization of shells are compared. Moreover, a shape control technique which permits obtaining smooth surfaces is studied.

The *design model* defines, together with the selected criteria and restrictions expressed in (2.1), the formulation of the optimization problem. The structural optimization process, by which this problem is solved, is systematized as a group of modules or disciplines interacting between them. A scheme of the flow chart in a general structural optimization system is given in Figure 2.1. Further element involved is a system to control interactions between the different modules.

In structural optimization, the structural behavior of the design is considered in the search for a better design. This can be done by considering the strain energy as objective function, or by constraining the value of stresses or displacements.
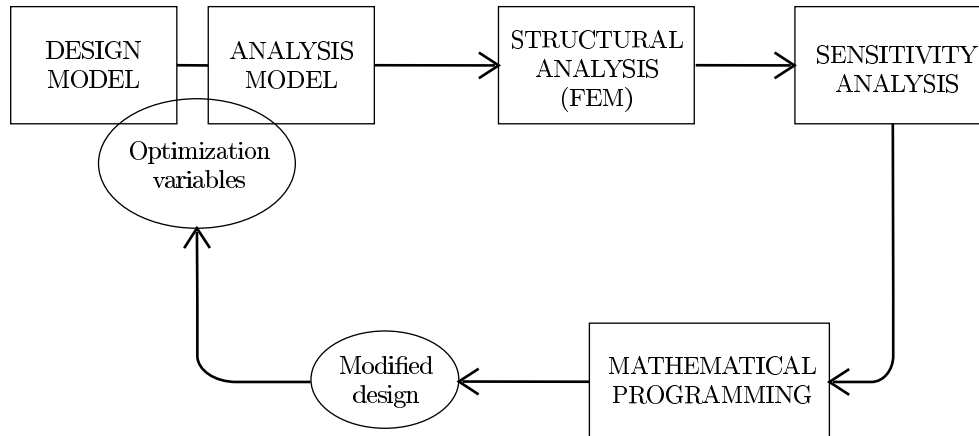
Figure 2.1: Scheme of a structural optimization system

For this reason, a structural analysis of the actual design is performed. In the case of continuum structures, this analysis is usually performed with the Finite Element Method. With the obtained structural response, the related objective function or constraint can be evaluated. However, in structural optimization other aspects which do not depend on the structural response (e.g. weight) can be considered as criteria or constraints. This is the case of weight, for instance, which can be computed based on the geometrical discretization considered in the analysis model used for structural analysis.

In Section 2.2, brief notes about continuum mechanics and the Finite Element Method are given in order to introduce the notation used in the following chapters.

In general, it is not only interesting to evaluate the objective function and constraints for the actual design, but also to predict their values for a potential modified design. Sensitivity analysis provides the derivatives of these functions with respect to the design variables. Based on this information, the optimization algorithm takes decisions about modifying the design. A review of the sensitivity analysis methods used in structural optimization is given in Chapter 4.

Mathematical programming is the discipline which deals with the techniques to solve problem (2.1). It comprises the optimization algorithm used to solve the problem. This is the most abstract part of the structural optimization loop. However, the selection of the mathematical programming technique depends on the formulation of the optimization problem (Papalambros and Wilde, 2000). Optimization algorithms can be classified as those for constrained or unconstrained problems, although many strategies for constrained problems generate

14

unconstrained subproblems. Algorithms used in the present work are gradient based, that is, they take decisions based on the values of objective function and constraints and on the values of their first order derivatives. This gradient information is provided by sensitivity analysis. In the present work, sequential quadratic programming (SQP) algorithms are used for constrained problems and conjugate gradient methods for unconstrained problems. A detailed exposition of the different optimization algorithms is given by Haftka and Gürdal (1999) and Kirsch (1998).

## 2.2 Structural analysis

For the comprehension of the present work, fundamental knowledge of Continuum Mechanics and of the Finite Element Method is required. Many references can be found on these matters. An introduction to Continuum Mechanics is given by Malvern (1969) and Marsden and Hughes (1983). An introduction to the Finite Element Method is given by Hughes (2000) for linear elastics and dynamics, Zienkiewicz and Taylor (2000a), Becker et al. (1981) and Carey and Oden (1983). The present section does not pretend to be a detailed introduction to Continuum Mechanics and the Finite Element Method, whose fundamental concepts are assumed to be known, but rather an introduction to the notation used in the following work.

There are three fundamental types of equations in Continuum Mechanics, which constitute the analytical model of structural mechanics. These equations can be expressed in tensor form and, thus, in an invariant form in all coordinate systems.

First, the *kinematic equations* determine the relations between strains and displacements in the domain and the prescribed displacement values at boundaries. Through these equations different models of calculus can be considered, for instance small displacements and small strains, or large displacements and small strains. The general form of the linear kinematic equation is given by

$$\boldsymbol{\varepsilon} = \mathbf{L}(\mathbf{u}) \tag{2.2}$$

where $\boldsymbol{\varepsilon}$ are the strains, $\mathbf{u}$ are the displacements and $\mathbf{L}$ is a linear differential operator.

The *constitutive equation* defines the material behavior and relates kinematic variables and stresses. In the present work, only linear elastic materials are

considered. For these cases, the constitutive equation reads

$$\boldsymbol{\sigma} = \mathbf{D} \cdot (\boldsymbol{\varepsilon} - \boldsymbol{\varepsilon}^0) + \boldsymbol{\sigma}^0 \qquad (2.3)$$

where $\boldsymbol{\sigma}$ are the stresses, $\mathbf{D}$ is the material tensor and $\boldsymbol{\varepsilon}^0$ and $\boldsymbol{\sigma}^0$ are the initial strains and stresses, respectively.

The operator $\cdot$ implies the contraction of inner indices, i.e. $\mathbf{A} \cdot \mathbf{B} = A_{ij}b_{jk}$. For vectors, it corresponds to the scalar product or dot product, that is $\mathbf{a} \cdot \mathbf{b} = a_i b_i$.

The *equilibrium equations* constitute an undetermined system of differential equations which relates internal and external forces of the structure. The boundary conditions are given by the support conditions of the structure. The equilibrium equations can be written in terms of the Principle of Virtual Work as

$$\int_{\Omega} \boldsymbol{\sigma} \cdot \delta\boldsymbol{\varepsilon}\, d\Omega = \int_{\Omega} \mathbf{f} \cdot \delta\mathbf{u}\, d\Omega \qquad (2.4)$$

where $\delta\boldsymbol{\varepsilon}$ and $\delta\mathbf{u}$ are the virtual strains and displacements, respectively, $\mathbf{f}$ is the external force vector and $\Omega$ the domain of the structure. This expression is a weak form of the equilibrium equations and is independent of constitutive and kinematic equations.

Expression (2.4) can be also obtained by writing equilibrium equations as integral equations in a weighted residual form. The variational index, which is the highest derivative order of the displacements, can be reduced by applying the divergence theorem or partial integration, obtaining expression (2.4). This expression is called weak form of the problem in contrast to the strong or classical form. The reduction of the variational index has the advantage of relaxing the continuity requirements of the solutions to the system of equations.

In certain structural typologies, in addition to these equations, other assumptions related to the deformed and tensional state are considered. In the case of thin structures, such as plates and shells, they permit the analysis of these three-dimensional structures as two-dimensional ones. These assumptions determine the different plate or shell theories.

In the Finite Element Method, the domain $\Omega$ is discretized by a mesh of subdomains called elements. Geometry and state variables are approximated by an interpolation of related values at the nodes of the mesh. The functions used for the interpolation are called shape functions. If nodes and shape functions used for the interpolation of geometry and state variables are the same, the interpolation is said to be isoparametric. The approximation of geometry and displacements is given by

$$\mathbf{x} = \mathbf{N} \cdot \mathbf{r} \qquad (2.5)$$

$$\mathbf{u} = \mathbf{N} \cdot \mathbf{d} \tag{2.6}$$

where $\mathbf{x}$ is the nodal position vector, $\mathbf{r}$ is the vector of nodal geometrical parameters, $\mathbf{u}$ is the nodal displacement vector, $\mathbf{d}$ is the vector of nodal degrees of freedom and $\mathbf{N}$ is the global matrix of shape functions.

Substituting (2.2), (2.3) and (2.6) in (2.4), we get to the following discrete system of equations

$$\mathbf{K} \cdot \mathbf{d} = \mathbf{F} \tag{2.7}$$

where $\mathbf{K}$ is the global stiffness matrix and $\mathbf{F}$ is the global vector of consistent nodal forces. The global stiffness matrix is obtained through assembling of the different contributions of elemental stiffness matrices, which are given in the general form as

$$\mathbf{k}^e = \int_{\Omega_e} \mathbf{B}^T \cdot \mathbf{D} \cdot \mathbf{B} \ d\Omega_e \tag{2.8}$$

In this expression $\mathbf{B}$ is the strain-displacement operator, which relates the approximated strains to the nodal degrees of freedom of the element. That is,

$$\mathbf{B} = \mathbf{L} \cdot \mathbf{N}^e \tag{2.9}$$

$\mathbf{N}^e$ being the matrix containing the shape functions related to element $e$. A detailed explanation of the assembling process can be found in Hughes (2000).

# Chapter 3

# A Shell Element with Reissner-Mindlin Kinematics

## 3.1  Introduction

Plate and shell elements are characterized by the slenderness $\lambda$, a parameter defined as the minimum value of the two ratios: the relation of a typical element length $h$ and the element thickness $t$, and the relation of $h$ and the radius of curvature $R$ of the element. Hence,

$$\lambda = min \left( \frac{h}{t}, \frac{h}{R} \right) \tag{3.1}$$

In the *thin shell* theory, the Kirchhoff condition leads to the appearance of second order derivatives of the unknown function in the strain definition. Consequently, in order to avoid kinks at the element boundaries in the deformed shell, $C_1$-continuity is required in the shape functions. The shape functions needed to satisfy this requirement are significantly more difficult than those used for $C_0$-continuity.

In the *thick shell* theory, as a consequence of the relaxation of the Kirchhoff assumptions, the strain definition contains only the unknown functions and their first derivatives. Therefore, the shape functions are only required to satisfy $C_0$-continuity. As a consequence, the formulation of a finite element with Reissner-Mindlin kinematics is much easier.

19

This chapter studies in depth a shell element with Reissner-Mindlin kinematics. The main points of the formulation are taken from Zienkiewicz and Taylor (2000b).

The element considered is a displacement element with five degrees of freedom: three global displacements and two rotations. Displacement degrees of freedom will affect the position of nodes, while rotation degrees of freedom will have influence on the direction in which the thickness of the shell element will be measured.

The parametrization of rotational degrees of freedom is closely related to the geometric definition of the element. To describe the spatial rotation of an arbitrary vector only two vectors, not coplanar with the first one, are needed. However, to describe the rotation of two or more vectors whose relative angle must remain unchanged, three vectors are required. These facts are the characteristics of two different main groups of definitions of shell element kinematics.

First, it is considered an element defined by the position of its nodes and the normal vectors to the element at its nodes, which are called director vectors. These vectors indicate the direction in which the element thickness is considered. As a consequence, the number of the defined director vectors at a node is equal to that of the non-coplanar elements sharing that node (see Figure 3.1). According to aforementioned affirmations, three rotation degrees of freedom are required to describe any arbitrary rotation of the cluster of director vectors of a node, if their relative positions are to be preserved.
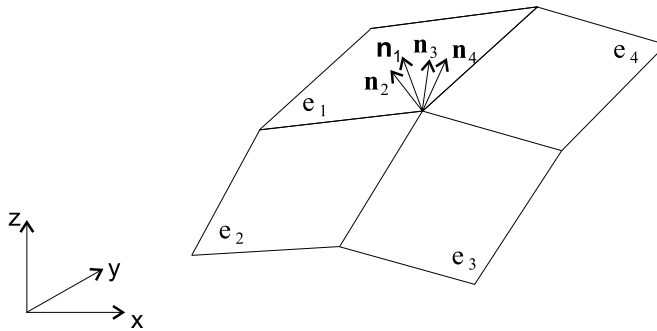


Figure 3.1: Multiple director vector definition at a node.

A drawback of this approach is the presence of gaps and overlappings of material at the inter-element boundaries (see Figure 3.2). The error introduced by this fact is usually neglected and, anyway, it will be considerably reduced with mesh refinement.
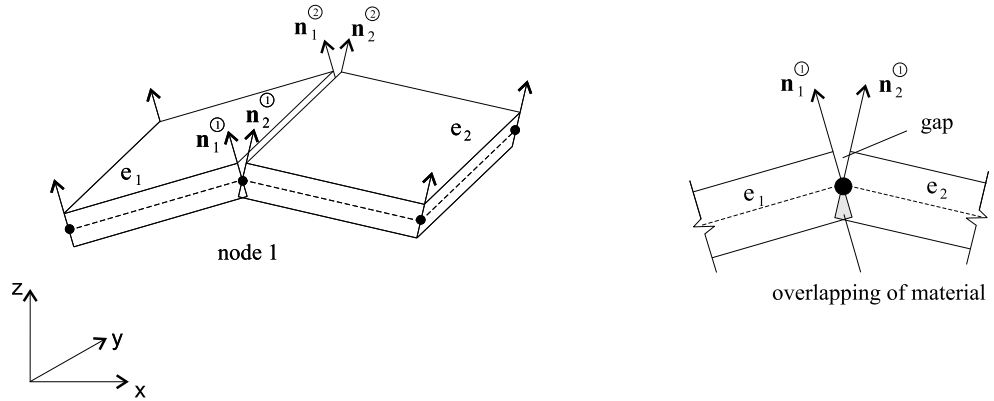
Figure 3.2: Gaps and overlappings of material at inter-element boundaries in a shell element definition with multiple director vectors.

The most important disadvantage of this shell element definition can be illustrated in an example. Consider the analysis of a plate using shell elements with six degrees of freedom: three displacements $\{u, v, w\}$ and three rotations $\{r_1, r_2, r_3\}$ as shown in Figure 3.3.
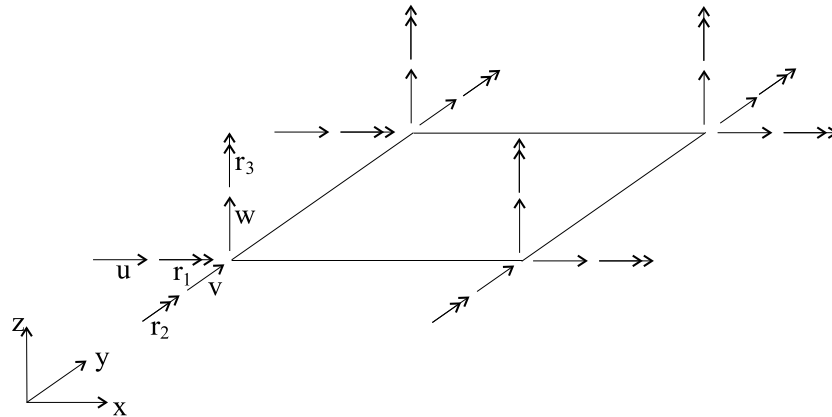


Figure 3.3: Plate element with six degrees of freedom at each node.

In this case, rotations $r_1$ and $r_2$ are associated with bending stiffness of the plate in $x$ and $y$ directions respectively. But, on the contrary, the drilling rotation $r_3$ has no physical meaning and cannot be related to any stiffness of the plate. As a consequence, the elemental stiffness matrix will be singular. Similar problems may appear in the case of a shell structure where the elements are coplanar or almost coplanar. Here, the system stiffness matrix may not be singular, but ill-conditioned. There are several methods to avoid this problem: A small stiffness may be added for drilling rotation, a penalty approach may be used or, in the

case of a plate, drilling rotation degree of freedom can be fixed and not taken into account in the assembling of the global stiffness matrix (Büchter, 1992).

To overcome the drawbacks of these shell elements, a new definition of a shell element considering only one director vector per node was proposed. As it was mentioned before, only two rotation degrees of freedom are needed to describe an arbitrary rotation of director vector. The only two requirements are that axes of rotation must not be coplanar with the director vector, and that they must be unique for each node. The direction of the director vector can be, in principle, arbitrary, with the restriction that it can not be contained in the mid-plane of the shell. Under these considerations, different shell elements were developed with respect to different definitions of the director vector.
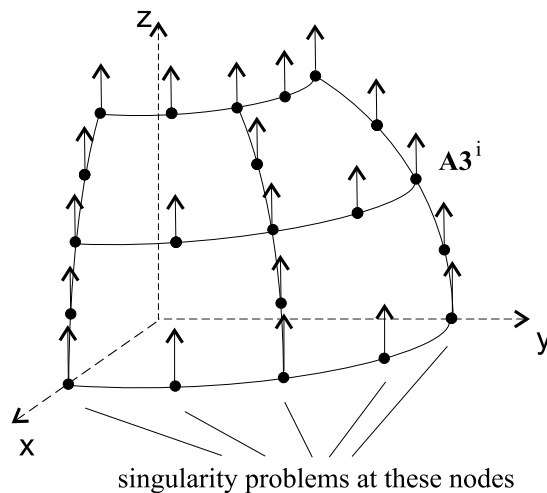


Figure 3.4: Spherical shell discretized with 8-node Lagrangian elements with global director vectors

One possibility is to choose the global Cartesian $z$-axis as the direction of the director vector at each node. However, this choice will lead to singularity problems if at any node the director vector is tangent to the shell element mid-plane. This is the case of the spherical sector shell discretized with 8-node Lagrangian elements shown in Figure 3.4. Here, director vectors of nodes located on the $xy$-coordinate plane are tangent to the shell element mid-plane at those points.

Another alternative is to calculate the director vector direction as the average of normal vectors to the elements at each node. This shell theory analyzes arbitrary shell geometries without difficulties related to singularities or bad-conditioning and without considering a third rotation degree of freedom.

Other alternative procedures to define the director vector are presented by Bischoff (1999).

The Reissner-Mindlin shell element studied in the present chapter, is considered within the framework of this averaged director shell theory and therefore, only two rotation degrees of freedom are required.

First, several aspects related to the geometrical definition of the element are discussed. Attention is paid to its derivation from the degeneration concept and to the definition of the director coordinate systems. Probably, the most difficult task related to shell finite elements is to deal with the numerous coordinate systems that are to be considered in each formulation. In order to clarify this point, the different coordinate systems used in the present formulation are presented and the relations between them are established. Calculation of strains and stresses is shown and the general expression for the elemental stiffness matrix is indicated.

Since the early days of the Finite Element Method, it has been observed that finite elements based on the Principle of Virtual Work suffer from so-called locking phenomena. These phenomena are characterized by the appearance of inaccuracies in relation with a certain parameter. Many alternative formulations to the standard displacement formulation have been proposed to avoid the locking effects. One of these, the DSG method, is formulated for the shell element presented in this chapter. Due to its efficiency and simplicity, the DSG shell element is very suitable for structural optimization.

## 3.2   Derivation of a shell element from the degeneration concept

The shell element studied is derived from the *degeneration concept* introduced by Ahmad (1969). The core of this concept is the discretization of a three-dimensional mathematical model with three-dimensional elements and their subsequent reduction into two-dimensional elements. The shell element is the most general level of the family of two-dimensional finite elements.

Figure 3.5 shows a typical three-dimensional element. Both top and bottom layers of the element have curved edges, while the edges in the thickness direction are straight lines. The nodes are located at the top and bottom of the element faces.

3D element · 2D shell element
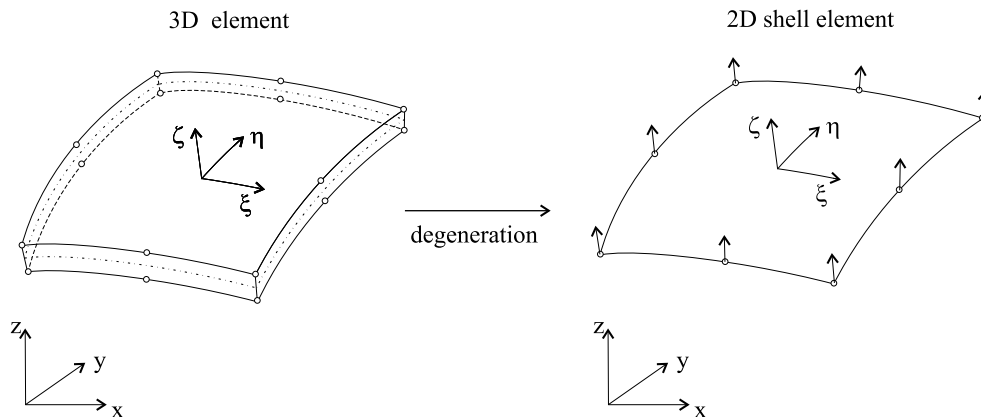
degeneration

Figure 3.5: Degeneration of a three-dimensional shell element into a two-dimensional one.

A curvilinear coordinate system $\{\xi, \eta, \zeta\}$ with origin in the mid-plane of the shell element is defined. $\xi$ and $\eta$ are curvilinear coordinates contained in the mid-plane, which range from $-1$ to $1$. $\zeta$ is a linear coordinate in the thickness direction, also ranging from $-1$ to $1$. The global Cartesian coordinates of an arbitrary point of the shell element can be expressed as a function of the curvilinear coordinates in the form

$$\begin{Bmatrix} x \\ y \\ z \end{Bmatrix} = \sum_a N_a(\xi, \eta) \left( \frac{1+\zeta}{2} \begin{Bmatrix} x_a \\ y_a \\ z_a \end{Bmatrix}_{top} + \frac{1-\zeta}{2} \begin{Bmatrix} x_a \\ y_a \\ z_a \end{Bmatrix}_{bottom} \right) \tag{3.2}$$

where $\{x_a, y_a, z_a\}^T_{top}$ and $\{x_a, y_a, z_a\}^T_{bottom}$ are the position vectors of node $a$ at top and bottom element faces respectively and $N_a(\xi, \eta)$ are the standard two-dimensional shape functions.

The degeneration of this three-dimensional shell element is done by melting the nodes with the same $\xi, \eta$ coordinates into a single node located at the mid-plane of the element, as shown in Figure 3.5.

The mathematical reduction of the three-dimensional geometrical definition of the shell element is done in two steps. First, the coordinates of the nodes located on the mid-plane of the element are calculated as

$$\begin{Bmatrix} x_a \\ y_a \\ z_a \end{Bmatrix}_{mid} = \frac{1}{2} \left( \begin{Bmatrix} x_a \\ y_a \\ z_a \end{Bmatrix}_{top} + \begin{Bmatrix} x_a \\ y_a \\ z_a \end{Bmatrix}_{bottom} \right) \tag{3.3}$$

Second, the information of the direction in which the thickness is considered is saved in a vector $\widehat{\mathbf{A3}}_a$ that connects the upper and lower points of the element (see Figure 3.6). This vector is obtained as

$$\widehat{\mathbf{A3}}_a = \left\{\begin{array}{c} x_a \\ y_a \\ z_a \end{array}\right\}_{top} - \left\{\begin{array}{c} x_a \\ y_a \\ z_a \end{array}\right\}_{bottom} \tag{3.4}$$
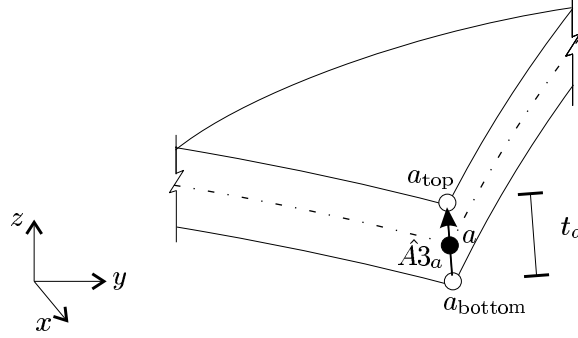


Figure 3.6: Vector $\widehat{\mathbf{A3}}_a$ containing the thickness information after the degeneration of the element.

Now, (3.2) may be rewritten as

$$\left\{\begin{array}{c} x \\ y \\ z \end{array}\right\} == \sum_{a=1}^{n_{en}} N_a(\xi, \eta) \left(\left\{\begin{array}{c} x_a \\ y_a \\ z_a \end{array}\right\}_{mid} + \frac{1}{2}\zeta\widehat{\mathbf{A3}}_a\right) \tag{3.5}$$

$n_{en}$ being the number of nodes at the element.

The length of the vector $\widehat{\mathbf{A3}}_a$ is the thickness of the shell element at the node $a$. If we normalize it, we obtain the unit vector $\mathbf{A3}_a$, called *director vector*, and the geometrical description of the two-dimensional degenerated shell element becomes

$$\left\{\begin{array}{c} x \\ y \\ z \end{array}\right\} = \sum_{a} N_a(\xi, \eta) \left(\left\{\begin{array}{c} x_a \\ y_a \\ z_a \end{array}\right\}_{mid} + \frac{1}{2}\zeta t_a \mathbf{A3}_a\right) \tag{3.6}$$

Hence, the discretized three-dimensional elements have been *degenerated* into two-dimensional shell elements.

It should be noted that this degeneration process is not explicitly done in the analysis of a structure. In fact, the director vectors are not really obtained from the melting process of an upper and lower previous nodes. The calculation process of the director vectors is explained in Section 3.4.

## 3.3 Geometric definition of an element

As it was explained in section 3.2, the geometry of the two-dimensional Reissner-Mindlin shell element studied is described by the position vector $\mathbf{x_a}$ and the director vector $\mathbf{A3_a}$ of each node $a$ (see Figure 3.7). The global Cartesian coordinates of an arbitrary point of the shell element are given by

$$\mathbf{x} = \sum_{a=1}^{n_{en}} N_a(\xi, \eta) \left( \mathbf{x}_a + \frac{1}{2}\zeta t_a \mathbf{A3}_a \right) \tag{3.7}$$

$n_{en}$ being the number of nodes of the element.
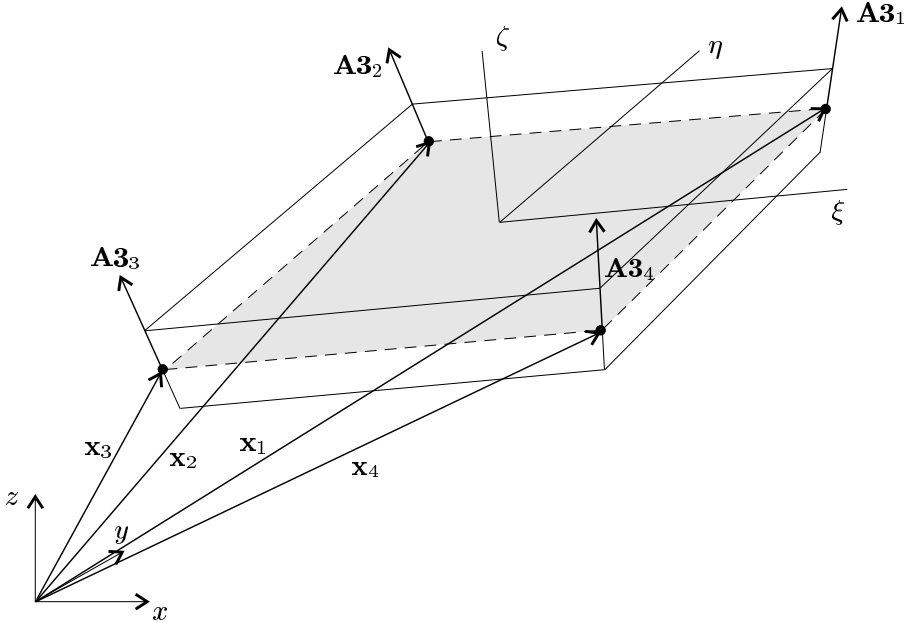


Figure 3.7: Geometric definition of the Reissner-Mindlin shell element studied.

Two contributions can be clearly distinguished. The first term indicates the position of the projection of the point into the shell mid-plane according to the thickness direction. $N_a(\xi, \eta)$ are the standard Lagrangian two-dimensional shape functions, and $\xi$ and $\eta$ are the curvilinear coordinates in the mid-surface of the shell which which range from $-1$ to $1$. Curved boundaries of the shell element can be considered by using higher order shape functions. Standard Lagrangian two-dimensional shape functions for different element types are given in Appendix A.1.

The second term describes the distance from the considered point to the mid-plane measured in the thickness direction. Here, $\zeta$ is a linear coordinate in the

thickness direction, that is, in the direction of the director vector, also ranging from $-1$ to $1$, and $t_a$ is the thickness of the shell at the node $a$. Figure 3.8 illustrates both contributions.
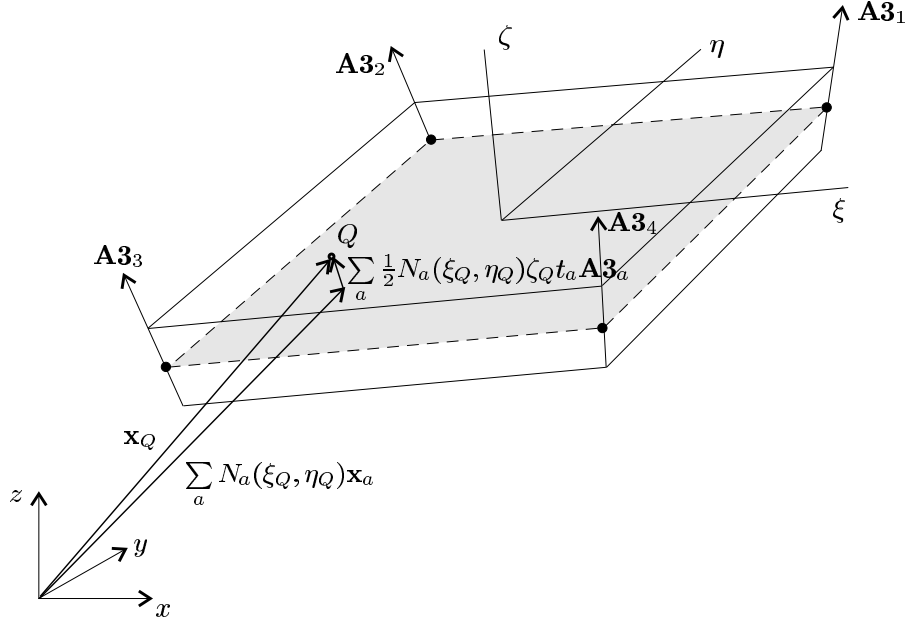


Figure 3.8: Location of an arbitrary point P in the shell element.

## 3.4 Calculation of the director coordinate systems

The director coordinate systems are local Cartesian systems defined at each node $P$ and constituted by the director vector at that node and two other vectors that complete a Cartesian basis. It should be noted that $P$ refers to the global node number and $a$ to the local node number.

As it was shown in Section 3.3, the director vector $\mathbf{A3}_P$ takes part in the geometric definition of the shell element, indicating the direction in which the thickness is to be considered. The other two vectors, called $\mathbf{A1}_P$ and $\mathbf{A2}_P$, are the axes of rotation of the rotation degrees of freedom.

The definition of the director vector $\mathbf{A3}_P$ depends on the shell theory chosen. As explained in Section 3.1, for the present Reissner-Mindlin shell element the

director vector direction is considered to be the average of the normal vectors to the elements at each node.

In this section, the calculation procedure for the director coordinate system is explained in detail. As it will be shown in Chapter 5, this procedure is of major importance for the calculation of the derivatives of the state variables in the sensitivity analysis.

We define the normal vector at node $a$ of element $e_k$ as

$$\mathbf{A3}_P^{e_k} = \left. \frac{\mathbf{x}_{,\xi} \times \mathbf{x}_{,\eta}}{|\mathbf{x}_{,\xi} \times \mathbf{x}_{,\eta}|} \right|_{\substack{\xi=\xi_a \\ \eta=\eta_a \\ \zeta=0}} \tag{3.8}$$

where $\xi_a$, $\eta_a$ and $\zeta = 0$ are the local curvilinear coordinates of node $P$ in element $e_k$, and the vectors $\mathbf{x}_{,\xi}$ and $\mathbf{x}_{,\eta}$ are given by

$$\left. \mathbf{x}_{,\xi} \right|_{\zeta=0} = \sum_{b=1}^{n_{en}} N_{b,\xi} \, \mathbf{x}_b \tag{3.9}$$

$$\left. \mathbf{x}_{,\eta} \right|_{\zeta=0} = \sum_{b=1}^{n_{en}} N_{b,\eta} \, \mathbf{x}_b \tag{3.10}$$

(Note that $N_{b,\xi} = \frac{\partial N_b}{\partial \xi}$).

However, in general the node $P$ will not only belong to element $e_k$, but also to other adjacent elements. Thus, we may apply the same procedure to calculate the normal vector at node $P$ considering the other adjacent elements. As Figure 3.9 shows, if not every element sharing node $P$ is on the same plane, different normal vectors and, therefore, different director coordinate systems, will be obtained.

To overcome this inconsistency, a unique director vector must be defined per node. There may be different ways to achieve this. One method is to calculate the averaged unit director vector at node $P$ as

$$\mathbf{A3_P} = \frac{\sum\limits_{k=1}^{nae} \mathbf{A3}_P^{e_k}}{|\sum\limits_{k=1}^{nae} \mathbf{A3}_P^{e_k}|} \tag{3.11}$$

*nae* being the number of adjacent elements at the node.

28
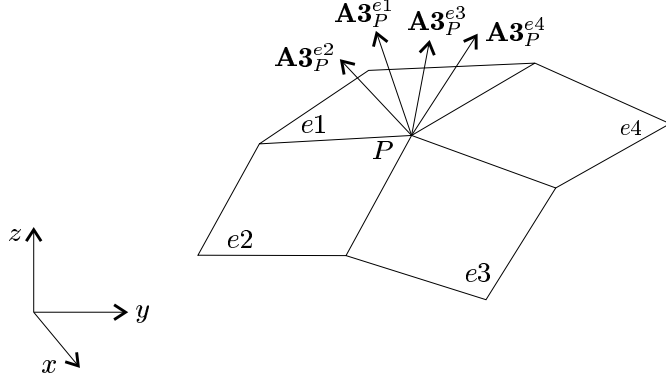
Figure 3.9: Normal vectors to the adjacent elements of a node.

It must be remarked that, in general, this director vector will be no longer normal to any adjacent element, but only an approximation of the normal direction of the shell. The thickness of the shell will be considered in the direction indicated by the director vector.

In order to complete the director coordinate system at each node, two other base vectors must be defined. The director coordinate system is a Cartesian system and, therefore, the three vectors must be orthogonal to each other. As the director vector has approximately the shell thickness direction, the other two vectors must be contained in the orthogonal plane, that is, the tangential plane to the shell surface at the considered node. There is obviously an infinite number of pairs of orthogonal vectors contained in that plane. There are several alternative procedures to choose a certain pair of these vectors in order to ensure a unique definition of the tangential plane. In this work, the scheme proposed by Ahmad (1969) and Zienkiewicz et al. (1971) is adopted.

Once the smallest component of the vector $\mathbf{A3}_P$ is found, the vector $\mathbf{A1}_P$ is calculated as the normalized vector product of the unit vector in this direction and the vector $\mathbf{A3}_P$. Let us consider that the director vector $\mathbf{A3}_P$ is expressed in vector representation as

$$\mathbf{A3}_P = x\mathbf{i} + y\mathbf{j} + z\mathbf{k} \tag{3.12}$$

where $\mathbf{i}$, $\mathbf{j}$ and $\mathbf{k}$ are the coordinate base vectors of the global Cartesian system. Thus,

$$\mathbf{A1}_P = \frac{\mathbf{l} \times \mathbf{A3}_P}{|\mathbf{l} \times \mathbf{A3}_P|} \tag{3.13}$$

29

where

$$\mathbf{l} = \begin{cases} \mathbf{i} & if \quad A3_P^1 = min\left\{A3_P^1, A3_P^2, A3_P^3\right\} \\ \mathbf{j} & if \quad A3_P^2 = min\left\{A3_P^1, A3_P^2, A3_P^3\right\} \\ \mathbf{k} & if \quad A3_P^3 = min\left\{A3_P^1, A3_P^2, A3_P^3\right\} \end{cases} \tag{3.14}$$

If, for example, the smallest component of $\mathbf{A3}_P$ is the $x$ component, the vector $\mathbf{A1}_P$ will be given by

$$\mathbf{A1}_P = \frac{\mathbf{i} \times \mathbf{A3}_P}{|\mathbf{i} \times \mathbf{A3}_P|} \tag{3.15}$$

As the vector $\mathbf{A2}_P$ is required to be perpendicular to the vectors $\mathbf{A1}_P$ and $\mathbf{A3}_P$, it will be calculated as the normalized vector product of these two vectors, that is,

$$\mathbf{A2}_P = \frac{\mathbf{A3}_P \times \mathbf{A1}_P}{|\mathbf{A3}_P \times \mathbf{A1}_P|} \tag{3.16}$$
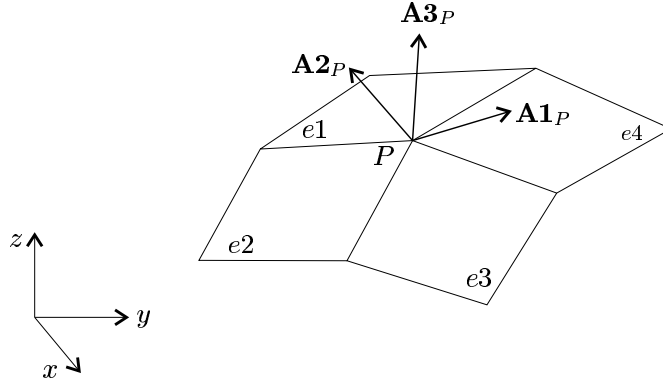
Figure 3.10: Director coordinate system at a node of a patch of bilinear shell elements.

It should be emphasized that all three vectors $\mathbf{A1}_P$, $\mathbf{A2}_P$ and $\mathbf{A3}_P$, are unit vectors. Figure 3.10 illustrates the director coordinate system at a node $P$ of a patch of bilinear shell elements.

## 3.5 Displacement field

The approximate displacement of an arbitrary point of the shell element in the global Cartesian axis is given by

$$\begin{Bmatrix} u \\ v \\ w \end{Bmatrix} = \sum_{a=1}^{n_{en}} N_a(\xi, \eta) \left( \begin{Bmatrix} u_a \\ v_a \\ w_a \end{Bmatrix} + \frac{1}{2}\zeta t_a \begin{bmatrix} \mathbf{A1}_a & -\mathbf{A2}_a \end{bmatrix} \cdot \begin{Bmatrix} \alpha_a \\ \beta_a \end{Bmatrix} \right) \tag{3.17}$$

As it can be noted, there are five degrees of freedom at each node: three global Cartesian displacements $u_a$, $v_a$ and $w_a$ and two rotation degrees of freedom $\alpha_a$ and $\beta_a$, which represent the rotation of the director at node $a$ around the vectors $\mathbf{A2}_a$ and $\mathbf{A1}_a$ respectively. As it was explained in Section 3.1, only one director vector per node is used in the geometrical definition of this shell element and, therefore, only two rotational degrees of freedom are required. Figure 3.11 illustrates the displacements of a point $Q$ located in the thickness direction at node $a$, due to the rotation degrees of freedom.
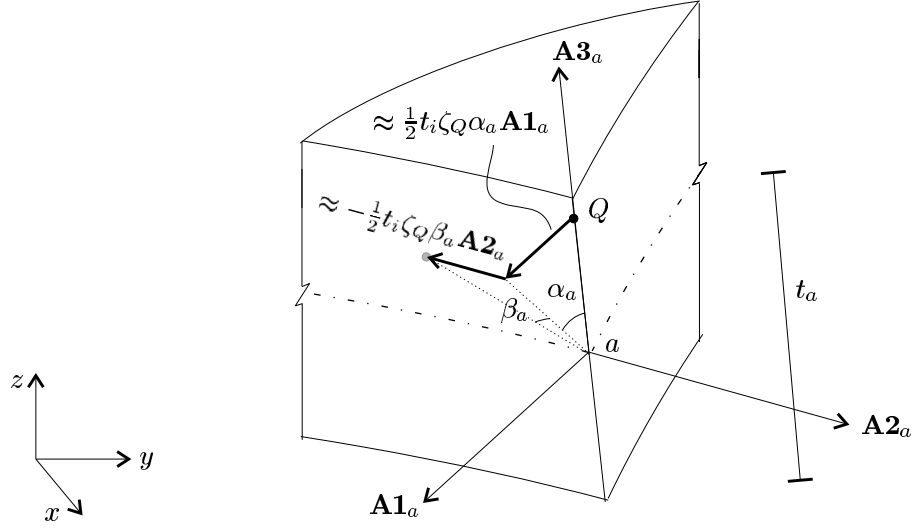


Figure 3.11: Displacements of a point $P$ due to the rotation degrees of freedom.

The usual form of (3.17) is

$$\mathbf{u} = \sum_{a=1}^{n_{en}} \mathbf{N_a}(\xi, \eta, \zeta) \cdot \mathbf{d_a} \tag{3.18}$$

where, in this case,

$$\mathbf{N_a}(\xi, \eta, \zeta) = \begin{pmatrix} N_a & 0 & 0 & \frac{1}{2}\zeta t_a N_a \mathbf{A1}_a^1 & -\frac{1}{2}\zeta t_a N_a \mathbf{A2}_a^1 \\ 0 & N_a & 0 & \frac{1}{2}\zeta t_a N_a \mathbf{A1}_a^2 & -\frac{1}{2}\zeta t_a N_a \mathbf{A2}_a^2 \\ 0 & 0 & N_a & \frac{1}{2}\zeta t_a N_a \mathbf{A1}_a^3 & -\frac{1}{2}\zeta t_a N_a \mathbf{A2}_a^3 \end{pmatrix} \tag{3.19}$$

and $\mathbf{d}_a$ is the vector of nodal displacements and rotations, that is,

$$\mathbf{d_a} = \begin{Bmatrix} u_a \\ v_a \\ w_a \\ \alpha_a \\ \beta_a \end{Bmatrix} \tag{3.20}$$

31

## 3.6 Relation between the different coordinate systems

A look back into the previous sections reveals that different coordinate systems are used simultaneously to define an element. In addition, in Section 3.7 additional coordinate systems will be used to obtain the strain tensor. In order to clarify this task, a brief review and further remarks are presented and the relations between the different coordinate systems are specified. Figure 3.12 illustrates the different coordinate systems and their location with respect to an element.
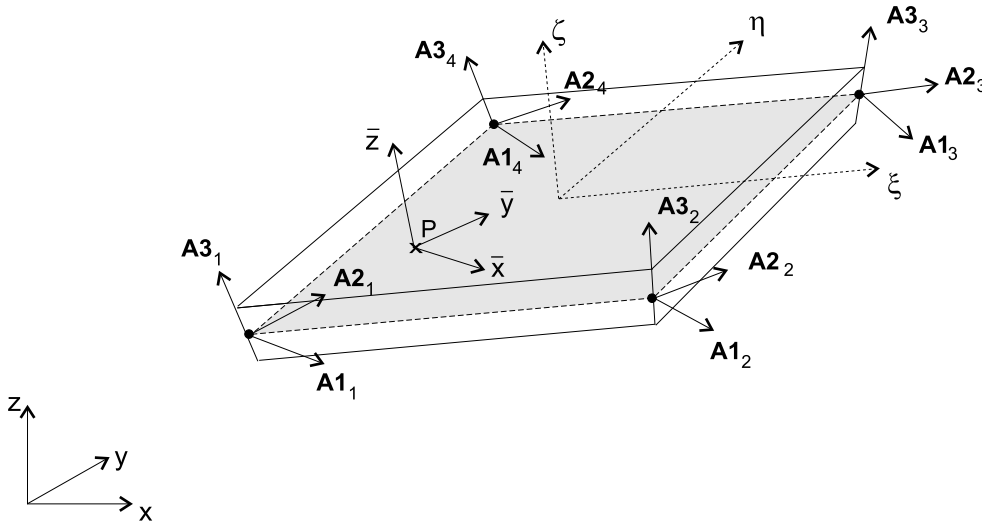


Figure 3.12: Different coordinate systems used in the present shell element formulation.

As a global reference, the *global Cartesian* coordinate system of the structure is used. It will be denoted by $\{x, y, z\}$ and the other coordinate systems will be related to it.

At each node $a$, the *director Cartesian coordinate system* $\{\mathbf{A1}_a, \mathbf{A2}_a, \mathbf{A3}_a\}$ is defined as explained in Section 3.4. The director vector $\mathbf{A3}_a$ is a parameter in the geometric definition of the element and points in thickness direction of the shell. As it was mentioned before, the director vector $\mathbf{A3}_a$ is not necessarily perpendicular to any element adjacent to node $a$, since it is an average of the normals to the adjacent elements at node $a$. The vectors $\mathbf{A1}_a$ and $\mathbf{A2}_a$ are approximately tangential to the mid-plane of the shell and are related to the rotational degrees of freedom of the node.

32

The *local curvilinear coordinate system* is defined locally for each element and has its origin at the element center. Two different bases are defined: the contravariant and the covariant basis. The covariant basis $\{\mathbf{g}_1, \mathbf{g}_2, \mathbf{g}_3\}$ is associated with the contravariant coordinates $\{\hat{x}^1, \hat{x}^2, \hat{x}^3\}$, here also denoted as $\{\xi, \eta, \zeta\}$, which are commonly used in the geometrical definition of finite elements. The coordinates $\xi$ and $\eta$ are tangential to the element mid-plane. The coordinates vary between $-1$ and $1$ on the respective faces of the element. The two-dimensional Lagrange shape functions are expressed in this system and the Gauss integration will be performed on it. For this reason, transformations and changes of variables into this system will be required in order to express the integrand as a function of $\xi$, $\eta$ and $\zeta$.

The relation between the global Cartesian and the local curvilinear contravariant coordinates is given by (3.7). The Jacobian of the transformation is

$$\mathbf{J} = \begin{pmatrix} x_{,\xi} & y_{,\xi} & z_{,\xi} \\ x_{,\eta} & y_{,\eta} & z_{,\eta} \\ x_{,\zeta} & y_{,\zeta} & z_{,\zeta} \end{pmatrix} = \begin{pmatrix} \mathbf{x}_{,\xi}^T \\ \mathbf{x}_{,\eta}^T \\ \mathbf{x}_{,\zeta}^T \end{pmatrix} \tag{3.21}$$

The expression (3.7) gives the global Cartesian coordinates of an arbitrary point of the shell as a function of the curvilinear coordinates. Therefore, the different terms of the Jacobian matrix can be easily obtained by simply deriving this expression with respect to the suitable curvilinear coordinate

$$\mathbf{x}_{,\xi} = \sum_a \frac{\partial N_a(\xi, \eta)}{\partial \xi} \left( \mathbf{x}_a + \frac{1}{2} \zeta t_a \mathbf{A3}_a \right) \tag{3.22}$$

$$\mathbf{x}_{,\eta} = \sum_a \frac{\partial N_a(\xi, \eta)}{\partial \eta} \left( \mathbf{x}_a + \frac{1}{2} \zeta t_a \mathbf{A3}_a \right) \tag{3.23}$$

$$\mathbf{x}_{,\zeta} = \sum_a N_a(\xi, \eta) \frac{1}{2} t_a \mathbf{A3}_a \tag{3.24}$$

And thus, we obtain

$$\mathbf{J} = \sum_a \begin{pmatrix} N_{a,\xi} \left( x_a + \frac{1}{2}\zeta t_a A3_a{}^1 \right) & N_{a,\xi} \left( y_a + \frac{1}{2}\zeta t_a A3_a{}^2 \right) & N_{a,\xi} \left( z_a + \frac{1}{2}\zeta t_a A3_a{}^3 \right) \\ N_{a,\eta} \left( x_a + \frac{1}{2}\zeta t_a A3_a{}^1 \right) & N_{a,\eta} \left( y_a + \frac{1}{2}\zeta t_a A3_a{}^2 \right) & N_{a,\eta} \left( z_a + \frac{1}{2}\zeta t_a A3_a{}^3 \right) \\ \frac{1}{2} N_a t_a A3_a{}^1 & \frac{1}{2} N_a t_a A3_a{}^2 & \frac{1}{2} N_a t_a A3_a{}^3 \end{pmatrix} \tag{3.25}$$

where $A3_a{}^i$ is the *ith*-component of vector $\mathbf{A3}_a$

The covariant curvilinear basis vectors can be obtained from the components of the Jacobian matrix as,

$$\mathbf{g}_i = \mathbf{x},_i \tag{3.26}$$

where, following the usual convention for Latin indices, $i = 1, 2, 3$.

Note that,

$$\mathbf{J} = \begin{pmatrix} x,_\xi & y,_\xi & z,_\xi \\ x,_\eta & y,_\eta & z,_\eta \\ x,_\zeta & y,_\zeta & z,_\zeta \end{pmatrix} = \begin{Bmatrix} \mathbf{g}_1^T \\ \mathbf{g}_2^T \\ \mathbf{g}_3^T \end{Bmatrix} \tag{3.27}$$

The contravariant basis $\{\mathbf{g}^1, \mathbf{g}^2, \mathbf{g}^3\}$ is associated with covariant coordinates $\{\hat{x}_1, \hat{x}_2, \hat{x}_3\}$. As it will be shown in Section 3.7, the strain tensor is computed first on this basis. The transformation from covariant components into contravariant components is done through the covariant metric coefficient matrix $\mathbf{G} = \{g_{ij}\}$. That is,

$$\{\hat{x}^j\} = \{g_{ij}\}^{-T}\{\hat{x}_i\} \tag{3.28}$$

where $\{\hat{x}^j\}$ and $\{\hat{x}_i\}$ are column vectors containing the covariant and contravariant coordinates, respectively.

The contravariant metric coefficient matrix $\mathbf{G}^{-1} = \{g^{ij}\} = \{g_{ij}\}^{-1}$ is the contravariant metric coefficient matrix. The covariant metric coefficient matrix is given by

$$\mathbf{G} = \{g_{ij}\} = \{\mathbf{g}_i \cdot \mathbf{g}_j\} = \begin{pmatrix} \mathbf{g}_1 \cdot \mathbf{g}_1 & \mathbf{g}_1 \cdot \mathbf{g}_2 & \mathbf{g}_1 \cdot \mathbf{g}_3 \\ \mathbf{g}_2 \cdot \mathbf{g}_1 & \mathbf{g}_2 \cdot \mathbf{g}_2 & \mathbf{g}_2 \cdot \mathbf{g}_3 \\ \mathbf{g}_3 \cdot \mathbf{g}_1 & \mathbf{g}_3 \cdot \mathbf{g}_2 & \mathbf{g}_3 \cdot \mathbf{g}_3 \end{pmatrix} \tag{3.29}$$

For rectangular elements, the contravariant and covariant basis coincide and $\mathbf{G}$ is the identity matrix.

For the definition of the strain and stress vector in an arbitrary point of the shell, a *local Cartesian coordinate system* at that point is introduced. This coordinate system will be denoted by $\{\bar{\mathbf{x}}, \bar{\mathbf{y}}, \bar{\mathbf{z}}\}$ and the unit base vectors of the system by $\{\bar{\mathbf{e}}_1, \bar{\mathbf{e}}_2, \bar{\mathbf{e}}_3\}$. The main important advantage of the choice of this system, is that the components of the strain vector will have a clear physical meaning, so no transformation will be necessary in the postprocessing. Moreover, further advantages of this local Cartesian coordinate system will be acknowledged in the sensitivity analysis of the element.

Another alternative would be to express the strain vector in the local curvilinear coordinate system. However, the physical meaning of the strain components would be lost and, moreover, additional difficulties would be introduced in the

sensitivity analysis of the element. This point will be explained in detail in Chapter 5.

In the integration of the stiffness matrix with a Gauss quadrature, the strain vector will be evaluated at the Gauss points. Thus, local Cartesian coordinate systems will be defined at these points.

For the determination of this coordinate system, the director vectors of the element nodes are taken into account. The base vector $\bar{\mathbf{e}}_3$ associated with the $\bar{z}$ axis will be calculated as the normalized interpolation of the director coordinate systems of the element nodes. Hence,

$$\bar{\mathbf{e}}_3 = \frac{\sum_a N_a(\xi, \eta)\mathbf{A3}_a}{\left|\sum_a N_a(\xi, \eta)\mathbf{A3}_a\right|} \tag{3.30}$$

As it was explained in Section 3.4, the director vector at an element node is not necessarily perpendicular to the element mid-plane, because it is calculated as an average of the perpendicular vectors to mid-planes of all adjacent elements at that node (see (3.11)). Therefore, it must be noted that, in general, $\bar{\mathbf{e}}_3$ will also not be perpendicular to the element mid-plane but its direction will be considered as the thickness direction.

The procedure chosen to compute the other two base vectors $\bar{\mathbf{e}}_1$ and $\bar{\mathbf{e}}_2$ is analogous to the calculation of the vectors $\mathbf{A1}_a$ and $\mathbf{A2}_a$ explained in Section 3.4. Therefore, the vector $\bar{\mathbf{e}}_1$ will be calculated as the normalized cross-product of the global base vector associated with the smallest component of $\bar{\mathbf{e}}_3$ and this vector $\bar{\mathbf{e}}_3$. Thus,

$$\bar{\mathbf{e}}_1 = \frac{\mathbf{l} \times \bar{\mathbf{e}}_3}{|\mathbf{l} \times \bar{\mathbf{e}}_3|} \tag{3.31}$$

where

$$\mathbf{l} = \begin{cases} \mathbf{i} & if & \bar{e}_3^1 = min\left\{\bar{e}_3^1, e_3^2, \bar{e}_3^3\right\} \\ \mathbf{j} & if & \bar{e}_3^2 = min\left\{\bar{e}_3^1, e_3^2, \bar{e}_3^3\right\} \\ \mathbf{k} & if & \bar{e}_3^3 = min\left\{\bar{e}_3^1, e_3^2, \bar{e}_3^3\right\} \end{cases} \tag{3.32}$$

and $\bar{e}_3^j$ is the $j$-component of the vector $\bar{\mathbf{e}}_3$.

The base vector $\bar{\mathbf{e}}_2$ completes the local Cartesian coordinate system and is calculated as a unitary perpendicular vector to the other two base vectors obtained. That is,

$$\bar{\mathbf{e}}_2 = \frac{\bar{\mathbf{e}}_3 \times \bar{\mathbf{e}}_1}{|\bar{\mathbf{e}}_3 \times \bar{\mathbf{e}}_1|} \tag{3.33}$$

It must be noted that $\bar{\mathbf{e}}_1$, $\bar{\mathbf{e}}_2$ and $\bar{\mathbf{e}}_3$ are unitary vectors.

Taking into account the calculation process of the base vectors $\{\bar{\mathbf{e}}_1, \bar{\mathbf{e}}_2, \bar{\mathbf{e}}_3\}$, we obtain the transformation matrix between this and the global Cartesian coordinate system

$$\boldsymbol{\Theta} = \{\theta_i{}^j\} = \begin{pmatrix} x_{,\bar{x}} & x_{,\bar{y}} & x_{,\bar{z}} \\ y_{,\bar{x}} & y_{,\bar{y}} & y_{,\bar{z}} \\ z_{,\bar{x}} & z_{,\bar{y}} & z_{,\bar{z}} \end{pmatrix} = \begin{pmatrix} \bar{e}_1^1 & \bar{e}_2^1 & \bar{e}_3^1 \\ \bar{e}_1^2 & \bar{e}_2^2 & \bar{e}_3^2 \\ \bar{e}_1^3 & \bar{e}_2^3 & \bar{e}_3^3 \end{pmatrix} = \begin{Bmatrix} \bar{\mathbf{e}}_1 & \bar{\mathbf{e}}_2 & \bar{\mathbf{e}}_3 \end{Bmatrix} \qquad (3.34)$$

where $\bar{e}_i^j$ is the $j$-component of the vector $\bar{\mathbf{e}}_i$.

Since this matrix links two Cartesian coordinate systems, it is orthogonal, that is:

$$\boldsymbol{\Theta}^T = \boldsymbol{\Theta}^{-1} \qquad (3.35)$$

Therefore, the transformation of the coordinates of a vector from the global coordinate system into the local coordinate system reads

$$\{\bar{x}^j\} = \{\theta_i{}^j\}^T \{x^i\} \qquad (3.36)$$

The transformation matrices $\mathbf{J}$, $\mathbf{G}$ and $\boldsymbol{\Theta}$ will have an important role in establishing the relations between the different coordinate systems in the integration of the element stiffness matrices.

At this point it becomes clear that the inherent difficulty of shell finite element formulations are the multiple coordinate systems that are involved and transformations between them. For this reason it is very important to keep the overview of all coordinate systems used. Figure 3.13 summarizes the different coordinate systems and the relations between them. This scheme will be very helpful to follow the transformations applied to the strain tensor in Section 3.7. In the Figure, for each coordinate system a sketch of each system in the element is given, except for the global Cartesian system, which, as its name indicates, is valid for all systems. Both top and side view of the element are presented. It can be noted that in general $\hat{x}_3$, $\hat{x}^3$ and $\bar{z}$ are not perpendicular to the element mid-plane, since they are determined by the averaged director vectors at the nodes. Moreover, $\hat{x}_1$, $\hat{x}_2$, $\hat{x}^1$ and $\hat{x}^2$ are contained in the element mid-plane. However, $\bar{x}$ and $\bar{y}$ are in general not contained in the element mid-plane, as they are part of a Cartesian system and they have to be normal to $\bar{z}$.

## 3.7 Definition of strains

As it was mentioned in Section 3.6, the strain and stress vector at a certain point of the element are expressed in the local Cartesian system $\{\bar{\mathbf{x}}, \bar{\mathbf{y}}, \bar{\mathbf{z}}\}$, which is

**LOCAL CURVILINEAR SYSTEM. CONTRAVARIANT BASIS**

$\hat{x}_2$     $\hat{x}_3$     $\hat{x}_1$

Basis: $\{\mathbf{g}^1, \mathbf{g}^2, \mathbf{g}^3\}$
Coordinates: $\{\hat{x}_i\}$

$$\{\mathbf{g}^1 \quad \mathbf{g}^2 \quad \mathbf{g}^3\} = \{\mathbf{g}_1 \quad \mathbf{g}_2 \quad \mathbf{g}_3\}\mathbf{G}^{-1}$$

$$\{\hat{x}^j\} = \{g^{ij}\}^T\{\hat{x}_i\} = \{g_{ij}\}^{-T}\{\hat{x}_i\}$$

$$\mathbf{G} = \{g_{ij}\} = \{\mathbf{g}_i \cdot \mathbf{g}_j\} = \begin{pmatrix} \mathbf{g}_1 \cdot \mathbf{g}_1 & \mathbf{g}_1 \cdot \mathbf{g}_2 & \mathbf{g}_1 \cdot \mathbf{g}_3 \\ \mathbf{g}_2 \cdot \mathbf{g}_1 & \mathbf{g}_2 \cdot \mathbf{g}_2 & \mathbf{g}_2 \cdot \mathbf{g}_3 \\ \mathbf{g}_3 \cdot \mathbf{g}_1 & \mathbf{g}_3 \cdot \mathbf{g}_2 & \mathbf{g}_3 \cdot \mathbf{g}_3 \end{pmatrix}$$

**LOCAL CURVILINEAR SYSTEM. COVARIANT BASIS**

$\hat{x}^2 \equiv \eta$     $\hat{x}^3 \equiv \zeta$     $\hat{x}^1 \equiv \xi$

Basis: $\{\mathbf{g}_1, \mathbf{g}_2, \mathbf{g}_3\}$
Coordinates: $\{\hat{x}^i\} = \{\xi, \eta, \zeta\}$

$$\{\mathbf{g}_1 \quad \mathbf{g}_2 \quad \mathbf{g}_3\} = \{\mathbf{e}_1 \quad \mathbf{e}_2 \quad \mathbf{e}_3\}\mathbf{J}^T$$

$$\{x^j\} = \{j_i{}^j\}^T\{\hat{x}^i\}$$

$$\mathbf{J} = \begin{pmatrix} x_{,\xi} & y_{,\xi} & z_{,\xi} \\ x_{,\eta} & y_{,\eta} & z_{,\eta} \\ x_{,\zeta} & y_{,\zeta} & z_{,\zeta} \end{pmatrix}$$

**GLOBAL CARTESIAN SYSTEM**

$z$     $y$     $x$

Basis: $\{\mathbf{e}_1, \mathbf{e}_2, \mathbf{e}_3\}$
Coordinates: $\{x^i\} = \{x, y, z\}$

$$\{\bar{\mathbf{e}}_1 \quad \bar{\mathbf{e}}_2 \quad \bar{\mathbf{e}}_3\} = \{\mathbf{e}_1 \quad \mathbf{e}_2 \quad \mathbf{e}_3\}\Theta$$

$$\{\bar{x}^j\} = \{\theta_i{}^j\}^T\{x^i\}$$

$$\Theta = \begin{pmatrix} x_{,\bar{x}} & x_{,\bar{y}} & x_{,\bar{z}} \\ y_{,\bar{x}} & y_{,\bar{y}} & y_{,\bar{z}} \\ z_{,\bar{x}} & z_{,\bar{y}} & z_{,\bar{z}} \end{pmatrix} = \begin{pmatrix} \bar{e}_1{}^1 & \bar{e}_2{}^1 & \bar{e}_3{}^1 \\ \bar{e}_1{}^2 & \bar{e}_2{}^2 & \bar{e}_3{}^2 \\ \bar{e}_1{}^3 & \bar{e}_2{}^3 & \bar{e}_3{}^3 \end{pmatrix}$$

**LOCAL CARTESIAN SYSTEM**

$\bar{y}$     $\bar{x}$     $\bar{z}$

Basis: $\{\bar{\mathbf{e}}_1, \bar{\mathbf{e}}_2, \bar{\mathbf{e}}_3\}$
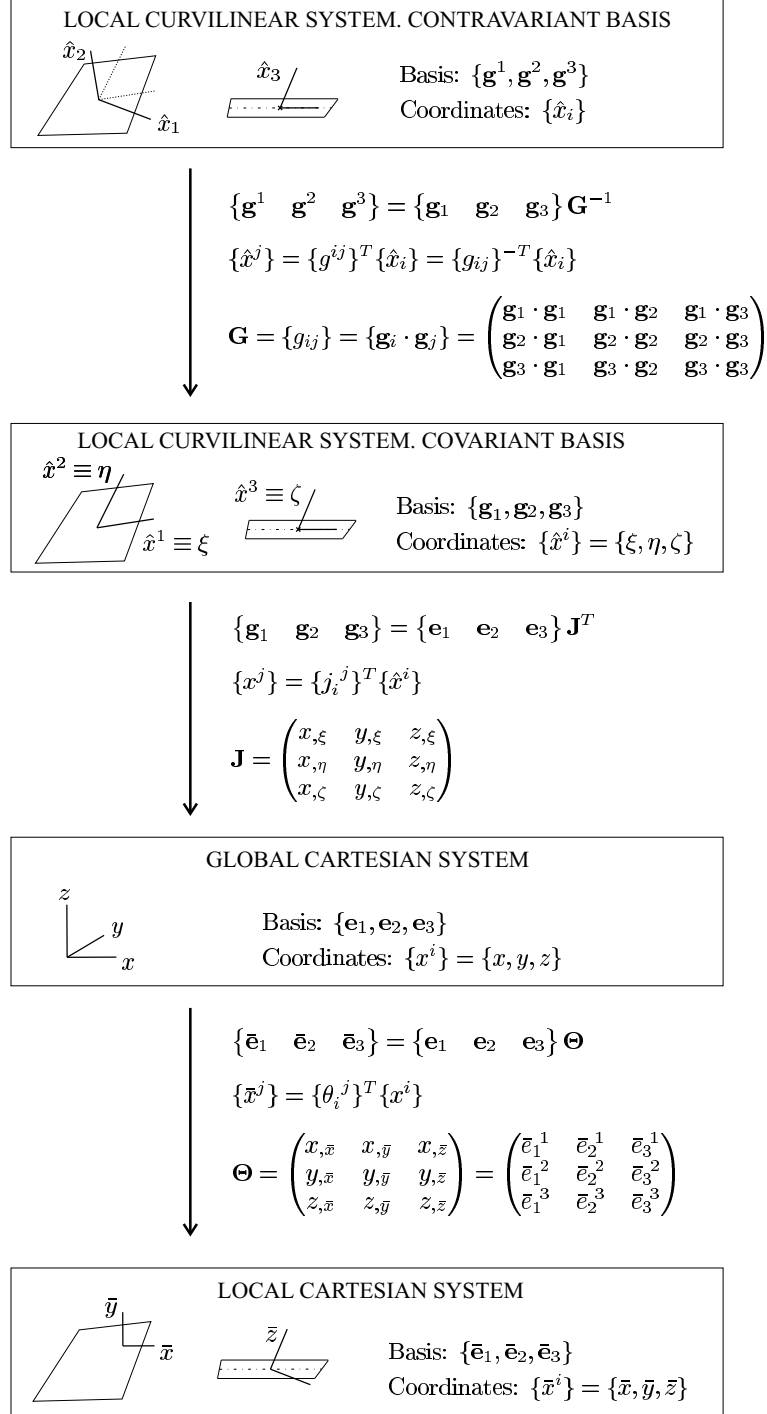Coordinates: $\{\bar{x}^i\} = \{\bar{x}, \bar{y}, \bar{z}\}$

Figure 3.13: Relation between the different coordinate systems used in the present shell formulation

defined at that point.

According to the shell assumptions, the strain components in the direction perpendicular to the mid-plane of the shell are negligible. As the strain vector is expressed in a local Cartesian coordinate system whose $\bar{z}$ direction coincides with the thickness direction, the contribution of $\varepsilon_{\bar{z}}$ to the potential strain energy of the system is neglected. It should be noted that, in fact, the $\bar{z}$ axis is not exactly perpendicular to the mid-plane of the shell, but it is assumed it is a good approximation.

Consequently, the strain vector of theory of first order in the local Cartesian system $\{\bar{x}, \bar{y}, \bar{z}\}$ is given by

$$\bar{\varepsilon} = \begin{Bmatrix} \varepsilon_{\bar{x}} \\ \varepsilon_{\bar{y}} \\ \gamma_{\bar{x}\bar{y}} \\ \gamma_{\bar{y}\bar{z}} \\ \gamma_{\bar{z}\bar{x}} \end{Bmatrix} = \begin{Bmatrix} \bar{u}_{,\bar{x}} \\ \bar{v}_{,\bar{y}} \\ \bar{u}_{,\bar{y}} + \bar{v}_{,\bar{x}} \\ \bar{v}_{,\bar{z}} + \bar{w}_{,\bar{y}} \\ \bar{w}_{,\bar{x}} + \bar{u}_{,\bar{z}} \end{Bmatrix} \tag{3.37}$$

where $\gamma_{\bar{x}\bar{y}} = 2\varepsilon_{\bar{x}\bar{y}}$ and so on. After discretization, the strain vector $\bar{\varepsilon}$ can be expressed as a function of the nodal degrees of freedom. Thus,

$$\bar{\varepsilon} = \bar{\mathbf{B}}\left(\xi, \eta, \zeta\right) \cdot \mathbf{d}^e \tag{3.38}$$

where $\mathbf{d}^e$ is a vector containing the vectors $\mathbf{d}_a$.

There are two possible ways to calculate the strain vector $\bar{\varepsilon}$ at a point. Following is the presentation of both.

## 3.7.1   Strains in local Cartesian system

In the first option, derivatives of the local Cartesian displacements with respect to the local Cartesian coordinates are obtained. For simplicity, these derivatives will be arranged in a matrix $\bar{\mathbf{H}}$

$$\bar{\mathbf{H}} = \begin{pmatrix} \bar{u}_{,\bar{x}} & \bar{v}_{,\bar{x}} & \bar{w}_{,\bar{x}} \\ \bar{u}_{,\bar{y}} & \bar{v}_{,\bar{y}} & \bar{w}_{,\bar{y}} \\ \bar{u}_{,\bar{z}} & \bar{v}_{,\bar{z}} & \bar{w}_{,\bar{z}} \end{pmatrix} = \begin{pmatrix} \frac{\partial}{\partial \bar{x}} \\ \frac{\partial}{\partial \bar{y}} \\ \frac{\partial}{\partial \bar{z}} \end{pmatrix} \begin{pmatrix} \bar{u} & \bar{v} & \bar{w} \end{pmatrix} = \nabla_{\bar{\mathbf{x}}} \bar{\mathbf{u}}^T \tag{3.39}$$

where $\nabla_{\bar{\mathbf{x}}}$ is the differential operator containing the derivatives with respect to the coordinate system designed by its index.

To obtain these derivatives, three sets of transformations are needed.

First, the local Cartesian displacements should be transformed into the global displacements, which are the ones we are using in the interpolation of the displacement field (see (3.17)). As it was shown in (3.36), the transformation of a vector in the local Cartesian system into a vector in the global system is done through the matrix $\boldsymbol{\Theta}$, defined in (3.34). Applying this transformation to equation (3.39) we obtain

$$\bar{\mathbf{H}} = \nabla_{\bar{\mathbf{x}}}\ \mathbf{u}^T \cdot \boldsymbol{\Theta} \tag{3.40}$$

In this expression the functional interpolation (3.17) can be substituted to obtain the strains as a function of the displacements and rotation degrees of freedom at the nodes of the element. Since in (3.17) the global displacements are a function of the curvilinear coordinates of an element, further transformations have to be done in the derivatives in order to express them in terms of the curvilinear variables. It should be noted that the local Cartesian coordinate system at a point is not directly related with the curvilinear coordinate system of the element. Therefore, two more sets of transformations are needed: from the local Cartesian to the global Cartesian system and, then, from the global Cartesian to the curvilinear system. The transformation into the global Cartesian derivatives involves the transpose of the matrix $\boldsymbol{\Theta}$ and leads to

$$\bar{\mathbf{H}} = \boldsymbol{\Theta}^T \cdot \nabla_{\mathbf{x}}\mathbf{u}^T \cdot \boldsymbol{\Theta} \tag{3.41}$$

Last, the derivatives with respect to the global Cartesian variables are transformed into derivatives with respect to the curvilinear variables through the inverse of the Jacobian matrix $\mathbf{J}$ defined in (3.21). Thus, we obtain

$$\bar{\mathbf{H}} = \boldsymbol{\Theta}^T \cdot \mathbf{J}^{-1} \cdot \nabla_{\xi}\ \mathbf{u}^T \cdot \boldsymbol{\Theta} \tag{3.42}$$

which in explicit form is

$$\bar{\mathbf{H}} = \begin{pmatrix} x_{,\bar{x}} & y_{,\bar{x}} & z_{,\bar{x}} \\ x_{,\bar{y}} & y_{,\bar{y}} & z_{,\bar{y}} \\ x_{,\bar{z}} & y_{,\bar{z}} & z_{,\bar{z}} \end{pmatrix} \cdot \begin{pmatrix} x_{,\xi} & y_{,\xi} & z_{,\xi} \\ x_{,\eta} & y_{,\eta} & z_{,\eta} \\ x_{,\zeta} & y_{,\zeta} & z_{,\zeta} \end{pmatrix}^{-1} \cdot \begin{pmatrix} \frac{\partial}{\partial \xi} \\ \frac{\partial}{\partial \eta} \\ \frac{\partial}{\partial \zeta} \end{pmatrix} \begin{pmatrix} u & v & w \end{pmatrix} \cdot \begin{pmatrix} x_{,\bar{x}} & x_{,\bar{y}} & x_{,\bar{z}} \\ y_{,\bar{x}} & y_{,\bar{y}} & y_{,\bar{z}} \\ z_{,\bar{x}} & z_{,\bar{y}} & z_{,\bar{z}} \end{pmatrix} \tag{3.43}$$

If we define the matrix containing the derivatives of the global Cartesian coordinates with respect to the curvilinear coordinates as

$$\mathbf{H}\left(\xi, \eta, \zeta\right) = \begin{pmatrix} u_{,\xi} & v_{,\xi} & w_{,\xi} \\ u_{,\eta} & v_{,\eta} & w_{,\eta} \\ u_{,\zeta} & v_{,\zeta} & w_{,\zeta} \end{pmatrix} \tag{3.44}$$

and substitute it into (3.42), we obtain:

$$\bar{\mathbf{H}} = \mathbf{\Theta}^T \cdot \mathbf{J}^{-1} \cdot \mathbf{H}\,(\xi, \eta, \zeta) \cdot \mathbf{\Theta} \tag{3.45}$$

which gives the relation between the derivatives contained in the definition of the strain vector (3.37) and the derivatives of the global displacements with respect to the curvilinear coordinates. If we insert the approximation of the displacements given by (3.17) in (3.45), we obtain the approximation of $\bar{\mathbf{H}}$

$$\bar{\mathbf{H}} = \mathbf{\Theta}^T \cdot \mathbf{J}^{-1} \cdot \nabla_\xi \sum_a \mathbf{d}_a^T \cdot \mathbf{N_a}(\xi, \eta, \zeta)^{\mathbf{T}} \cdot \mathbf{\Theta} \tag{3.46}$$

The expression (3.46) allows us to obtain the approximation of the strain components as a function of the displacements and rotational degrees of freedom, as in (3.38).

### 3.7.2 Strains in curvilinear coordinate system

In the second option, the strain tensor is first computed in the contravariant basis of the local curvilinear system, and then a set of transformations are performed in order to obtain it in the local Cartesian basis. The strain tensor expressed in the contravariant basis of the local curvilinear system is

$$\boldsymbol{\varepsilon} = \hat{\varepsilon}_{ij}\mathbf{g}^i \otimes \mathbf{g}^j \tag{3.47}$$

The covariant components $\hat{\varepsilon}_{ij}$ of the strain tensor are given by

$$\hat{\varepsilon}_{ij} = \frac{1}{2}\left(\mathbf{u}_{,i} \cdot \mathbf{g}_j + \mathbf{u}_{,j} \cdot \mathbf{g}_i\right) \tag{3.48}$$

where $\mathbf{g}_j$ is a covariant base vector of the curvilinear basis and $\mathbf{u}_{,i}$ is the derivative of the displacement vector with respect to the contravariant component $\hat{x}^i$.

The displacement vector expressed in the global Cartesian coordinate system is given by

$$\mathbf{u} = u^k \mathbf{e}_k \tag{3.49}$$

Substituting (3.49) in (3.48), gives

$$\hat{\varepsilon}_{ij} = \frac{1}{2}\left((u^k \mathbf{e}_k)_{,i} \cdot \mathbf{g}_j + (u^k \mathbf{e}_k)_{,j} \cdot \mathbf{g}_i\right) \tag{3.50}$$

As the displacements $\mathbf{u}$ are expressed in the global Cartesian basis, the derivative of the base vector $\mathbf{e}_k$ with respect to the curvilinear coordinates vanishes. Thus,

$$\hat{\varepsilon}_{ij} = \frac{1}{2}\left(u^k{}_{,i}\,\mathbf{e}_k \cdot \mathbf{g}_j + u^k{}_{,j}\,\mathbf{e}_k \cdot \mathbf{g}_i\right) = \frac{1}{2}\left(u^k{}_{,i}\,\frac{\partial x^k}{\partial \hat{x}^j} + u^k{}_{,j}\,\frac{\partial x^k}{\partial \hat{x}^i}\right) \qquad (3.51)$$

If in this expression, (3.18) and (3.26) are substituted, the components of the strain tensor are obtained as a function of the nodal degrees of freedom.

However, as already explained, for the computation of the stiffness matrix, the strain and stress vector at a certain point of the element are expressed in the local Cartesian system $\{\bar{x}, \bar{y}, \bar{z}\}$. For that reason, the transformation of the strain components from the local curvilinear contravariant system into the local Cartesian system is required. That is,

$$\boldsymbol{\varepsilon} = \hat{\varepsilon}_{ij}\mathbf{g}^i \otimes \mathbf{g}^j = \bar{\varepsilon}^{mn}\bar{\mathbf{e}}^m \otimes \bar{\mathbf{e}}^n \qquad (3.52)$$

where $\bar{\varepsilon}^{mn}$ are the components of the modified strain tensor expressed in the local Cartesian frame. As in the previous section, the upper hat indicates the curvilinear system and the upper bar the local Cartesian system.

The objective now is to compute the new components $\bar{\varepsilon}^{mn}$. In order to achieve the required change of basis and according to the known relations between the different coordinate systems explained in Section 3.6 and summarized in Figure 3.13, three sets of transformations are to be performed.

In the first transformation, the contravariant coefficients of the strain tensor are obtained from the covariant coefficients. That is,

$$\begin{aligned}
\boldsymbol{\varepsilon} &= \hat{\varepsilon}_{ij}\mathbf{g}^i \otimes \mathbf{g}^j = \hat{\varepsilon}_{ij}\left(g^{ik}\mathbf{g}_k\right) \otimes \left(g^{jl}\mathbf{g}_l\right) \\
&= \hat{\varepsilon}_{ij}g^{ik}g^{jl}\mathbf{g}_k \otimes \mathbf{g}_l = \hat{\varepsilon}^{kl}\mathbf{g}_k \otimes \mathbf{g}_l
\end{aligned} \qquad (3.53)$$

where the coefficients $g^{ik}$ are the components of the contravariant metric coefficient matrix $\mathbf{G}^{-1}$, which is calculated as the inverse of the covariant metric coefficient matrix $\mathbf{G}$, as explained in Section 3.6.

The second transformation changes the components of the strain tensor from the covariant curvilinear basis into the global Cartesian basis. Thus, it can be written

$$\begin{aligned}
\boldsymbol{\varepsilon} &= \hat{\varepsilon}_{ij}g^{ik}g^{jl}\mathbf{g}_k \otimes \mathbf{g}_l = \hat{\varepsilon}_{ij}g^{ik}g^{jl}\left(j_k{}^m\mathbf{e}_m\right) \otimes \left(j_l{}^n\mathbf{e}_n\right) \\
&= \hat{\varepsilon}_{ij}g^{ik}g^{jl}j_k{}^m j_l{}^n\mathbf{e}_m \otimes \mathbf{e}_n = \varepsilon^{mn}\mathbf{e}_m \otimes \mathbf{e}_n
\end{aligned} \qquad (3.54)$$

41

where $j_k{}^m$ are the components of the Jacobian matrix $\mathbf{J}$ defined in (3.21).

Lastly, what remains to be done is the transformation from the global Cartesian basis into the local Cartesian basis. Thus, we obtain

$$
\begin{aligned}
\boldsymbol{\varepsilon} &= \hat{\varepsilon}_{ij} g^{ik} g^{jl} j_k{}^m j_l{}^n \mathbf{e}_m \otimes \mathbf{e}_n = \hat{\varepsilon}_{ij} g^{ik} g^{jl} j_k{}^m j_l{}^n \left( \theta_m{}^p \bar{\mathbf{e}}_p \right) \otimes \left( \theta_n{}^q \bar{\mathbf{e}}_q \right) \\
&= \hat{\varepsilon}_{ij} g^{ik} g^{jl} j_k{}^m j_l{}^n \theta_m{}^p \theta_n{}^q \bar{\mathbf{e}}^p \otimes \bar{\mathbf{e}}^q = \bar{\varepsilon}^{pq} \bar{\mathbf{e}}^p \otimes \bar{\mathbf{e}}^q
\end{aligned}
\tag{3.55}
$$

where $\theta_m{}^p$ are the components of the transformation matrix $\boldsymbol{\Theta}$ defined in (3.34).

Now, the transformation of the components of the strain tensor from the contravariant curvilinear system into the local Cartesian system can be expressed in matrix form as

$$
\begin{aligned}
\{\bar{\varepsilon}^{mn}\} &= \{\theta_m{}^p\}^T \{j_k{}^m\}^T \{g^{ik}\}^T \{\hat{\varepsilon}_{ij}\} \{g^{jl}\} \{j_l{}^n\} \{\theta_n{}^q\} \\
&= \boldsymbol{\Theta}^T \cdot \mathbf{J}^T \cdot \mathbf{G}^{-T} \cdot \{\hat{\varepsilon}_{ij}\} \cdot \mathbf{G}^{-1} \cdot \mathbf{J} \cdot \boldsymbol{\Theta}
\end{aligned}
\tag{3.56}
$$

Taking into account that

$$
\{\bar{\varepsilon}^{mn}\} = \begin{pmatrix} \varepsilon_{\bar{x}} & \varepsilon_{\bar{x}\bar{y}} & \varepsilon_{\bar{x}\bar{z}} \\ \varepsilon_{\bar{y}\bar{x}} & \varepsilon_{\bar{y}} & \varepsilon_{\bar{y}\bar{z}} \\ \varepsilon_{\bar{z}\bar{x}} & \varepsilon_{\bar{z}\bar{y}} & \varepsilon_{\bar{z}} \end{pmatrix}
\tag{3.57}
$$

the components of the strain tensor can be reordered into the strain vector (3.37), and thus the $\bar{\mathbf{B}}$ operator defined in (3.38) can be obtained.

## 3.8    Calculation of stresses and stress resultants

Once the strain vector (3.37) at a point is obtained, the stress vector can also be computed. In the linear elastic case, the stresses corresponding to these strains, are

$$
\bar{\boldsymbol{\sigma}} = \begin{Bmatrix} \sigma_{\bar{x}} \\ \sigma_{\bar{y}} \\ \tau_{\bar{x}\bar{y}} \\ \tau_{\bar{y}\bar{z}} \\ \tau_{\bar{z}\bar{x}} \end{Bmatrix} = \bar{\mathbf{D}} \cdot (\bar{\boldsymbol{\varepsilon}} - \bar{\boldsymbol{\varepsilon}}_0) + \bar{\boldsymbol{\sigma}}_0
\tag{3.58}
$$

where $\bar{\boldsymbol{\varepsilon}}_0$ and $\boldsymbol{\sigma}_0$ are the initial strains and stresses. Note that these stresses are also given in the local Cartesian system. For an isotropic material, the material

matrix is

$$
\bar{\mathbf{D}} = \frac{E}{1-\nu^2}
\begin{pmatrix}
1 & \nu & 0 & 0 & 0 \\
\nu & 1 & 0 & 0 & 0 \\
0 & 0 & \frac{(1-\nu)}{2} & 0 & 0 \\
0 & 0 & 0 & \frac{\kappa(1-\nu)}{2} & 0 \\
0 & 0 & 0 & 0 & \frac{\kappa(1-\nu)}{2}
\end{pmatrix}
\tag{3.59}
$$

where $E$ is the Young's modulus and $\nu$ the Poisson's ratio.

In (3.37) it can be seen that the shear strain distribution $\gamma_{\bar{y}\bar{z}}$ and $\gamma_{\bar{z}\bar{x}}$ will be constant in the thickness. However, in reality the distribution for elastic behavior is approximately quadratic, due to the presence of warping. In order to better approximate the shear stress resultants, the shear correction factor $\kappa = \frac{5}{6}$ is included in the related components of the material matrix.

The stress resultants are computed in the local Cartesian axes and they are given by

$$
m_{\bar{x}} = \int_{-\frac{h}{2}}^{\frac{h}{2}} \bar{z} \; \sigma_{\bar{x}} \; d\bar{z}
\tag{3.60}
$$

$$
m_{\bar{y}} = \int_{-\frac{h}{2}}^{\frac{h}{2}} \bar{z} \; \sigma_{\bar{y}} \; d\bar{z}
\tag{3.61}
$$

$$
m_{\bar{x}\bar{y}} = \int_{-\frac{h}{2}}^{\frac{h}{2}} \bar{z} \; \tau_{\bar{x}\bar{y}} \; d\bar{z}
\tag{3.62}
$$

$$
q_{\bar{x}} = \int_{-\frac{h}{2}}^{\frac{h}{2}} \tau_{\bar{z}\bar{x}} \; d\bar{z}
\tag{3.63}
$$

$$
q_{\bar{y}} = \int_{-\frac{h}{2}}^{\frac{h}{2}} \tau_{\bar{y}\bar{z}} \; d\bar{z}
\tag{3.64}
$$

$$
n_{\bar{x}} = \int_{-\frac{h}{2}}^{\frac{h}{2}} \sigma_{\bar{x}} \; d\bar{z}
\tag{3.65}
$$

$$
n_{\bar{y}} = \int_{-\frac{h}{2}}^{\frac{h}{2}} \sigma_{\bar{y}} \; d\bar{z}
\tag{3.66}
$$

$$n_{\bar{x}\bar{y}} = \int_{-\frac{h}{2}}^{\frac{h}{2}} \tau_{\bar{x}\bar{y}} \ d\bar{z} \qquad (3.67)$$

## 3.9 Element stiffness matrix

In Section 3.6, the suitability of expressing the strain and stress vector in the local Cartesian system was explained. Now, the element stiffness matrix can be computed with the B-operator and the material matrix can also be expressed in this system. Therefore,

$$\mathbf{k}^e = \iiint_{V_e} \bar{\mathbf{B}}^T \cdot \bar{\mathbf{D}} \cdot \bar{\mathbf{B}} dV \qquad (3.68)$$

It should be observed that, even though the present shell finite element formulation is based on the degeneration concept, no previous integration in thickness direction is performed. For this reason, integration over the element volume is required to compute the stiffness matrix. Since curvilinear coordinates are preferred for the numerical integration, we may express the infinitesimal volume as

$$dV = d\bar{x}d\bar{y}d\bar{z} = dxdydz = Jd\xi d\eta d\zeta \qquad (3.69)$$

where $J$ is the determinant of the Jacobian matrix $\mathbf{J}$. Thus, the element stiffness matrix is given by

$$\mathbf{k}^e = \int_{-1}^{1} \int_{-1}^{1} \int_{-1}^{1} \bar{\mathbf{B}}^T(\xi, \eta, \zeta) \cdot \bar{\mathbf{D}} \cdot \bar{\mathbf{B}}(\xi, \eta, \zeta) Jd\xi d\eta d\zeta \qquad (3.70)$$

The number of Gauss points needed for numerical integration in $\xi$ and $\eta$ directions depends on the polynomial order of the shape functions. For instance, for bilinear shape functions, two Gauss points in each direction are required, and for parabolic or cubic shape functions, three or four respectively. Since the variation of strain components through the shell thickness is at most linear with respect to $\zeta$, and does not depend on the shape functions used, two Gauss points will be sufficient for exact integration through the thickness.

## 3.10 External loads

The nodal force vector at node $a$ is given by

$$\mathbf{f}_a = \begin{pmatrix} F_{ax} \\ F_{ay} \\ F_{az} \\ m_{a\alpha} \\ m_{a\beta} \end{pmatrix} \tag{3.71}$$

Analogously to the nodal displacement vector (3.17), in the nodal force vector the nodal forces are expressed in the global Cartesian system and the nodal moments $m_{a\alpha}$ and $m_{a\beta}$ are related to the axis $\mathbf{A2}_a$ and $\mathbf{A1}_a$ of the director vector Cartesian system. The force components are depicted in Figure 3.14. The definition of the director vector Cartesian system is explained in detail in Section 3.4.
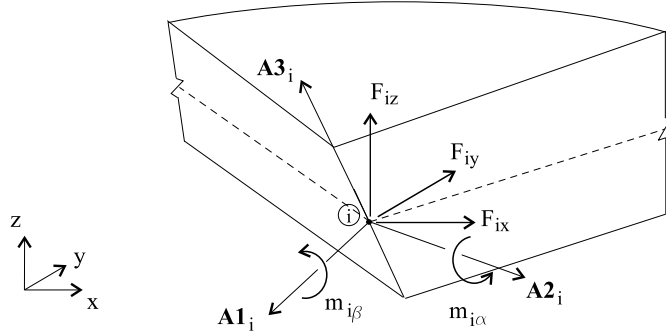


Figure 3.14: Nodal forces

Let us now consider the particular load case of volume forces. The most common volume force is self-weight. However, a general volume force $\mathbf{b}^T = \{b_x, b_y, b_z\}$ expressed in the global Cartesian system is considered.

The elemental force vector containing the consistent nodal forces is given by

$$\mathbf{f}^e = \iiint_{V_e} \sum_{a=1}^{n_{en}} \mathbf{N}_a^T \cdot \mathbf{b} \; dV \tag{3.72}$$

where $n_e n$ is the number of nodes per element and $\mathbf{N}_a$ is given by (3.19).

It should be noted that, as no thickness integration is performed in advance in the present element formulation, integration of the volume forces $\mathbf{b}$ has also to be done over the thickness direction. Substituting (3.19) and (3.69) into (3.72), we obtain

45

$$\mathbf{f}^e = \iiint_{V_e} \sum_a \mathbf{N}_a^T(\xi, \eta, \zeta) \cdot \mathbf{b} \; dV$$

$$= \int_{-1}^1 \int_{-1}^1 \int_{-1}^1 \sum_a \begin{pmatrix} N_a & 0 & 0 \\ 0 & N_a & 0 \\ 0 & 0 & N_a \\ \frac{1}{2}\zeta t_a N_a A1_a^1 & \frac{1}{2}\zeta t_a N_a A1_a^2 & \frac{1}{2}\zeta t_a N_a A1_a^3 \\ -\frac{1}{2}\zeta t_a N_a A2_a^1 & -\frac{1}{2}\zeta t_a N_a A2_a^2 & -\frac{1}{2}\zeta t_a N_a A2_a^3 \end{pmatrix} \cdot \begin{Bmatrix} b_x \\ b_y \\ b_z \end{Bmatrix} \; J \; d\xi d\eta d\zeta$$

$$= \int_{-1}^1 \int_{-1}^1 \int_{-1}^1 \sum_a \begin{Bmatrix} N_a b_x \\ N_a b_y \\ N_a b_z \\ \frac{1}{2}\zeta t_a N_a \left( b_x A1_a^1 + b_y A1_a^2 + b_z A1_a^3 \right) \\ -\frac{1}{2}\zeta t_a N_a \left( b_x A2_a^1 + b_y A2_a^2 + b_z A2_a^3 \right) \end{Bmatrix} \; J \; d\xi d\eta d\zeta$$

(3.73)

where $A1_a^i$ and $A2_a^i$ are the $i^{th}$-components of $\mathbf{A1}_a$ and $\mathbf{A2}_a$, respectively.

Generally, in the present shell finite element formulation, applied forces will not only produce nodal forces, but also nodal moments. This effect is illustrated in Figure 3.15 for the case of self weight. Here, the volume of the element above the mid-plane is different from the volume under it. This is a consequence of the averaged director vector formulation. As a result, the general equivalent system consists of nodal forces and nodal moments. This effect can also be observed in (3.73).
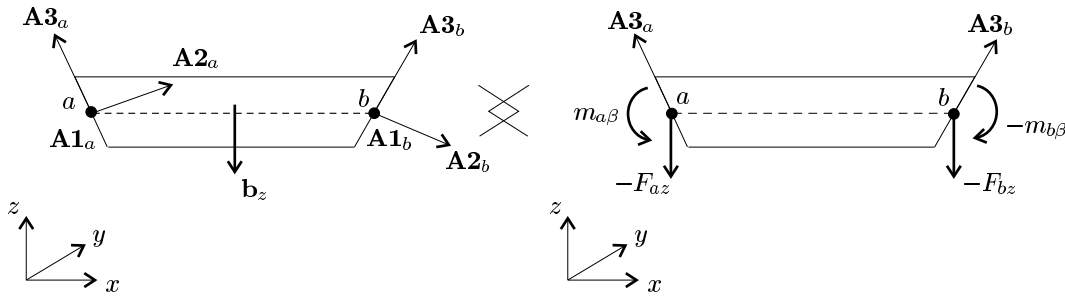


Figure 3.15: Self-weight load case. Equivalence between volume force and consistent nodal forces and moments

## 3.11 Locking phenomena

As early as in the sixties, it was realized that under certain circumstances displacement elements yield inaccurate results. Hughes et al. (1977) named this effect *locking*, because its main characteristic is that the element *locks* itself and displacements obtained are underestimated.

From the mechanical point of view, the locking effect is characterized by the presence of parasitic stresses, that is, stresses that are not present in the exact solution of the problem. These parasitic stresses produce a parasitic internal energy and, consequently, structural stiffness is overestimated. As a consequence, a reduced rate of convergence is observed. This additional artificial stiffness depends on a geometrical or material parameter, in such a way that when this parameter tends to a certain value, the locking effect becomes more pronounced.

A heuristic method to determine if an element suffers from locking is explained by (Hughes, 2000). The method consists of determining the so-called *constraint ratio* of the element and comparing it with an optimal value, which is the constraint ratio of the continuous problem. The constraint ratio $r$ for a certain element is defined as the relation between the number of degrees of freedom and the number of constraints of the global system. If the constraint ratio of an element is lower than the optimal value, the element will lock. If they coincide, it will, in principle, not lock. This approach, although lacking mathematical precision, provides a useful hint about the element behaviour.

In the case of shear deformable thin structures, the constraints are the Kirchoff conditions and the locking becomes more pronounced when the slenderness of the element tends to zero. Under these circumstances, parasitic transverse shear stresses appear in pure bending states.

Locking effects can be classified depending on the parasitic stresses appearing. Principally, one can be distinguish between *transverse shear locking*, *membrane locking*, *in-plane shear locking* and *volumetric locking*. A review of the different locking phenomena can be found in Bischoff (1999).

Transverse shear locking appears in beam, plate and shell elements subjected to bending. In pure bending, parasitic transverse shear stresses can be observed. Shear locking may appear in beam and shell elements and even 2D and 3D solid elements used to model thin structures. Membrane locking occurs in curved beam and shell elements. The parasitic stresses are membrane stresses in the case of pure bending.

Contrary to other kinds of locking effects, volumetric locking is not related to the slenderness of an element, but to a material parameter, the *bulk modulus*. This kind of locking appears in nearly incompressible problems, and the related constraint is the incompressibility condition.

Another kind of locking is *curvature thickness locking*, also called *trapezoidal locking*. It was first observed by Ramm et al. (1994) (see also Ramm et al. (1995)) and only appears in certain cases of shell formulations considering thickness changes.

Unfortunatelly, shell elements with Reissner Mindlin kinematics are in principle candidates for be affected by all kinds of locking effects. The use of 3D elements to model a shell structure does not circumvent the locking problem.

Since the late seventies, numerous studies have been done about the influence of locking phenomena in structural analysis and many alternatives to the displacement element formulation have been proposed in order to avoid locking. A review can be found in Bathe (1996), Zienkiewicz and Taylor (2000a) and Zienkiewicz and Taylor (2000b).

However, the consequences of locking in the overall shape optimization process have been underestimated. In Chapter 6, the influence of locking in shape optimization of shells is studied with the help of some numerical experiments. The aim of this work is not to study the causes of the locking phenomena, but to present the scope of its effects in shape optimization. To perform these numerical examples, a formulation which avoids locking is needed. To this purpose, the DSG method, a simple but efficient approach, is chosen. In the following section, the application of this method to the shell element studied in the present chapter is outlined.

## 3.12  A DSG shell element

The DSG method (*Discrete Shear Gap*), proposed by Bletzinger et al. (2000), is one of the numerous techniques used to avoid locking. The method was originally developed to avoid transverse shear locking in beams, plates and shells (Bletzinger et al., 2000; Bischoff, 1999). The basic idea is to compute a modified transverse shear distribution free of parasitic parts by interpolation of the *discrete shear gaps* across the element domain. Discrete shear gaps at node $a$ are defined as the integration of the discrete shear strain of the displacement element. Bischoff and Bletzinger (2001) proposed a stabilized version of the

DSG method, which helps to reduce oscillations of transverse shear forces and to reduce sensitivity to mesh distortions.

Later, Koschnick et al. (2002, 2004) extended the basic idea of the method to avoid membrane and shear locking. This generality of the method led to renaming DSG as *Discrete Strain Gap*.

Some main characteristics of the DSG method motivated its application to optimization problems. These are:

1. The method is particularly attractive because it can be applied to both triangles and quads and its formulation is independent of the polynomial order of the element. This is not the case of many other locking free formulations.

2. No additional degrees of freedom are introduced, making the method particularly efficient.

3. The method is based on one unique, simple rule by which modified strains free of parasitic parts are computed. The only modification with respect to a standard displacement element is the calculation of the strain-displacement operator. Therefore, the implementation of the method into an existing code is easy.

4. A further advantage, as it will be shown in Chapter 5 is the simplicity of the implementation of sensitivity analysis. Moreover, once the implementation of sensitivity analysis has been done, sensitivity analysis of the DSG shell element differs only on the $\mathbf{B}$ operator and on its derivatives with respect to design variables.

5. The numerical integration order required for computation of elemental stiffness matrix is not increased with respect to the standard displacement formulation. Therefore, computational cost is not significantly increased. Moreover, in the case of linear elements only one Gauss point is needed in contrast to the three Gauss points needed for the same case in the standard displacement formulation.

Due to these characteristics, the DSG method turns out to be very efficient and suitable for structural optimization.

Linear and bilinear elements are used in the numerical experiments given in Chapter 6 to study the influence of locking in shape optimization of thin shells.

In these cases, elements suffer from transverse shear locking, the rest of locking effects being subsidiary. For this reason, the DSG concept is applied here to avoid transverse shear locking.

The DSG concept for transverse shear strains is explained for the case of a Timoschenko beam in Bletzinger et al. (2000). The Timoschenko beam offers the possibility of explaining this concept attaining the simplicity of a 1D element. Explaining directly the essence of this concept for a shell element may be more complex. However, to this point one should be familiarized enough with the shell element formulation used herein.

First, the biunit square element depicted in Figure 3.16.a is considered. Director vectors are not normal to element mid-plane and, as a consequence the $\zeta$ axis (see Section 3.4) is not either.

(a)



(b)
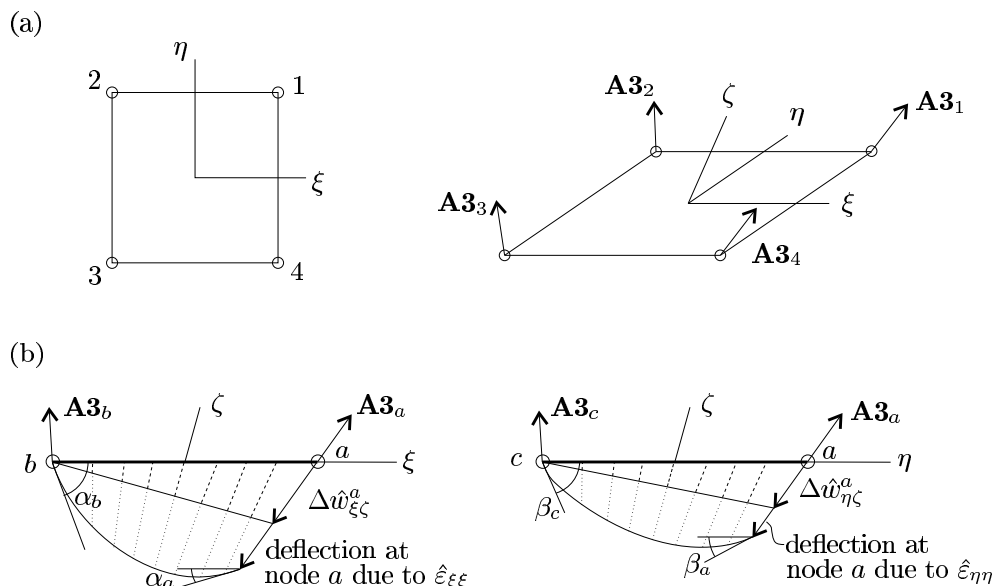


Figure 3.16: (a) Biunit square element with director vectors not normal to its mid-plane. (b) Scheme of discrete shear gaps.

The deflection of the element due to rotations $\alpha$ and $\beta$ is sketched in Figure 3.16.b, respectively. The total displacement in $\zeta$ direction of a certain point of the element is the sum of the contributions of deflection due to pure bending and shear. The deflection of a certain point due to shear is called shear gap and it is the difference between the total deflection at the point and the deflection due to bending. It can be computed by integration of the corresponding shear strain along the coordinate line associated to it. In a shell element two shear

strains are considered ($\varepsilon_{\xi\zeta}$ and $\varepsilon_{\eta\zeta}$) and therefore, two discrete shear gaps for each node $a$ can be defined. That is,

$$\Delta \hat{w}^a_{\xi\zeta} = \int_{\xi=-1}^{\xi_a} \hat{\varepsilon}_{\xi\zeta} d\xi \bigg|_{\substack{\eta=\eta_a \\ \zeta=0}} \tag{3.74}$$

$$\Delta \hat{w}^a_{\eta\zeta} = \int_{\eta=-1}^{\eta_a} \hat{\varepsilon}_{\eta\zeta} d\eta \bigg|_{\substack{\xi=\xi_a \\ \zeta=0}} \tag{3.75}$$

A hat in the shear gaps denotes that the deflection is considered in the curvilinear $\zeta$ direction. It is important to note that strains $\varepsilon_{\xi\zeta}$ and $\varepsilon_{\eta\zeta}$ are not related to a deflection normal to the element mid-plane, but to a deflection in $\zeta$ direction. To emphasize this fact, an upper hat, related to curvilinear coordinate system (see Section 3.6), is included in the notation of the strain gaps.

Coordinate lines $\xi = -1$ and $\eta = -1$ are taken as reference edges for each shear gap respectively. That is, at these edges the deflection due to the related shear is arbitrarily supossed to be null. Consequently, nodes located at these reference edges for a certain integration direction have null discrete shear gaps. This assumption does not imply loss of generality of the method. It should be noted that in the computation of the discrete shear gaps it does not matter that the element is not rectangular, since integration is performed in the curvilinear axis. Evaluation of discrete shear gaps is done at $\zeta = 0$, because all nodes of the present shell formulation lay at the mid-plane.

The discretized strains $\hat{\varepsilon}_{ij}$, that enter in the computation of the discrete shear gaps, are the covariant components of the strain tensor expresed in the curvilinear basis. As explained in Section 3.7.2, they can be computed according to formula (3.50). That is

$$\hat{\varepsilon}_{ij} = \frac{1}{2} \left( \mathbf{u}_{,i} \cdot \mathbf{g}_j + \mathbf{u}_{,j} \cdot \mathbf{g}_i \right) \tag{3.76}$$

It is important to remark that integration of shear gaps can be performed analytically, so the computational cost of DSG elements is not increased with respect to standard displacement elements.

Once discrete shear gaps are obtained, they are interpolated in order to obtain the related shear gap distributions over the element. That is,

$$\Delta \hat{w}_{\xi\zeta} = \sum_a N_a(\xi, \eta) \Delta \hat{w}_{\xi\zeta}^a \tag{3.77}$$

$$\Delta \hat{w}_{\eta\zeta} = \sum_a N_a(\xi, \eta) \Delta \hat{w}_{\eta\zeta}^a \tag{3.78}$$

From these strain gaps distributions, new modified strains can be recovered by differentiation. The main characteristic of these modified strains is that they are free of parasitic parts. These modified strains are given by

$$\varepsilon_{\xi\zeta}^{\text{DSG}} = \frac{\partial \hat{\Delta} w_{\xi\zeta}}{\partial \xi} = \sum_a N_{a,\xi} \Delta \hat{w}_{\xi\zeta}^a \tag{3.79}$$

$$\varepsilon_{\eta\zeta}^{\text{DSG}} = \frac{\partial \Delta \hat{w}_{\eta\zeta}}{\partial \eta} = \sum_a N_{a,\eta} \Delta \hat{w}_{\eta\zeta}^a \tag{3.80}$$

The superscript $^{\text{DSG}}$ indicates that these are modified strains with respect to those computed for the standard displacement formulation given by (3.50).

It should be remarked that the modified strain components computed above according to the DSG method rule, are covariant components, that is, they are expressed in the contravariant base. This was also the case for the original strain components (3.50) used in the displacement formulation.

Therefore, the same coordinate transformations explained in Section 3.7.2 for the displacement shell element have to be performed for the DSG shell element, in order to get the strain tensor components in the local Cartesian basis.

The only modification that the DSG method introduces with respect to the standard displacement formulation is in the strain-displacement operator. The rest of the formulation remains the same. As a consequence, implementation of this method into an existing code is very simple.

# Chapter 4

# Sensitivity Analysis

## 4.1    Introduction

In general, the concept of sensitivity analysis means the study of the dependence of a function from a certain parameter. That is, how this function changes when a parameter is changed. In an optimization process, this information is required by gradient based optimization algorithms to predict how a certain modification of the actual design is going to affect the objective function or constraints. Based on these predictions, the optimization algorithm takes a decision about modifying the actual design. Therefore, the main contribution of the sensitivity analysis to the optimization process is the possibility of studying the influence of design changes in a certain function without requiring trial and error experiments, which may be expensive and time consuming.

Apart from the optimization field, sensitivity analysis is widespread in science, engineering, and economy because of its applications in model analysis. In numerical modeling, sensitivity analysis is used to study and improve performance of the model itself. The study of the relationship between input information and provided output is used to calibrate the model, to study its quality and to reduce it to a simpler one by identifying the model parameters that are not relevant, a technique known as variable screening (Saltelli et al., 2000).

In statistics, sensitivity analysis is used to perform a robust design. The aim is to achieve insensitivity of the system with respect to small deviations from the input assumptions. In structural analysis, sensitivities may also be used to predict the structural response in probabilistic terms by the Probabilistic Finite Element Method (see Liu et al. (1986)).

In structural optimization, the two major areas of sensitivity analysis are sensitivity of static and transient response and sensitivity of vibration and buckling eigenproblems. A clear distinction between these to areas os required, because the solution methods are significantly different.

Sensitivity analysis of transient response is more complex than in the static case, because the additional variable of time has to be considered in the derivations. In the static case, sensitivity analysis is significantly more complex for nonlinear structural problems than for linear problems. For this reason, most of the studies in this field are focused on linear problems. However, some important contributions were presented by Cardoso and Arora (1988) for path-independent nonlinear problems and by Tsay and Arora (1990), Tsay et al. (1990) and Kemmler (2004) for path-dependent nonlinear problems. In the present work, attention is focused on sensitivity analysis of linear static response.

In Chapter 2, a brief description of the three basic types of structural optimization problems was given. Sensitivity analysis for shape optimization problems is significantly more difficult than for sizing problems. In sizing, the design variable is typically the cross section of a bar or the thickness of a shell, and usually they enter in the governing equation of the system multiplying or dividing. In this case, it is not very difficult to obtain the derivatives even, in some cases, analytically.

In shape optimization, design variables are geometrical properties of the structure in a most general sense. In this case, derivation of the governing equations is more complex, since design variables affect not only these equations but also the domain. If the Finite Element Method is used for structural analysis, a change in the design variables implies a change in the finite element model. As a consequence, shape design variables may affect the domain of integration of element stiffness matrices, the B-operator and even the material matrix.

For these reasons, in shape optimization the computation of sensitivities was historically always done by the global finite difference method. This is the easiest way to compute sensitivities and it does not require much knowledge of the code or the finite element formulation used. However, as it will be explained in section 4.2, sensitivities obtained by this method are not very accurate.

An efficient and accurate computation of design sensitivities is of main importance in the overall structural optimization process. Accuracy of sensitivities may be decisive in the success of the optimization problem and in the number of iterations needed to obtain the optimal design. Moreover, sensitivity analysis represents a large part of the computational effort required to solve an optimiza-

tion problem (Haftka and Gürdal, 1999). For these reasons a lot of research was done related to sensitivity analysis in the search for more efficient and accurate methods. Especially in the eighties, sensitivity analysis was a very important area of engineering research. As a result, a wide variety of sensitivity analysis techniques were developed.

In structural optimization, sensitivity analysis implies the derivation of the state equation of the considered structural model. Two general approaches can be distinguished. Both are based on the principle of virtual work, but the main difference is the moment in which differentiation is done: before or after discretization. These two methods are:

1. discrete approach or implicit differentiation, where the state equation is first discretized and then differentiated

2. variational approach, where the continuum equations are first differentiated and then discretized.

In addition, there are two general ways of performing sensitivity analysis: the direct method and the adjoint method. In the direct method, sensitivities of state variables are computed and, with these, sensitivity of response functional $\psi$ is obtained. In the adjoint method, sensitivity of response functional is obtained directly, with no intermediate computation of derivatives of the state variables. However, to achieve this the solution of an adjoint problem is necessary. Along the present Chapter, the different types of sensitivity analysis are presented. Almost for each type, a distinction between direct and adjoint method will be made.

The present chapter is focused on first order sensitivity analysis. Computation of second and higher order derivatives is significantly more difficult and results obtained have less accuracy.

The objective of the sensitivity analysis is to calculate the total dependence of a certain functional with respect to the design variables. In structural optimization a certain objective function has to be minimized for certain design variables simultaneously fulfilling some constraints. In the most general case, this objective function or constraints depend on the design variables and on the state variables, i.e. the displacements. In a general structural problem, state variables are function of the geometry of the structure, its mechanical properties and the loads. In a general case of structural shape optimization, geometry, mechanical properties, and loads are function of the design variables. Therefore,

the dependence of the objective function, or constraints, with respect to the design variables is set in two ways: directly or indirectly through the dependence on the displacements.

In the following, it will be considered a general response functional needing design sensitivity analysis given by

$$\psi = \psi(\mathbf{s}, \mathbf{u}) \tag{4.1}$$

where $\mathbf{s} = \{s_i\}$, $i = 1,...ns$ is the vector of design variables and $\mathbf{u}$ is the vector of state variables, i.e. displacements. The functional $\psi$ may represent the objective function of the optimization problem or constraints on stresses, strains, displacements, reaction forces, etc.

Once a design is set, the state variables can be computed by a structural analysis. These state variables are highly non-linear with respect to the design variables. This fact is the key to the difficulties related to shape optimization.

In the present chapter, a review of the different sensitivity analysis techniques is presented. Main characteristics, advantages and disadvantages of the methods are outlined. First, the global finite difference method is briefly studied, since it is the most intuitive sensitivity analysis technique. Then, special attention is paid to other discrete sensitivity approaches: the semi-analytical and the analytical method. Lastly, an overview of the variational sensitivity analysis is given and principal differences to the discrete approach are outlined. As already mentioned, only sensitivity analysis of static linear elastic systems is considered in the present chapter.

## 4.2 Discrete sensitivity analysis by global finite differences

The global finite difference is the simplest sensitivity analysis technique. The main advantage of this approach is its easy implementation in a general purpose finite element program, since no much knowledge of the code of the structural analysis program is required.

In this method, sensitivities of a function are approximated by finite differences. The simplest approximation uses the first order forward (or backward) finite differences scheme. Using the forward finite differences scheme, the derivative of a function $\psi$ (4.1) with respect to design variable $s_i$ can be expressed as

$$\frac{\partial \psi(\mathbf{s})}{\partial s_i} = \frac{\psi(s_1, ..., s_i + \Delta s_i, ...s_{ns}) - \psi(s_1, ..., s_i, ...s_{ns})}{\Delta s_i} + O(\Delta s_i) \qquad (4.2)$$

where $O(\Delta s_i)$ is the truncation error given by

$$O(\Delta s_i) = -\frac{\Delta s_i}{2} \frac{\partial^2 \psi}{\partial s_i^2}\bigg|_{(s_1, ..., s_i + \varepsilon \Delta s_i, ...s_{ns})} \qquad (4.3)$$

with $0 \leq \varepsilon \leq 1$.

Therefore, the sensitivity of $\psi$ can be approximated by

$$\frac{\partial \psi(\mathbf{s})}{\partial s_i} \approx \frac{\Delta \psi(s_1, ...s_{ns})}{\Delta s_i} = \frac{\psi(s_1, ..., s_i + \Delta s_i, ...s_{ns}) - \psi(s_1, ..., s_i, ...s_{ns})}{\Delta s_i} \qquad (4.4)$$

As it can be deduced from (4.4), in order to compute sensitivity $\frac{\partial \psi(\mathbf{s})}{\partial s_i}$, it is necessary to evaluate $\psi$ for an additional perturbed design with $s_i + \Delta s_i$. If sensitivities of $\psi$ are to be computed with respect to $ns$ design variables, the global finite difference method requires $ns$ additional analysis of perturbed designs. Therefore, from the computational point of view, this method is very expensive.

Accuracy of this method strongly depends on the incremental step (perturbation step) of the design variables. In first order finite differences schemes, the truncation error (4.3) depends linearly on the step size. Therefore, small step sizes minimize this source of error. However, too small step sizes may yield large condition errors, i.e. algorithmic and computational round-off errors. The difficulty on choosing a suitable size step is the so-called step-size dilemma (Haftka and Adelman, 1989). An extended discussion about this issue is given by Haftka and Gürdal (1999).

Finite difference approximations of higher order significantly reduce the truncation error. However, these schemes require the computation of additional perturbed designs with the consequent increase of the computational cost.

Although it lacks accuracy and implies a high computational effort, this approach has been widely used because of its simplicity, specially in shape optimization. Nowadays, the importance of sensitivity accuracy in the optimization process has been recognized. As a consequence, more accurate approaches are preferred. However, the global finite difference approach remains as a good reference method.

## 4.3 Discrete sensitivity analysis of state variable constraints

The lack of accuracy of the global finite difference technique motivated to search for more accurate alternative approaches to the computation of sensitivities.

In the discrete sensitivity approach, also known as implicit sensitivity approach, the governing equations are first discretized and then differentiated with respect to the design variables. As already explained in Chapter 2, in the discretization process geometry and displacements are approximated by a linear combination of global shape functions (Hughes, 2000). Displacements $\mathbf{u}$ are approximated by

$$\mathbf{u} = \sum_a \mathbf{N}_a \cdot \mathbf{d}_a \qquad (4.5)$$

where $\mathbf{N}_a$ is the matrix containing the shape functions and $\mathbf{d}_a$ are the nodal degrees of freedom of node $a$. Both $\mathbf{N}_a$ and $\mathbf{d}_a$ depend on the kind of element considered. In the case of the shell element studied in Chapter 3, their expressions are given by (3.19) and (3.20), respectively.

Therefore, after discretization, the functional $\psi$ given by (4.1) is approximated by

$$\psi = \psi(\mathbf{s}, \sum_a \mathbf{N}_a \cdot \mathbf{d}_a) \qquad (4.6)$$

In sizing and shape optimization problems, geometrical variables are taken as design variables. Thus, the global stiffness matrix and the load vector are functions of these design variables. Therefore, the governing system of equations turns out to be

$$\mathbf{K}(\mathbf{s}) \cdot \mathbf{d} = \mathbf{F}(\mathbf{s}) \qquad (4.7)$$

where $\mathbf{s}$ is the vector of design variables. Thus, the vector of displacements obtained as solution to the structural analysis also depends on the design variables, that is $\mathbf{d} = \mathbf{d}(\mathbf{s})$.

Considering this, the sensitivity of the functional $\psi$ (4.6) with respect to the vector of design variables $\mathbf{s}$ is given by

$$\frac{d\psi}{d\mathbf{s}} = \frac{\partial\psi}{\partial\mathbf{s}} + \frac{\partial\psi}{\partial\mathbf{d}} \cdot \frac{\partial\mathbf{d}}{\partial\mathbf{s}} \tag{4.8}$$

It should be noted that the shape functions do not depend on the design variables. Derivatives $\frac{\partial\psi}{\partial\mathbf{s}}$ and $\frac{\partial\psi}{\partial\mathbf{d}}$ are determined explicitly from expression (4.6). The computation of derivatives of the state variables, that is $\frac{\partial\mathbf{d}}{\partial\mathbf{s}}$, is the main task of discrete sensitivity analysis.

There are different methods to compute these sensitivities. Depending on the way to organize the operations, it can be distinguished between direct and adjoint sensitivity analysis. In both cases, the computation of the so-called pseudo load vector, which will be introduced next, is required. Depending on the way the pseudo load vector is computed, semi-analytical and analytical sensitivities can be distinguished. As a result of the combination of these factors, discrete sensitivity analysis of state variables can be performed in four different ways.

In the present section, both the adjoint and direct method, as well as the semi-analytical and analytical approaches are explained and their computational advantages are outlined.

### 4.3.1 Discrete direct sensitivity analysis

In order to obtain the derivatives of the nodal degrees of freedom, the system equilibrium equation 4.7 must be derived with respect to the design variable $s_i$. That is,

$$\mathbf{K} \cdot \frac{d\mathbf{d}}{ds_i} + \frac{d\mathbf{K}}{ds_i} \cdot \mathbf{d} = \frac{d\mathbf{F}}{ds_i} \tag{4.9}$$

Derivatives of the degrees of freedom with respect to the design variables can be obtained by solving the system of equations

$$\mathbf{K} \cdot \frac{d\mathbf{d}}{ds_i} = \mathbf{F}_i^* \tag{4.10}$$

where $\frac{d\mathbf{d}}{ds_i}$ is the vector of unknowns and $\mathbf{F}_i^*$ is the pseudo load vector for design variable $i$, which is given by

$$\mathbf{F}_i^* = \frac{d\mathbf{F}}{ds_i} - \frac{d\mathbf{K}}{ds_i} \cdot \mathbf{d} \tag{4.11}$$

It must be noted that both systems (4.7) and (4.10) have the same system matrix. From the computational point of view, this may be a great advantage, if in the finite element analysis the system of equations was solved by a factorization method (Cholesky or Crout). In this case, for the solution of (4.10), the factorization of $\mathbf{K}$ is already available, and only forward and backward substitution are needed to solve the intermediate triangular systems of equations. Consequently, computational time is saved. At this point, it can be easily understood that $\mathbf{F}_i^*$ is called the pseudo load vector, since it can be interpreted as a new load case in the structural analysis.

The system of equations (4.10) has to be solved for each design variable $s_i$ and for each load case. Therefore, $ns$ being the number of design variables and $nl$ the number of load cases, the system (4.10) has to be solved $nl * ns$ times (although always with the same system matrix). Once the derivatives of nodal displacements are obtained, the sensitivity of functional $\psi$ can be obtained by (4.8).

As aforementioned, semi-analytical and analytical sensitivities are distinguished on the basis of how the pseudo load vector is computed. In the semi-analytical approach, the pseudo load vector is approximated by finite differences. In the analytical method, this vector is computed deriving analytically the stiffness matrix and load vector of the system.

## 4.3.2   Discrete adjoint sensitivity analysis

The adjoint sensitivity analysis can be explained as just another way to organize the operations different to the direct approach. As it will be shown, the reason for choosing one approach or the other is mainly computational.

From (4.8) and (4.10), it can be obtained that the derivative of functional $\psi$ with respect to design variable $s_i$ is given by

$$\frac{d\psi}{ds_i} = \frac{\partial\psi}{\partial s_i} + \left(\frac{\partial\psi}{\partial \mathbf{d}}\right)^T \cdot \mathbf{K}^{-1}(s) \cdot \mathbf{F}_i^* \tag{4.12}$$

where $\mathbf{F}^*$ is the pseudo load vector defined in (4.11).

The vector of adjoint variables is defined as

$$\boldsymbol{\lambda} := \mathbf{K}^{-1}(\mathbf{s}) \cdot \frac{\partial\psi}{\partial \mathbf{d}} \tag{4.13}$$

From (4.13) can be deduced, that the adjoint operator $\boldsymbol{\lambda}$ can be computed from the system of equations

$$\mathbf{K(s)} \cdot \boldsymbol{\lambda} = \frac{\partial \psi}{\partial \mathbf{d}} \tag{4.14}$$

Now, considering the symmentry of $\mathbf{K}$, the total derivative of functional $\psi$ is given by

$$\frac{d\psi}{ds_i} = \frac{\partial \psi}{\partial s_i} + \boldsymbol{\lambda}^T \cdot \mathbf{F}_i^* \tag{4.15}$$

To study the computational cost of this approach and compare it with the direct method, attention should be focused on system of equations (4.14) (Haug et al., 1986). As in the case of the direct method, the factorization of the system matrix may already be available from the structural analysis. The system has to be solved for each functional $\psi$. If $nc$ is the number of constraints in the optimization problem, it can be considered that system (4.14) has to be solved $nc$ times.

To determine which approach (direct or adjoint) is more suitable to be used in a certain optimization problem, the number of systems of equations needed to be solved in each case has to be analyzed. If $ns*nl < nc$, then direct differentiation method is preferred. These are cases with high number of constraints and low number of design variables and load cases.

However, in structural optimization it is usual that the number of active constraints must be smaller than the number of design variables and thus $ns*nl > nc$. Therefore, in most cases the direct adjoint sensitivity analysis will be more efficient from the computational point of view. Highly recommendable is the use of adjoint sensitivity analysis in optimization problems where a large number of design variables is applicable. Chapter 7 explains that the number of design variables is directly related to the kind of design parametrization chosen. In general, in design parametrizations based on the finite element mesh, a large number of design variables is considered. In these cases, especially for large problems, the use of adjoint techniques of sensitivity analysis is of crucial importance, in order to attain a reasonable computational cost.

### 4.3.3  Semi-analytical design sensitivities

As it has been already explained, in both discrete adjoint and discrete direct sensitivity approaches, the computation of the pseudo load vector (4.11) is required. The computation of the pseudo load vector can be done either numerically or analytically.

In the semi-analytical method the sensitivity analysis is formulated analytically, but the derivative of the pseudo load vector is computed numerically. For this reason, the semi-analytical sensitivity analysis can be seen as an intermediate technique between the global finite difference scheme and the analytical approach.

Many finite differences schemes have been used for numerical evaluation of the pseudo load vector. In the case of forward finite differences, the pseudo load vector is given by

$$
\begin{aligned}
\mathbf{F}_i^* &= \frac{d\mathbf{F}}{ds_i} - \frac{d\mathbf{K}}{ds_i} \cdot \mathbf{d} \\
&\approx \frac{1}{\Delta s_i} \Big[ \mathbf{F}(s_1, ..., s_i + \Delta s_i, ...s_{nd}) - \mathbf{F}(\mathbf{s}) + \\
&\quad \Big( \mathbf{K}(s_1, ..., s_i + \Delta s_i, ...s_{nd}) - \mathbf{K}(\mathbf{s}) \Big) \cdot \mathbf{d} \Big]
\end{aligned}
\tag{4.16}
$$

where $\Delta s_i$ is a small but finite increment in design variable $s_i$.

It should be noted that the global pseudo load vector is computed by assembling the individual contributions of the elemental pseudo load vectors $\mathbf{f}_i^{*e}$. The contribution of element $e$ to the pseudo load vector is given by

$$
\mathbf{f}_i^{*e} \approx \frac{1}{\Delta s_i} \Big[ \mathbf{f}^e(s_1, ..., s_i + \Delta s_i, ...s_{nd}) - \mathbf{f}^e(\mathbf{s}) + \Big( \mathbf{k}^e(s_1, ..., s_i + \Delta s_i, ...s_{nd}) - \mathbf{k}^e(\mathbf{s}) \Big) \mathbf{d}^e \Big]
\tag{4.17}
$$

Here, as well as in the global finite difference sensitivity analysis, a perturbed design has to be considered. Nevertheless, in the case of the semi-analytical approach it is not necessary to perform the whole structural analysis for the perturbed design, since just the elemental stiffness matrices $\mathbf{k}^e(s_1, ..., s_i + \Delta s_i, ...s_{nd})$ and the elemental load vectors $\mathbf{f}^e(s_1, ..., s_i + \Delta s_i, ...s_{nd})$ are required.

It should be noted that in some cases the considered load cases are independent of the design. In those cases, the term $\frac{d\mathbf{F}}{ds_i}$ vanishes.

The advantages of this method are basically two (Haftka and Adelman, 1989). First, the computational efficiency of the method is better than in the finite difference method (Haftka and Adelman, 1989; Olhoff et al., 1993). Second, the implementation on an existing code is only slightly more difficult than for the finite difference method, but significantly easier than the implementation of the analytical method. As it can be noticed, the semi-analytical approach does not depend on the finite element formulation used. On the contrary, as it will be shown in Section 4.3.4, the analytical approach does depend on the finite element formulation used and, therefore, it has to be implemented for each finite element of the code.

In the late 80's, Barthelemy et al. (1988) and Barthelemy and Haftka (1988) proved that severe accuracy problems may appear in sensitivities obtained by the semi-analytical method and they may even increase with mesh refinement. Soon, further studies about these accuracy problems were published (Cheng et al., 1989; Pedersen et al., 1989; Fenyes and Lust, 1991; Olhoff and Rassmunsen, 1991). Three important conclusions of these studies can be outlined.

First, it was concluded that the computation of the pseudo load vector was the key of these accuracy problems. Particularly, these errors are due to the numerical differentiation of the elemental stiffness matrices (by finite differences), which only occurs in the semi-analytical method.

Second, it was found that the slenderness of the structure and the mesh density influence strongly the accuracy of semi-analytical sensitivities.

Third, Barthelemy et al. (1988) studied local error indicators and concluded that the accuracy problems of the pseudo load vector were strongly related to rigid body motions of elements. Cheng and Olhoff (1993) formulated an accuracy indicator for the semi-analytical sensitivities.

Numerous attempts have been made to improve performance of semi-analytical sensitivities. These attempts can be classified in two groups depending on the way in which the performance of the method is improved.

1. In the first group, efforts on improving the accuracy of numerical differentiation of stiffness matrix are considered.

   It is well known that the forward finite differences scheme used in 4.16 has first order accuracy. More accurate schemes (eg. central differences) were used to approximate the pseudo load vector (Barthelemy and Haftka (1988), Cheng et al. (1989) and Olhoff and Rassmunsen (1991)). However,

an important disadvantage in these cases is that more design perturbations are needed, which implies a significant increment of computational effort.

An alternative approach to improve accuracy of semi-analytical sensitivities was proposed by Olhoff et al. (1993). The so-called *exact* semi-analytical method compensates errors of the finite difference scheme by introducing some correction factors, which can be precomputed in an initial step of sensitivity analysis. This approach can be viewed as a hybrid of semi-analytical and analytical methods.

2. In the second group, efforts to improve accuracy of semi-analytical sensitivities by improving the differentiation of rigid body modes are considered. As it was mentioned above, Barthelemy et al. (1988) stated the influence of the elemental rigid body motions on the quality of the pseudo load vector. In this second group of approaches, the element nodal displacement vector is decomposed into rigid body part and a part leading to deformations. Both parts are functions of the design variables.

   Inspired by the work of Cheng and Olhoff (1991), Mlejnek (1992) used an alternative finite differences scheme for the differentiation of the rigid body part and attained an improvement with respect to the traditional semi-analytical method.

   Later, the *refined semi-analytical* (RSA) method was proposed by van Keulen and de Boer (1998b). This approach is inspired by the work of Cheng and Olhoff (1993) and Mlejnek (1992). Here, the rigid body modes are exactly differentiated at element level. Improvements can be obtained when relatively large rigid body rotations can be identified for individual elements.

   This method, initially formulated for linear structures, was extended to linear buckling by van Keulen and de Boer (1998a) and to geometrically non-linear structures by de Boer and van Keulen (2000) and Parente and Vaz (2001).

   Later, RSA was extended by de Boer et al. (2002) to the computation of second order design sensitivities.

   It should be remarked that the rigid body modes and their derivatives do not depend on the finite formulation used, but just on the degrees of freedom. Thus, RSA, as well as the simple semi-analytical method, are of general applicability no matter what finite element formulation is used.

### 4.3.4 Analytical design sensitivities

As explained in Section 4.3.3, the core of the semi-analytical method is the numerical computation of the pseudo load $F_i^*$ (4.11) by finite differences. Contrary to the semi-analytical sensitivities, computation of pseudo load vector in the present case is performed analytically. This implies that stiffness matrix and load vector are derived analytically.

The main advantages of this method are its computational efficiency and reliability. Reliability and accuracy of sensitivities are very important in the optimization process. As it was already mentioned, sensitivity coefficients are used by the optimization algorithms as a prediction of the structural response of the modified system design. Therefore, accurate sensitivities are a determinant factor to ensure convergence of optimization algorithm and to increase the convergence rate.

As in the semi-analytical approach, the global pseudo load vector is computed by assembling the individual contributions of elemental pseudo load vectors. The elemental pseudo load vector is given by

$$\mathbf{f}^{*e} = \frac{d\mathbf{f^e}}{ds} - \frac{d\mathbf{k^e}}{ds} \cdot \mathbf{d^e} \tag{4.18}$$

In general, the stiffness matrix of an structural finite element is given by (Hughes, 2000)

$$\mathbf{k}_e = \int_{\Omega_e} \mathbf{B}^T \cdot \mathbf{D} \cdot \mathbf{B} d\Omega_e \tag{4.19}$$

where $\Omega_e$ is the element domain, $\mathbf{B}$ is the strain-displacement matrix and $\mathbf{D}$ is the material matrix.

The analytical calculation of the derivative of the element stiffness matrix is obtained by applying the chain rule to the integral expression (4.19). Thus,

$$\begin{aligned}
\mathbf{k}_e, s_i = \int_{\Omega_e} \mathbf{B}^T,_{s_i} \cdot \mathbf{D} \cdot \mathbf{B} d\Omega_e + \int_{\Omega_e} \mathbf{B}^T \cdot \mathbf{D},_{s_i} \cdot \mathbf{B} d\Omega_e + \\
\int_{\Omega_e} \mathbf{B}^T \cdot \mathbf{D} \cdot \mathbf{B},_{s_i} d\Omega_e + \int_{\Omega_e} \mathbf{B}^T \cdot \mathbf{D} \cdot \mathbf{B} (d\Omega_e),_{s_i}
\end{aligned} \tag{4.20}$$

It should be noted that, in general, the domain of integration of the stiffness matrix in shape optimization, also depends on the design variables. This introduces additional difficulties compared to sizing.

The computation of the derivative of the elemental load vector is done in an analogous manner to (4.20). Depending on the kind of load, it is either design dependent or not design dependent. Its design dependency may be due to the fact that its magnitude, domain in which it is applied, or direction in which it acts, is design dependent.

A drawback of this approach is that formulation and implementation are more difficult than for the semi-analytical method, and depend on the particular type of finite element used. The analytical differentiation of the stiffness matrix is more complex for more complex finite elements. However, once this differentiation is done and implemented in the code, the efficiency and reliability of the computed sensitivities are a clear advantage with respect to those computed by the semi-analytical method or global finite difference method.

Due to the complex formulation of this approach, the use of analytical sensitivities was historically restricted to size optimization problems. However, the need of more accurate sensitivity coefficients in order to enhance convergence of optimization methods legitimates the use of this approach for shape optimization problems (Schmit, 1986).

In Chapter 5, the analytical design sensitivity for the shell element studied in Chapter 3 is presented.

## 4.4 Variational sensitivity approach

The origin of variational sensitivity approach can be found in different contributions of Haug, Zolesio, Céa and Rousselet among other authors, presented in Haug and Céa (1981). The principal difference with respect to discrete sensitivity analysis is that in the variational approach, governing equations of the system are derived in its continuum form. This technique allows to compute derivatives of the structural response analytically. After this, and depending on the solution technique used, discretization may be done.

During the eighties and at the beginning of the nineties, a great effort was done in developing the variational sensitivity analysis both for sizing and shape optimization problems.

Dems and Mróz (1983) studied the variational sensitivity approach with the adjoint technique applied to structural optimization, using material parameters as design variables. They also extended this study to shape optimization in Dems and Mróz (1984).

Haug et al. (1986) presented a study of the different sensitivity analysis approaches using variational calculus and analyzed their mathematical basis. Later, Phelan and Haber (1989) introduced the concept of domain parametrization in variational sensitivity analysis of shape optimization problems. Application of variational sensitivity analysis to some prototype problems of shape optimal design was presented by Haug et al. (1984) and Barthelemy et al. (1989), among others.

The main motivation behind the variational sensitivity analysis is its easy implementation. As it will be explained, a deep knowledge of the code of the structural analysis program is not required. In Section 4.2, it was shown that also the global finite differences approach has this advantage. In that case, accuracy of this method strongly depends on the increment step chosen. However, the variational sensitivity analysis is best suited because no step size is required.

In the present section, sensitivity analysis for sizing problems and shape optimization problems is briefly described. As in the discrete sensitivity approach, the case of sizing is significantly easier than the case of shape optimization. The reason is that in shape optimization the domain of integration is design dependent and this fact has to be taken into account in differentiation. Finally, a comparison between discrete and variational sensitivity analysis is presented.

### 4.4.1 Variational sensitivity analysis for sizing

As in the case of discrete sensitivity analysis, direct and adjoint procedures can be distinguished in variational sensitivity analysis. In the direct approach, the sensitivity of structural response is computed by means of displacement sensitivities. In adjoint approach, sensitivity is computed through an adjoint problem.

#### 4.4.1.1 Direct Method

For the computation of the sensitivity coefficients by the direct method, equations governing the structural response have to be differentiated with respect to the design variables. This method is analogous to the discrete direct sensitivity method described in Section 4.3.1, but in the present case the equations are differentiated before discretization.

In Chapter 2, the basic governing equations for linear mechanical analysis were presented. The equilibrium equation written in terms of the Principle of Virtual

Work reads

$$\int_\Omega \boldsymbol{\sigma} \cdot \delta\boldsymbol{\varepsilon} d\Omega = \int_\Omega \mathbf{f} \cdot \delta\mathbf{u} d\Omega \tag{4.21}$$

the constitutive equation,

$$\boldsymbol{\sigma} = \mathbf{D} \cdot (\boldsymbol{\varepsilon} - \boldsymbol{\varepsilon}^0) \tag{4.22}$$

and the kinematic equation,

$$\boldsymbol{\varepsilon} = \mathbf{L}(\mathbf{u}) \tag{4.23}$$

where $\mathbf{L}$ is a linear differential operator.

Derivatives of (4.21), (4.22) and (4.23) with respect to design variable $s_i$ are

$$\int_\Omega \boldsymbol{\sigma},_{s_i} \cdot \delta\boldsymbol{\varepsilon} d\Omega = \int_\Omega \mathbf{f},_{s_i} \cdot \delta\mathbf{u} d\Omega \tag{4.24}$$

$$\boldsymbol{\sigma},_{s_i} = \mathbf{D} \cdot \boldsymbol{\varepsilon},_{s_i} + \mathbf{D},_{s_i} \cdot (\boldsymbol{\varepsilon} - \boldsymbol{\varepsilon}^0) \tag{4.25}$$

$$\boldsymbol{\varepsilon},_{s_i} = \mathbf{L}(\mathbf{u},_{\mathbf{s_i}}) \tag{4.26}$$

Comparing equations (4.21), (4.22) and (4.23) with (4.24), (4.25) and (4.26), it can be observed that sensitivities $u,_{s_i}$, $\boldsymbol{\varepsilon}$ and $\boldsymbol{\sigma}$ can be interpreted as the displacement field, strain field and stress field appearing in the original structure under a pseudo load $\mathbf{f}^*$. This pseudo load is determined by the pseudo initial strain $\boldsymbol{\varepsilon}^*$ and the derivative of the original load field with respect to the design variables, that is $\mathbf{f},_{s_i}$. The expression for the pseudo initial strain can be obtained rearranging terms in equation (4.25), that is,

$$\begin{aligned} \boldsymbol{\sigma},_{s_i} &= \mathbf{D} \cdot \boldsymbol{\varepsilon},_{s_i} + \mathbf{D},_{s_i} \cdot (\boldsymbol{\varepsilon} - \boldsymbol{\varepsilon}^0) \\ &= \mathbf{D} \cdot \left(\boldsymbol{\varepsilon},_{s_i} + \mathbf{D}^{-1} \cdot \mathbf{D},_{s_i} \cdot (\boldsymbol{\varepsilon} - \boldsymbol{\varepsilon}^0)\right) = \mathbf{D} \cdot (\boldsymbol{\varepsilon},_{s_i} - \boldsymbol{\varepsilon}^*) \end{aligned} \tag{4.27}$$

where

$$\boldsymbol{\varepsilon}^* = -\mathbf{D}^{-1} \cdot \mathbf{D},_{s_i} (\boldsymbol{\varepsilon} - \boldsymbol{\varepsilon}^0) \tag{4.28}$$

This analogy allows an easy computation of the sensitivities. The actual loading of the system is replaced by the pseudo load case and the structural analysis is again performed. As a result, the response sensitivity instead of the response of the system is obtained.

#### 4.4.1.2   Adjoint method

In the variational sensitivity analysis, the adjoint method results more convenient than the direct method when sensitivity of a function is not required over the entire domain but only at certain points (Haftka and Gürdal, 1999). This situation is frequent in structural optimization, since often displacement and stress constraints have to be satisfied at a certain critical point.

In this approach, a functional in integral form of the measure whose sensitivities are required is considered. The most common cases in structural optimization are displacement functionals and stress functionals. Sensitivities are obtained through differentiation of this functional with respect to design variables. In the differentiation of the functional, derivatives of displacement field or stress field appear. The computation of these derivatives is circumvented by the definition of an adjoint problem. This adjoint problem or adjoint structure can be interpreted as the original structure under an artificial load, which depends on the original system and the considered functional.

An excellent exposition of this method is given by Haug et al. (1986). They also present a discussion about differentiability requirements on design derivatives. (Haftka and Gürdal, 1999) study the approach for the cases of displacement functional and stress functional.

It can be observed that both in the direct and adjoint method, a pseudo load case is considered. However, in general the implementation of direct method is easier than for the adjoint method. In the adjoint approach, the computation of sensitivities of a stress field becomes especially complex.

### 4.4.2   Variational shape sensitivity

As in the case of discrete sensitivity analysis, variational sensitivity analysis for shape optimization is significantly more difficult than for sizing. The reason of this increasing complexity is that in shape optimization the integration domain is design dependent and this has to be taken into account in the derivatives.

Two general approaches of variational shape sensitivity can be distinguished: the material derivative approach and the domain parametrization approach. Following, a brief introduction to both approaches is given. A detailed presentation of the formulations can be found in the corresponding references.

### 4.4.2.1 Material derivative approach

This approach was first presented by Zolesio (1981) and Choi and Haug (1983). In the eighties, further development was made and numerous applications have been reported (Haug et al., 1986; Arora et al., 1992).

In this approach, the variation of the field variables is obtained using the material derivative concept of continuum mechanics. The use of the concept of material derivative is based on the identification of the iterative process of search for the optimum shape as a time dependent deformation of a system and the consequent identification of the design variable with a time variable. For simplicity, only one design variable $s$ is considered. In Figure 4.1, the movement of a material point in the optimization process is sketched. Initially, that is at $s = 0$, the position of the point is $\mathbf{x}$ and when the design variable takes a value of $s$ the new position is $\mathbf{x}^s$. The linearized relation between $\mathbf{x}^s$ and $\mathbf{x}$ is given by

$$\mathbf{x}^s = \mathbf{x} + s\mathbf{v} \tag{4.29}$$

where

$$\mathbf{v} = \mathbf{x}^s{,}_s \Big|_{s=0} \tag{4.30}$$

is the design velocity field which represents the change of the shape variation field with respect to a shape design variable.

Let us consider a function $f(\mathbf{x}, s)$, where $\mathbf{x}$ is a position vector and $s_i$ is a certain design variable. The material derivative of $f(\mathbf{x}, s)$ with respect to design variable $s$ is given by

$$Df = f{,}_s + \boldsymbol{\nabla}_{\mathbf{x}} f \cdot \mathbf{x}^s{,}_s \tag{4.31}$$

where $f{,}_s$ is the partial derivative of $f$ with respect to $s$.

This material derivative concept applied to design changes can be extended to vector fields (e.g. displacements), tensors (e.g. strain tensor or stress tensor), volume integrals and surface integrals (Arora et al., 1992). Through these, the sensitivity of any response functional $\psi$ can be computed. As in the case of variational sensitivity for sizing, a distinction between direct and adjoint methods is made. The procedure for variational shape sensitivity coincides with that of sizing, except that now the material derivative concept is used, instead of the local derivative. As in the case of sizing, the computation of a

pseudo load vector is also required. Detailed explanation of the method is given by Haug et al. (1986) and Arora (1993).

The material derivative approach can be presented in different forms, depending on the expression used for evaluation of the pseudo load. This expression can be in form of volume integrals or boundary integrals (Haug et al., 1986). The formulation of the pseudo load vector, using boundary integrals, implies a lower computational cost but yields less accurate results (Adelman and Haftka, 1986). A unification of these forms is presented by Arora (1993).
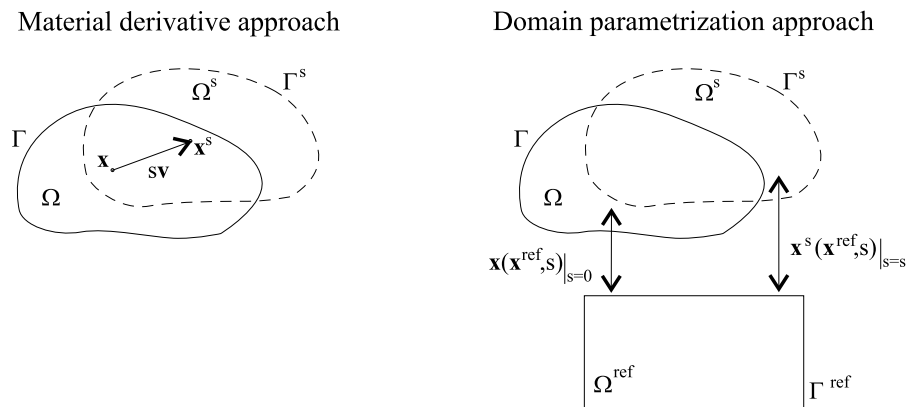


Figure 4.1: Sketch of mappings established in material derivative approach and domain parametrization approach

#### 4.4.2.2 Domain parametrization approach

The domain parametrization approach (also called control volume approach) was introduced by Phelan and Haber (1989), in order to overcome the difficulties related to domain variation. Here, the domain is parametrized, and all integrals are transformed to a fixed reference domain before differentiation. Then, variation of these integrals is performed without the need to account domain variation.

In Figure 4.1, the main differences between material approach and domain parametrization approach can be observed. In the material approach, mapping was established between actual configuration ($s = 0$) and a next configuration ($s \neq 0$), which is obtained as a result of a 'movement' of the actual configuration. In the domain parametrization approach, mapping is established between actual configuration and a reference domain. As design changes, this mapping

between actual domain and reference domain changes but the reference domain itself remains constant.

The idea behind this approach is analogous to the isoparametric finite elements concept (Arora et al., 1992). In the isoparametric method of finite element analysis, all elements of the same type are mapped into a fixed regular reference domain, where numerical integration is performed. In fact, when using isoparametric finite elements combined with this approach, the parent element is taken as reference domain.

Arora et al. (1992) showed the theoretical equivalence between material derivative and the domain parametrization approaches. Moreover, they showed that discretized forms of both approaches can also be implemented in the same way. A detailed exposition of both approaches is given by Haftka and Gürdal (1999).

### 4.4.3   Comparison between discrete and variational sensitivity analysis

Yang and Botkin (1986) presented a comparison between discrete and variational sensitivity analysis. In this context, the main advantage of the variational technique is its general application to any solution technique, i.e. finite element method or boundary method, for instance. In the particular case of the finite element method, the variational sensitivity analysis has the advantage of its easy implementation in a general purpose finite element program. It may seem that the variational approach is more accurate than the discrete approach because it does not directly depend on the finite element method and, as a consequence, it does not, in principle, involve numerical errors. However, as Yang and Botkin (1986) show, the accuracy of the variational sensitivities is also affected by the finite element solution. The reason is that the analytical expression obtained for the sensitivities depends on the boundary solution quantities obtained from the structural analysis. The main disadvantage is that the accurate evaluation of these quantities, for example stresses, on the boundaries is often difficult.

A disadvantage of the variational sensitivity analysis is the complexity of the mathematical proof associated with it. Differentiability of the structural response with respect to design variables should be studied in each case (Haug et al., 1986).

Arora et al. (1992) reached a conclusion that the discretized form of variational sensitivity analysis and expressions given by the discrete sensitivity approach

are similar. For simple examples, and when discretization for the structural and sensitivity analysis are consistent, results obtained by the variational method coincide with those obtained by the discrete approach.

# Chapter 5

# Analytical Sensitivity of a Shell Finite Element

## 5.1 Introduction

In Chapter 4, a review of the different sensitivity analysis methods was presented. The need for more accurate and reliable sensitivity coefficients legitimates the use of the analytical approach. This approach involves higher mathematical complexity but is more efficient and has lower computational costs. In addition, for optimization problems where a large number of design variables are considered the suitability of adjoint sensitivity techniques is shown.

As explained in Section 4.3, analytical sensitivity analysis depends on the finite element formulation at hand. The elemental pseudo load vector is given by

$$\mathbf{f}^{*e} = \frac{d\mathbf{f}^e}{ds} - \frac{d\mathbf{k}^e}{ds} \cdot \mathbf{d}^e \tag{5.1}$$

Therefore, analytical differentiation of the elemental stiffness matrix and elemental load vector are required.

Historically, this approach was mostly used in sizing problems. In these optimization problems, differentiation of elemental stiffness matrix is relatively easy. This is, for instance, the case of optimizing the sectional area of truss elements. In this case, design variables are factors in the elemental stiffness matrices.

However, applications of analytical sensitivity analysis to shape optimization can also be found in the literature. Wang et al. (1985) applied the discrete

analytical differentiation technique of sensitivity analysis to isoparametric brick elements. Brockman (1987) computed through this technique sensitivities of static displacements and stresses and sensitivities of natural vibration frequencies for two- and three-dimensional isoparametric finite elements.

Later, Brockman and Lung (1988) adapted these techniques to the sensitivity analysis for plate and flat shell finite elements. Design parameters of interest included material properties, thickness and geometrical variables which govern size and shape of the structure. Again, both displacement and stress sensitivities were considered for the static case and frequency and mode sensitivities for the dynamic case. Brockman and Lung (1988) showed that accuracy of the computed sensitivities is comparable in quality to that of the basic solution of the static analysis.

Kimmich (1990) presented a detailed formulation of sensitivity analysis for an isoparametric degenerated shell element. He calculated the derivative of elemental stiffness matrix and of different load vectors and used them to compute sensitivities of objective functions and stress constraints. Several numerical examples were presented.

Kimmich (1990) and Yamazaki and Vanderplaats (1993) extended the analytical differentiation technique to isoparametric curved shell elements. The improvement with respect to the work of Brockman and Lung (1988) is that now they considered the normal vector to the curved shell surface in the definition of the shell geometry. This introduced additional difficulties in differentiation of strain-displacement matrix. In particular, Yamazaki and Vanderplaats (1993) considered an eight-node isoparametric shell element based on Mindlin plate theory and derived analytically the element stiffness, geometric stiffness and mass matrices. Shell thickness and nodal coordinates were considered as design variables. Examples were given for a plate and a cylindrical shell for sensitivities of displacement, stress, buckling and natural frequency.

In this chapter, the analytical sensitivity technique is applied to the shell finite element studied in Chapter 3. First, analytical differentiation of elemental stiffness matrix of the displacement element is shown in detail. Attention is focused on differentiation of the different coordinate systems considered in the formulation. In Section 5.3, differentiation of the stiffness matrix for the DSG shell element is presented. It will be shown that the only difference with respect to the displacement element is the computation of the derivatives of the modified strain components. Differentiation of load vector is performed in Section 5.4. Some remarks about simplifications in the computation of derivatives in

sizing with respect to shape optimization are given in Section 5.5. Last, adjoint sensitivity analysis for the particular case of strain energy minimization is considered. It will be shown that in this case a simplified expression to compute derivatives of the objective function can be obtained.

In order to avoid clutter, only one design variable $s$ is considered.

## 5.2 Analytical sensitivity analysis for a shell displacement element

In Chapter 3, a shell element with Reissner-Mindlin kinematics was studied in detail. In order to use this element for shape optimization of shells, its analytical sensitivities are computed. Here, the analytical procedure to obtain derivatives of this displacement shell element is explained. Throughout the section, a continuous reference to matrices and vectors involved in the computation of the element stiffness matrix is made.

Calculation of the element stiffness matrix derivative is obtained by applying the chain rule to integral expression (3.70). Thus,

$$
\begin{aligned}
\mathbf{k}^e{}_{,s} = & \int_{-1}^{1} \int_{-1}^{1} \int_{-1}^{1} \bar{\mathbf{B}}_{,s}^{T}(\xi, \eta, \zeta) \cdot \bar{\mathbf{D}} \cdot \bar{\mathbf{B}}(\xi, \eta, \zeta) J d\xi d\eta d\zeta + \\
& \int_{-1}^{1} \int_{-1}^{1} \int_{-1}^{1} \bar{\mathbf{B}}^{T}(\xi, \eta, \zeta) \cdot \bar{\mathbf{D}}_{,s} \cdot \bar{\mathbf{B}}(\xi, \eta, \zeta) J d\xi d\eta d\zeta + \\
& \int_{-1}^{1} \int_{-1}^{1} \int_{-1}^{1} \bar{\mathbf{B}}^{T}(\xi, \eta, \zeta) \cdot \bar{\mathbf{D}} \cdot \bar{\mathbf{B}}_{,s}(\xi, \eta, \zeta) J d\xi d\eta d\zeta + \\
& \int_{-1}^{1} \int_{-1}^{1} \int_{-1}^{1} \bar{\mathbf{B}}^{T}(\xi, \eta, \zeta) \cdot \bar{\mathbf{D}} \cdot \bar{\mathbf{B}}(\xi, \eta, \zeta) J_{,s} d\xi d\eta d\zeta
\end{aligned}
\tag{5.2}
$$

Since strains and stresses at a point are expressed in a local Cartesian coordinate system, the material matrix $\bar{\mathbf{D}}$ is constant (see Section 3.8) and, therefore, its derivative is the zero matrix, assuming $s$ is not a material parameter.

As it can be observed in (5.2), the derivatives of the strain-displacement matrix $\bar{\mathbf{B}}$ and of the Jacobian determinant with respect to the design variables are needed. The calculation of these derivatives is explained next.

## 5.2.1 Differentiation of the strain-displacement matrix

The strain-displacement matrix $\bar{\mathbf{B}}$ relates the strain components in the local Cartesian system with the nodal degrees of freedom. That is,

$$\bar{\varepsilon} = \bar{\mathbf{B}}\left(\xi, \eta, \zeta\right) \cdot \mathbf{d}^e \tag{5.3}$$

In Section 3.7, two different ways to compute the strain-displacement matrix are presented. The difference between them lies in the coordinate system in which strain components are first computed. In the first method, strain components are directly computed in the local Cartesian system. In the second one, covariant strain components in the curvilinear system are first computed and then transformed into the local Cartesian basis. Obviously, the result obtained is the same in both cases. However, for practical reasons when considering modified strains in the DSG method, the second procedure is preferred.

In the following, the differentiation of the strain-displacement operator for both approaches is explained.

### 5.2.1.1 Strains in local Cartesian system

As it was explained in Section 3.7.1, the strain-displacement operator $\bar{\mathbf{B}}$, can be obtained byrearranging the components of $\bar{\mathbf{H}}$ defined in (3.39), which contains the local Cartesian derivatives of the local Cartesian displacements. Analogously, $\bar{\mathbf{B}}_{,s}$ can be obtained rearranging the components of $\bar{\mathbf{H}}_{,s}$. In order to calculate this last matrix, the product rule must be applied to (3.45). Hence,

$$\begin{aligned}\bar{\mathbf{H}}_{,s} =& \boldsymbol{\Theta}_{,s}^T \cdot \mathbf{J}^{-1} \cdot \mathbf{H} \cdot \boldsymbol{\Theta} + \boldsymbol{\Theta}^T \cdot (\mathbf{J}^{-1})_{,s} \cdot \mathbf{H} \cdot \boldsymbol{\Theta} \\ &+ \boldsymbol{\Theta}^T \cdot \mathbf{J}^{-1} \cdot \mathbf{H}_{,s} \cdot \boldsymbol{\Theta} + \boldsymbol{\Theta}^T \cdot \mathbf{J}^{-1} \cdot \mathbf{H} \cdot \boldsymbol{\Theta}_{,s}\end{aligned} \tag{5.4}$$

The matrix $\mathbf{H}$ contains the derivatives of global displacements with respect to curvilinear coordinates and it is approximated by

$$\mathbf{H} = \begin{pmatrix} \frac{\partial}{\partial \xi} \\ \frac{\partial}{\partial \eta} \\ \frac{\partial}{\partial \zeta} \end{pmatrix} \sum_a \mathbf{d}_a^T \cdot \mathbf{N}_a(\xi, \eta, \zeta)^T \tag{5.5}$$

Therefore, the derivative of $\mathbf{H}$ with respect to the design variables, is given by

$$\mathbf{H}_{,s} = \begin{pmatrix} \frac{\partial}{\partial \xi} \\ \frac{\partial}{\partial \eta} \\ \frac{\partial}{\partial \zeta} \end{pmatrix} \sum_a \mathbf{d}_a^T \cdot \mathbf{N}_a^T{}_{,s} \tag{5.6}$$

78

Differentiation of $\boldsymbol{\Theta}$ and $\mathbf{J}^{-1}$ with respect to design variables is explained in Sections 5.2.2 and 5.2.3.

### 5.2.1.2 Strains in curvilinear coordinate system

In this case, the strain tensor is first computed in the contravariant basis of the local curvilinear system and then a set of transformations is performed in order to obtain it in the local Cartesian basis. Once components of the strain tensor in the local Cartesian basis are obtained, they can be reordered into the strain vector (3.37), and thus $\bar{\mathbf{B}}$ can be obtained. In Section 3.7.2, both the computation of the covariant strain components in the curvilinear basis and a detailed explanation of the set of transformations required, are provided.

In an analogous way, $\bar{\mathbf{B}}$ is obtained by rearranging derivatives of strain components in the local Cartesian basis. These derivatives are obtained differentiating expression (3.56) with respect to design variable $s$. Thus, applying the product rule, we get

$$
\begin{aligned}
\{\bar{\varepsilon}^{mn}\}_{,s} = {} & \boldsymbol{\Theta}^T{}_{,s} \cdot \mathbf{J}^T \cdot \mathbf{G}^{-T} \cdot \{\hat{\varepsilon}_{ij}\} \cdot \mathbf{G}^{-1} \cdot \mathbf{J} \cdot \boldsymbol{\Theta} \\
& + \boldsymbol{\Theta}^T \cdot \mathbf{J}^T{}_{,s} \cdot \mathbf{G}^{-T} \cdot \{\hat{\varepsilon}_{ij}\} \cdot \mathbf{G}^{-1} \cdot \mathbf{J} \cdot \boldsymbol{\Theta} \\
& + \boldsymbol{\Theta}^T \cdot \mathbf{J}^T \cdot \mathbf{G}^{-T}{}_{,s} \cdot \{\hat{\varepsilon}_{ij}\} \cdot \mathbf{G}^{-1} \cdot \mathbf{J} \cdot \boldsymbol{\Theta} \\
& + \boldsymbol{\Theta}^T \cdot \mathbf{J}^T \cdot \mathbf{G}^{-T} \cdot \{\hat{\varepsilon}_{ij}\}_{,s} \cdot \mathbf{G}^{-1} \cdot \mathbf{J} \cdot \boldsymbol{\Theta} \\
& + \boldsymbol{\Theta}^T \cdot \mathbf{J}^T \cdot \mathbf{G}^{-T} \cdot \{\hat{\varepsilon}_{ij}\} \cdot \mathbf{G}^{-1}{}_{,s} \cdot \mathbf{J} \cdot \boldsymbol{\Theta} \\
& + \boldsymbol{\Theta}^T \cdot \mathbf{J}^T \cdot \mathbf{G}^{-T} \cdot \{\hat{\varepsilon}_{ij}\} \cdot \mathbf{G}^{-1} \cdot \mathbf{J}_{,s} \cdot \boldsymbol{\Theta} \\
& + \boldsymbol{\Theta}^T \cdot \mathbf{J}^T \cdot \mathbf{G}^{-T} \cdot \{\hat{\varepsilon}_{ij}\} \cdot \mathbf{G}^{-1} \cdot \mathbf{J} \cdot \boldsymbol{\Theta}_{,s}
\end{aligned}
\tag{5.7}
$$

It can be observed that in this expression derivatives of $\boldsymbol{\Theta}$, $\mathbf{J}$, $\mathbf{G}^{-1}$ and $\{\hat{\varepsilon}_{ij}\}$ appear. Derivatives of the covariant components of the strain tensor in the curvilinear basis are obtained by differentiation of expression (3.51). Thus,

$$
\hat{\varepsilon}_{ij},_s = \frac{1}{2}\left( (u^k{}_{,i})_{,s}\,\mathbf{e}_k \cdot \mathbf{g}_j + u^k{}_{,i}\,\mathbf{e}_k \cdot \mathbf{g}_{j,s} + (u^k{}_{,j})_{,s}\,\mathbf{e}_k \cdot \mathbf{g}_i + u^k{}_{,j}\,\mathbf{e}_k \cdot \mathbf{g}_{i,s} \right)
\tag{5.8}
$$

In the above expression, derivatives of the covariant curvilinear base vectors and of the displacements with respect to design variables are involved. Considering that the $i$-th row of the Jacobian matrix is the vector $\mathbf{g}_i$ (see equation (3.27)), $\mathbf{g}_{i,s}$ will be the $i$-th row of the derivative of the Jacobian matrix. Computation

of $\mathbf{J}_{,s}$ is explained in Section 5.2.3. Derivatives of displacement vector (3.18) with respect to design variable $s$ are given by

$$\mathbf{u}_{,s} = \sum_a \mathbf{N}_{a,s} \cdot \mathbf{d}_a \qquad (5.9)$$

where

$$\mathbf{N}_{a,s} = \begin{pmatrix} 0 & 0 & 0 & \frac{1}{2}\zeta N_a(t_{a,s}\,\mathbf{A1}_a^1 + t_a\mathbf{A1}_{a,s}^1) & -\frac{1}{2}\zeta N_a(t_{a,s}\,\mathbf{A2}_a^1 + t_a\mathbf{A2}_{a,s}^1) \\ 0 & 0 & 0 & \frac{1}{2}\zeta N_a(t_{a,s}\,\mathbf{A1}_a^2 + t_a\mathbf{A1}_{a,s}^2) & -\frac{1}{2}\zeta N_a(t_{a,s}\,\mathbf{A2}_a^2 + t_a\mathbf{A2}_{a,s}^2) \\ 0 & 0 & 0 & \frac{1}{2}\zeta N_a(t_{a,s}\,\mathbf{A1}_a^3 + t_a\mathbf{A1}_{a,s}^3) & -\frac{1}{2}\zeta N_a(t_{a,s}\,\mathbf{A2}_a^3 + t_a\mathbf{A2}_{a,s}^3) \end{pmatrix} \qquad (5.10)$$

As the considered design variables may be nodal coordinates or the thickness of the shell, these derivatives can be computed analytically. Computation of derivatives of the director base vectors is explained in Section 5.2.6.

In the following sections, the computation of derivatives of matrices $\mathbf{\Theta}$, $\mathbf{J}$ and $\mathbf{G}^{-1}$, as well as the differentiation of the determinant of the Jacobian matrix are explained.

## 5.2.2 Differentiation of $\mathbf{\Theta}$

The procedure to obtain the matrix $\mathbf{\Theta}$, which is the transformation matrix between the global and local Cartesian coordinate systems, was explained in detail in Section 3.6. Considering the expression (3.34), the derivative of the matrix $\mathbf{\Theta}$ with respect to the design variable $s$ is given by

$$\mathbf{\Theta}_{,s} = \begin{pmatrix} x_{,\bar{x}s} & x_{,\bar{y}s} & x_{,\bar{z}s} \\ y_{,\bar{x}s} & y_{,\bar{y}s} & y_{,\bar{z}s} \\ z_{,\bar{x}s} & z_{,\bar{y}s} & z_{,\bar{z}s} \end{pmatrix} = \begin{pmatrix} \bar{e}_{1,s}^1 & \bar{e}_{2,s}^1 & \bar{e}_{3,s}^1 \\ \bar{e}_{1,s}^2 & \bar{e}_{2,s}^2 & \bar{e}_{3,s}^2 \\ \bar{e}_{1,s}^3 & \bar{e}_{2,s}^3 & \bar{e}_{3,s}^3 \end{pmatrix} = \left\{ \bar{\mathbf{e}}_{1,s} \quad \bar{\mathbf{e}}_{2,s} \quad \bar{\mathbf{e}}_{3,s} \right\} \quad (5.11)$$

where $\bar{e}_{i,s}^j$ is the derivative with respect to $s$ of the $j$-component of the vector $\bar{\mathbf{e}}_i$. The components of $\mathbf{\Theta}_{,s}$ are calculated differentiating expressions (3.30), (3.31), and (3.33). In expression (3.30), it can be observed that $\bar{\mathbf{e}}_3$ is a normalized vector. Differentiation of a normalized vector is explained in Appendix A.2. According to this formula, we obtain

$$\bar{\mathbf{e}}_{3,s} = \frac{1}{\left| \sum_a N_a(\xi,\eta)\mathbf{A3}_a \right|^2} \left[ \left( \sum_a N_a(\xi,\eta)\mathbf{A3}_{a,s} \right) \left( \left| \sum_a N_a(\xi,\eta)\mathbf{A3}_a \right| \right) \right.$$
$$\left. - \left( \sum_a N_a(\xi,\eta)\mathbf{A3}_a \right) \left( \left| \sum_a N_a(\xi,\eta)\mathbf{A3}_a \right| \right)_{,s} \right] \qquad (5.12)$$

The expression for differentiation of the magnitude of a vector is given in Appendix A.3. The calculation procedure to obtain the derivative of director vector $\mathbf{A3}_a$ is explained in detail in Section 5.2.6. Note that $N_a(\xi, \eta)$ do not depend on $s$, since they are the usual two-dimensional shape functions (see Appendix A.1). They should not be confused with $\mathbf{N}_a(\xi, \eta)$, which is the shape function matrix defined in (3.19).

In a similar manner, derivatives of $\bar{\mathbf{e}}_1$ and $\bar{\mathbf{e}}_2$ are given by

$$\bar{\mathbf{e}}_{1,s} = \frac{(\mathbf{l} \times \bar{\mathbf{e}}_3)_{,s} \left| \mathbf{l} \times \bar{\mathbf{e}}_3 \right| - (\mathbf{l} \times \bar{\mathbf{e}}_3) \left| \mathbf{l} \times \bar{\mathbf{e}}_3 \right|_{,s}}{\left| \mathbf{l} \times \bar{\mathbf{e}}_3 \right|^2} \tag{5.13}$$

$$\bar{\mathbf{e}}_{2,s} = \frac{(\bar{\mathbf{e}}_3 \times \bar{\mathbf{e}}_1)_{,s} \left| \bar{\mathbf{e}}_3 \times \bar{\mathbf{e}}_1 \right| - (\bar{\mathbf{e}}_3 \times \bar{\mathbf{e}}_1) \left| \bar{\mathbf{e}}_3 \times \bar{\mathbf{e}}_1 \right|_{,s}}{\left| \bar{\mathbf{e}}_3 \times \bar{\mathbf{e}}_1 \right|^2} \tag{5.14}$$

Differentiation of a vector resulting from a cross product is indicated in Appendix A.4.

## 5.2.3   Differentiation of $\mathbf{J}$ and $\mathbf{J}^{-1}$

In case strains are obtained directly in the local Cartesian system, $\mathbf{J}^{-1}{}_{,s}$ is required for computation of $\bar{\mathbf{B}}_{,s}$ (see (5.4)). In case strain components are computed first in the curvilinear system and then transformed into the local Cartesian basis, $\mathbf{J}_{,s}$ is required instead (see (5.7)). Here, computation of $\mathbf{J}_{,s}$ and $(\mathbf{J}^{-1})_{,s}$ are presented.

Considering the definition of the Jacobian matrix given in (3.21), its derivative with respect to design variable $s$ reads

$$\mathbf{J}_{,s} = \begin{pmatrix} x_{,\xi s} & y_{,\xi s} & z_{,\xi s} \\ x_{,\eta s} & y_{,\eta s} & z_{,\eta s} \\ x_{,\zeta s} & y_{,\zeta s} & z_{,\zeta s} \end{pmatrix} = \begin{pmatrix} \mathbf{x}_{,\xi s}^T \\ \mathbf{x}_{,\eta s}^T \\ \mathbf{x}_{,\zeta s}^T \end{pmatrix} \tag{5.15}$$

The components of this matrix are obtained differentiating the expressions (3.22), (3.23) and (3.24) with respect to $s$. Thus,

$$\mathbf{x}_{,\xi s} = \sum_a N_{a,\xi} \left( \mathbf{x}_{a,s} + \frac{1}{2} \zeta t_{a,s} \mathbf{A3}_a + \frac{1}{2} \zeta t_a \mathbf{A3}_{a,s} \right) \tag{5.16}$$

$$\mathbf{x}_{,\eta s} = \sum_a N_{a,\eta} \left( \mathbf{x}_{a,s} + \frac{1}{2}\zeta t_{a,s}\,\mathbf{A3}_a + \frac{1}{2}\zeta t_a \mathbf{A3}_{a,s} \right) \tag{5.17}$$

$$\mathbf{x}_{,\zeta s} = \sum_a N_{a,\zeta} \frac{1}{2}\left( t_{a,s}\,\mathbf{A3}_a + t_a \mathbf{A3}_{a,s} \right) \tag{5.18}$$

In these expressions, derivatives of the nodal position vector with respect to design variable $s$ are involved. These derivatives will be different from zero when the position of node $a$ varies in the modified design. As in the case of calculation of $\mathbf{\Theta}_{,s}$, here, derivatives of the director coordinate base vectors are also required. The procedure to calculate these derivatives is presented in Section 5.2.6.

The derivative of the inverse Jacobian matrix is given by (Wang et al., 1985)

$$\mathbf{J}^{-1}_{,s} = -\mathbf{J}^{-1} \cdot \mathbf{J}_{,s} \cdot \mathbf{J}^{-1} \tag{5.19}$$

This expression can be obtained by differentiating

$$\mathbf{J}\mathbf{J}^{-1} = \mathbf{I} \tag{5.20}$$

with respect to design variable $s$. By doing this, it can be obtained

$$\mathbf{J}_{,s}\,\mathbf{J}^{-1} + \mathbf{J}\mathbf{J}^{-1}_{,s} = \mathbf{0} \tag{5.21}$$

which is equivalent to (5.19).

## 5.2.4  Derivative of $\mathbf{G}^{-1}$

Computation of derivatives of contravariant coefficient matrix $\mathbf{G}^{-1}$ is done analogously as the derivative of the inverse Jacobian matrix (5.19). Therefore,

$$\mathbf{G}^{-1}_{,s} = -\mathbf{G}^{-1} \cdot \mathbf{G}_{,s} \cdot \mathbf{G}^{-1} \tag{5.22}$$

Derivatives of covariant coefficient matrix are computed differentiating expression (3.29). That is,

$$\mathbf{G}_{,s} = \{g_{ik}\}_{,s} = \{\mathbf{g}_{i,s}\cdot\mathbf{g}_j + \mathbf{g}_i\cdot\mathbf{g}_{j,s}\} \tag{5.23}$$

82

Once the derivative of the Jacobian matrix is computed according to (5.15), the derivatives of the covariant base vectors required for the computation of (5.23) are known, since

$$\mathbf{J}_{,s} = \begin{pmatrix} x_{,\xi s} & y_{,\xi s} & z_{,\xi s} \\ x_{,\eta s} & y_{,\eta s} & z_{,\eta s} \\ x_{,\zeta s} & y_{,\zeta s} & z_{,\zeta s} \end{pmatrix} = \begin{Bmatrix} \mathbf{g}_{1}^{T}{}_{,s} \\ \mathbf{g}_{2}^{T}{}_{,s} \\ \mathbf{g}_{3}^{T}{}_{,s} \end{Bmatrix} \tag{5.24}$$

Therefore, $\mathbf{G}_{,s}$ can be easily obtained.

### 5.2.5 Derivative of the determinant of the Jacobian matrix

As it can be observed in (5.2), in order to calculate the derivative of the elemental stiffness matrix, the derivative of the determinant of the Jacobian matrix is required. This is given by (Wang et al., 1985; Navarrina, 1987)

$$|\mathbf{J}|_{,s} = |\mathbf{J}| tr \left( \mathbf{J}^{-1} \cdot \mathbf{J}_{,s} \right) \tag{5.25}$$

Note that $\mathbf{J}_{,s}$ is already available, since it is required for the computation of $\mathbf{B}_{,s}$.

### 5.2.6 Derivative of director coordinate systems

In Section 3.4, the procedure to obtain the director coordinate system was explained in detail. Differentiation of $\mathbf{A1}_P$, $\mathbf{A2}_P$ and $\mathbf{A3}_P$ is obtained applying recursively the product rule to the corresponding formulae.

It is important to remember that director vector $\mathbf{A3}_P$ is obtained as the average of the unit normal vectors to elements sharing node $P$. Therefore, the derivative of the director vector must take into account derivatives of these single contributions. Thus,

$$\mathbf{A3}_{P,s} = \frac{\left( \sum_{k=1}^{nae} \mathbf{A3}_{P}^{e_k}{}_{,s} \right) \left| \sum_{k=1}^{nae} \mathbf{A3}_{P}^{e_k} \right| - \left( \sum_{k=1}^{nae} \mathbf{A3}_{P}^{e_k} \right) \left| \sum_{k=1}^{nae} \mathbf{A3}_{P}^{e_k} \right|_{,s}}{\left| \sum_{k=1}^{nae} \mathbf{A3}_{P}^{e_k} \right|^2} \tag{5.26}$$

where

$$\left| \sum_{k=1}^{nae} \mathbf{A3}_P^{e_k} \right|_{,s} = \frac{\sum_{k=1}^{nae} \mathbf{A3}_P^{e_k} \mathbf{A3}_P^{e_k}{}_{,s}}{\left| \sum_{k=1}^{nel} \mathbf{A3}_P^{e_k} \right|} \tag{5.27}$$

It should be remembered that *nae* is the number of adjacent elements to node $P$, and $\mathbf{A3}_P^{e_k}$ is the normal vector to element $e_k$ at node $P$.

The proof of the expression which gives the derivative of the norm of a vector, can be found in Appendix A.3. The derivative of the unit normal vector to an element $e_k$ at node $P$ of natural coordinates $\xi = \xi_a$, $\eta = \eta_a$ and $\zeta = 0$ is given by

$$\mathbf{A3}_{P,s}^{e_k} = \left. \frac{(\mathbf{x}_{,\xi} \times \mathbf{x}_{,\eta})_{,s} \, |\mathbf{x}_{,\xi} \times \mathbf{x}_{,\eta}| - (\mathbf{x}_{,\xi} \times \mathbf{x}_{,\eta}) \, |\mathbf{x}_{,\xi} \times \mathbf{x}_{,\eta}|_{,s}}{|\mathbf{x}_{,\xi} \times \mathbf{x}_{,\eta}|^2} \right|_{\substack{\xi=\xi_a \\ \eta=\eta_a \\ \zeta=0}} \tag{5.28}$$

where, for each element $e_k$ with $n_e n$ nodes,

$$\left. \mathbf{x}_{,\xi s} \right|_{\zeta=0} = \sum_{b=1}^{n_{en}} N_{b,\xi} \, \mathbf{x}_{b,s} \tag{5.29}$$

$$\left. \mathbf{x}_{,\eta s} \right|_{\zeta=0} = \sum_{b=1}^{n_{en}} N_{b,\eta} \, \mathbf{x}_{b,s} \tag{5.30}$$

The derivative of a cross product and the derivative of the length of a vector are given in Appendices A.4 and A.3, respectively.

The fact that all contributions of adjacent elements have to be taken into account in the computation of the derivative of the director vector at a node, will have important consequences in sensitivity analysis. A structural optimization problem on a patch of bilinear shell elements, as shown in Figure 5.1.a, whit the $z$-coordinate of the central node considered as design variable, is analyzed.

A positive increment of the design variable is considered, as illustrated in Figure 5.1.b, where not only the position of central node $P$ changes out of the plane of the adjacent elements, but also the direction of the director vector at that node may vary. The element normals at $P$ in the modified design have been denoted by $\mathbf{A3}_P^{e_k*}$ and the director vector at this node by $\mathbf{A3}_P^*$.

As a direct consequence, the geometry of the elements sharing this central node $P$ will change. Apparently, this has no influence on the rest of elements of

the patch which do not share this central node. However, the change in the position of the central node makes the normal vectors at the other nodes of the adjacent elements change. Since these normal vectors are a contribution in the calculation of the *averaged* director vector at those nodes, the director vector of all nodes of the elements sharing the central node $P$ (in the Figure $e_k$, $k = 1, ...4$) may vary. As it was explained in Section 3.3, the director vectors, together with the nodal coordinates and nodal thicknesses, define the geometry of the element. Therefore, geometry of elements sharing these nodes will also be modified in the optimization process, even though they are not sharing the central node.

If at certain node $P$ the director vector changes, then the other two vectors completing the director vector coordinate system may also vary. The derivative of vector $\mathbf{A1}_P$ is given by

$$\mathbf{A1}_{P,s} = \frac{(\mathbf{l} \times \mathbf{A3}_P)_{,s} \left|\mathbf{l} \times \mathbf{A3}_P\right| - (\mathbf{l} \times \mathbf{A3}_P) \left|\mathbf{l} \times \mathbf{A3}_P\right|_{,s}}{\left|\mathbf{l} \times \mathbf{A3}_P\right|^2} \qquad (5.31)$$

Lastly, the derivative of $\mathbf{A2}_P$ is

$$\mathbf{A2}_{P,s} = \frac{(\mathbf{A3}_P \times \mathbf{A1}_P)_{,s} \left|\mathbf{A3}_P \times \mathbf{A1}_P\right| - (\mathbf{A3}_P \times \mathbf{A1}_P) \left|\mathbf{A3}_P \times \mathbf{A1}_P\right|_{,s}}{\left|\mathbf{A3}_P \times \mathbf{A1}_P\right|^2}$$

$$(5.32)$$

It should be remarked that, although the vectors $\mathbf{A1}_P$, $\mathbf{A2}_P$ and $\mathbf{A3}_P$ are normalized, the magnitude of their derivatives will in general be different from one.

## 5.3 Analytical sensitivity analysis for the DSG shell element

In Section 3.12, the DSG concept was applied to a Reissner Mindlin shell element. The main idea of the method is the computation of modified strain components free of parasitic parts. These distributions are obtained by interpolation of the correspondent strain gaps.
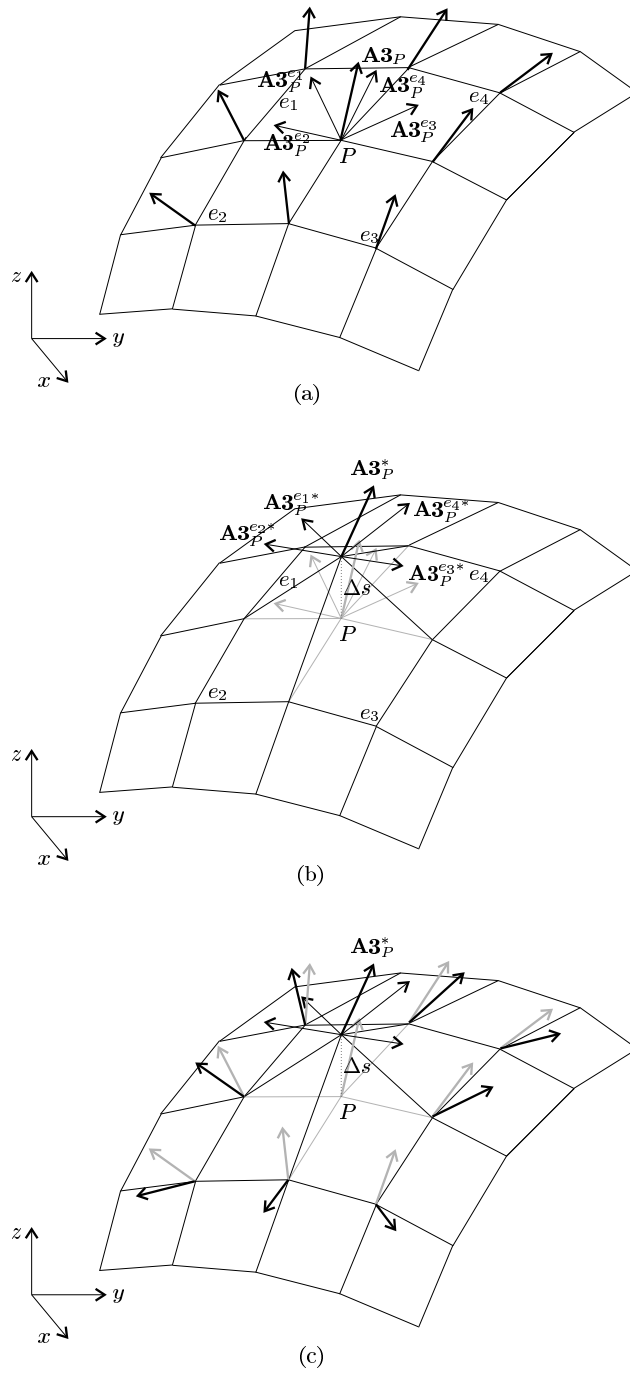
Figure 5.1: Patch of bilinear shell elements in a shape optimization problem: (a) initial configuration; (b) and (c) modified configuration (denoted with $*$) considering an increment $\Delta s$ in the $z$-coordinate of the central node $P$.

It was shown that the only modification with respect to standard displacement formulation lies on the strain-displacement operator. As a consequence, sensitivity analysis for the DSG shell element is done in a similar manner as for the displacement element. The only difference consists of the differentiation of the modified strains computed by the DSG method.

The DSG modified strains are given in equations (3.79) and (3.80). Differentiation of these strains with respect to design variable $s$ is given by

$$\varepsilon_{\xi\zeta}^{\mathrm{DSG}},_s = \left(\frac{\partial \Delta w_{\xi\zeta}}{\partial \xi}\right)_{,s} = \sum_a N_{a,\xi}\left(\Delta w_{\xi\zeta}^a\right),_s \tag{5.33}$$

$$\varepsilon_{\eta\zeta}^{\mathrm{DSG}},_s = \left(\frac{\partial \Delta w_{\eta\zeta}}{\partial \eta}\right)_{,s} = \sum_a N_{a,\eta}\left(\Delta w_{\eta\zeta}^a\right),_s \tag{5.34}$$

Note that shape functions do not depend on design variables. Derivatives of discrete strain gaps with respect to design variable $s$ are obtained differentiating the corresponding expressions given in Section 3.12. That is,

$$\Delta\hat{w}_{\xi\zeta}^a,_s = \int_{\xi=-1}^{\xi_i} \varepsilon_{\xi\zeta,s}\, d\xi \bigg|_{\substack{\eta=\eta_a \\ \zeta=0}} \tag{5.35}$$

$$\Delta\hat{w}_{\eta\zeta}^a,_s = \int_{\eta=-1}^{\eta_a} \varepsilon_{\eta\zeta,s}\, d\eta \bigg|_{\substack{\xi=\xi_a \\ \zeta=0}} \tag{5.36}$$

In Section 3.12, it was shown that the discrete shear gap of a node lying on the reference edge associated to that gap was zero. The reason was that the upper and lower limits of the integral domain coincide and thus its result vanishes. In the optimization process, nodes may change their global position, but their curvilinear coordinates in the parent domain remain constant. Consequently, derivatives of a discrete shear gap of a node lying on the related reference edge vanishes too.

The procedure to obtain derivatives of the strain components $\hat{\varepsilon}_{ij}$ with respect to design variables is already explained in Section 5.2.1.2 (see equation (5.8)), because their computation is also required for sensitivity analysis of standard displacement shell elements. These derivatives can be computed analytically. Moreover, integration in (5.35) and (5.36) can be also performed analytically. Consequently, the computation of analytical sensitivities for the DSG finite element formulation does not increase computational cost with respect to standard displacement formulation. This is a decisive aspect for the efficiency of DSG method and for its suitability for optimization problems.

## 5.4 Analytical differentiation of elemental load vector

In equation (5.1) it can be seen that derivatives of the load vector with respect to design variables are also required in sensitivity analysis. These derivatives will vanish, when a modification of the structural design does not affect the value of the external load or its distribution on the structure, as in the case of a single load at a fixed point in any direction of the global coordinate system.

Load vectors are the same for the displacement formulation and for the DSG method. The reason for this is that the difference between both approaches lays in the definition of the element strains, but in both cases the geometrical interpolation remains the same. Derivatives of elemental load vector with respect to design variables are also the same for both formulations.

The load self-weight explained in Section 3.10 is a design-dependent load. The load magnitude may be changed because the volume of the structure may vary. In order to compute the sensitivity of the load vector, (3.72) has to be differentiated with respect to the design variable $s_i$. The elemental force vector of consistent nodal forces is given by

$$\mathbf{f}^e = \iiint_{V_e} \sum_a \mathbf{N}_a^T(\xi, \eta, \zeta) \cdot \mathbf{b} \ dV \tag{5.37}$$

where $\mathbf{N}_a$ is given by (3.19) and $\mathbf{b}^T = \{b_x, b_y, b_z\}$ is the vector of volume forces expressed in the global Cartesian system. Thus, its derivative with respect to design variable $s$ is given by

$$\mathbf{f}^e = \int_{-1}^{1} \int_{-1}^{1} \int_{-1}^{1} \sum_a \left( \mathbf{N}_{a,s}^T \cdot \mathbf{b} \ J \ + \mathbf{N}_a^T \cdot \mathbf{b}_{,s} \ J \ + \mathbf{N}_a^T \cdot \mathbf{b} \ J_{,s} \ \right) d\xi d\eta d\zeta \tag{5.38}$$

where $\mathbf{N}_{a,s}$ is computed according to (5.10) and the derivative of the determinant of the Jacobian matrix with respect to the design variable is given by (5.25).

## 5.5 Some remarks about sizing

At this point some remarks about sizing and shape optimization should be made. In this chapter nodal coordinates, director vectors and nodal thickness have been

considered to be a function of $s$. This would be the most general case of shape optimization. However, in the case of sizing optimization nodal thickness is the typical design variable, while nodal positions and director vectors remain unchanged throughout the optimization process. Therefore, in the particular case of sizing optimization

$$\mathbf{x}_{P,s} = 0 \qquad \text{and} \qquad \mathbf{A3}_{P,s} = 0 \qquad (5.39)$$

A brief review of the different derivatives explained until here, shows the important consequences derived from this fact. The computation of the derivatives of both element stiffness matrix and load vector are significantly simplified.

The first immediate consequence of (5.39) is that derivatives of director vector system will also vanish. Therefore, the derivative of the shape function matrix $\mathbf{N}_a$ and of the Jacobian matrix, given in (5.10) and (5.15) respectively, will become simpler. At first, it may appear strange that the derivative of the Jacobian matrix is not vanishing for sizing problems. Generally, a shell element is two-dimensional and by changing its thickness, we are changing a property, but not its geometry. However, one may remember that in this case a 3D formulation of a shell element is considered. Therefore, thickness is not just a property, but defines actually the element shape. For this reason, the derivative of the Jacobian matrix will, in general, not vanish, if thickness at any element node is varying, but it will be much simpler than for the case of shape optimization. As a consequence, the computation of $\mathbf{J}^{-1}{}_{,s}$, $\mathbf{G}_{,s}$ and $J_{,s}$ (see (5.19), (5.22) and (5.25)) is also simplyfied.

In the case of $\boldsymbol{\Theta}$, the transformation matrix between global and local Cartesian systems, its derivative will vanish. The reason is that, as derivatives of director vector coordinate systems at nodes vanish, so do derivatives of local Cartesian systems. Therefore, the relation between global and local Cartesian system remains the same, because none of them changes in the optimization process.

Derivatives of external loads depend on the type of load considered. In sizing, the most intuitive case may seem differentiation of self weight load vector. Element weight depends on element volume, and this depends on element thickness. So, it seems clear that the magnitude of the self weight load vector will change with thickness variations. However, it should be noted that even in the case of sizing, not only the magnitude of the consistent nodal forces may change, but also the consistent nodal moments.

Even though if the magnitude of the load per unit of surface remains constant, derivatives of surface loads may not vanish in the case of sizing. The reason

is that surface loads are applied on the top or bottom face of the shell and a change in the thickness implies in general that these areas are becoming smaller or larger. Therefore, derivatives of consistent forces and moments will, in general, not vanish.

Even though, in general, derivatives of external volume and surface forces will not vanish for the case of sizing optimization, its computation will be much easier than for the case of shape optimization.

At this point, it becomes clear that analytical sensitivity analysis in shape optimization is much more complex than in sizing.

## 5.6   A particular case of adjoint sensitivity analysis

To consider a large number of design variables in a shape optimization problem means to enlarge the set of admissible designs, where the optimum is searched. This topic and related ones are treated in Chapter 7. An important aspect to consider in optimization problems with many design variables is the use of adjoint techniques in sensitivity analysis. As explained in Section 4.3.2, in these cases the computational cost of sensitivity coefficients is significantly lower than in the direct approach.

In optimization problems where strain energy is to be minimized and no constraints are considered, adjoint sensitivity analysis can be performed in a particular way, which is presented in this section.

An objective function $\psi(\mathbf{s}, \mathbf{d})$ is considered, where, as before, $\mathbf{s}$ is the vector of design variables and $\mathbf{d}$ is the vector of degrees of freedom. The variation of the objective function is given by

$$\delta\psi = \frac{\partial\psi}{\partial\mathbf{s}} \cdot \delta\mathbf{s} + \frac{\partial\psi}{\partial\mathbf{d}} \cdot \delta\mathbf{d} \tag{5.40}$$

Normally, if we take into account that displacements depend on design variables, i.e. $\mathbf{d}(\mathbf{s})$, equilibrium is automatically implicit. However, if $\mathbf{d}$ and $\mathbf{s}$ are considered as independent variables, in order to ensure equilibrium, the equilibrium equation has to be imposed as an additional constraint. The equilibrium equation is of the form

$$g(\mathbf{s}, \mathbf{d}) = 0 \tag{5.41}$$

And its variation is given by

$$\frac{\partial g}{\partial \mathbf{s}} \cdot \delta \mathbf{s} + \frac{\partial g}{\partial \mathbf{d}} \cdot \delta \mathbf{d} = 0 \tag{5.42}$$

If the equilibrium equation is considered as a constraint, its variation can be added to the variation of objective function, as an additional term multiplied by the adjoint parameter $\lambda$. That is,

$$\delta f = \frac{\partial \psi}{\partial \mathbf{s}} \cdot \delta \mathbf{s} + \frac{\partial \psi}{\partial \mathbf{d}} \cdot \delta \mathbf{d} + \lambda \left( \frac{\partial g}{\partial \mathbf{s}} \cdot \delta \mathbf{s} + \frac{\partial g}{\partial \mathbf{d}} \cdot \delta \mathbf{d} \right) \tag{5.43}$$

Rearranging terms, it can be obtained

$$\delta \psi = \left( \frac{\partial \psi}{\partial \mathbf{s}} + \lambda \frac{\partial g}{\partial \mathbf{s}} \right) \cdot \delta \mathbf{s} + \left( \frac{\partial \psi}{\partial \mathbf{d}} + \lambda \frac{\partial g}{\partial \mathbf{d}} \right) \cdot \delta \mathbf{d} \tag{5.44}$$

Because of (5.42), expression (5.44) is valid for all $\lambda$. Now, $\lambda$ is chosen such that

$$\frac{\partial \psi}{\partial \mathbf{d}} + \lambda \frac{\partial g}{\partial \mathbf{d}} = \mathbf{0} \tag{5.45}$$

and thus

$$\lambda = -\frac{\partial \psi}{\partial \mathbf{d}} \cdot \left( \frac{\partial g}{\partial \mathbf{d}} \right)^{-1} \tag{5.46}$$

Substituting (5.46) in expression (5.44), the variation of the objective function $\psi$ is given by

$$\delta \psi = \left[ \frac{\partial \psi}{\partial \mathbf{s}} - \frac{\partial \psi}{\partial \mathbf{d}} \cdot \left( \frac{\partial g}{\partial \mathbf{d}} \right)^{-1} \cdot \frac{\partial g}{\partial \mathbf{s}} \right] \delta \mathbf{s} \tag{5.47}$$

As it can be seen, under these circumstances the variation (5.44) of the objective function depends only on the variation of the design variables.

It should be now considered that the objective function to be minimized is the strain energy. In the discrete case, strain energy is given by

$$\psi = \frac{1}{2} (\mathbf{d})^T \cdot \mathbf{K} \cdot \mathbf{d} \tag{5.48}$$

and the equilibrium equation is given by

$$g = \mathbf{K} \cdot \mathbf{d} - \mathbf{F} \tag{5.49}$$

91

Note that as $\mathbf{d}$ and $\mathbf{s}$ are independent variables, no chain rule is applied.

Derivatives of objective function (5.48) with respect to design variables and the displacements are

$$\frac{\partial \psi}{\partial \mathbf{s}} = \frac{1}{2}\mathbf{d}^T \cdot \frac{\partial \mathbf{K}}{\partial \mathbf{s}} \cdot \mathbf{d} \qquad (5.50)$$

$$\frac{\partial \psi}{\partial \mathbf{d}} = \mathbf{K} \cdot \mathbf{d} \qquad (5.51)$$

Analogously, derivatives of the equilibrium equation (5.49) with respect to design variables and displacements are given by

$$\frac{\partial g}{\partial \mathbf{s}} = \frac{\partial \mathbf{K}}{\partial \mathbf{s}} \cdot \mathbf{d} - \frac{\partial \mathbf{F}}{\partial \mathbf{s}} \qquad (5.52)$$

$$\frac{\partial g}{\partial \mathbf{d}} = \mathbf{K} \qquad (5.53)$$

Substituting (5.50), (5.51), (5.52) and (5.53) in (5.47), and taking into account the symmetry of $\mathbf{K}$, we obtain

$$\frac{\psi}{s} = \frac{1}{2}\mathbf{d}^T \cdot \frac{\partial \mathbf{K}}{\partial \mathbf{s}} \cdot \mathbf{d} - (\mathbf{K} \cdot \mathbf{d})^T \cdot \mathbf{K}^{-1} \cdot \frac{\partial \mathbf{K}}{\partial \mathbf{s}} \cdot \mathbf{d} - \frac{\partial \mathbf{F}}{\partial \mathbf{s}} = -\frac{1}{2}\mathbf{d}^T \cdot \frac{\partial \mathbf{K}}{\partial \mathbf{s}} \cdot \mathbf{d} - \frac{\partial \mathbf{F}}{\partial \mathbf{s}} \quad (5.54)$$

Variation $\delta\psi$ can be computed by adding the different contributions of this expression at element level. That is,

$$\frac{\partial \psi}{\partial s} = \sum_e \frac{\partial \psi^e}{\partial s} \qquad (5.55)$$

where

$$\frac{\partial \psi^e}{\partial s} = -\frac{1}{2}\mathbf{d}^{eT} \cdot \frac{\partial \mathbf{k}^e}{\partial \mathbf{s}} \cdot \mathbf{d}^e - \frac{\partial \mathbf{f}^e}{\partial \mathbf{s}} \qquad (5.56)$$

Thus, in this particular case, adjoint sensitivity analysis is very simple to implement and requires low computational time.

# Chapter 6

# Influence of Locking in Structural Optimization.

## 6.1   Introduction

In structural shape optimization, the optimization algorithm takes decisions about improving the actual design based on information provided by finite element analysis and sensitivity analysis. Finite element analysis is used to evaluate objective function and constraints. Sensitivity analysis computes derivatives of the objective function and constraints required by gradient-based optimization algorithms. Therefore, the quality of the underlying structural and sensitivity analysis is of crucial importance. Two main factors determine the quality of these analyses.

The first factor is the technique of sensitivity analysis. Discussion about the different sensitivity analysis techniques for structural optimization is given in Chapter 4. The analytical technique appears as the more suitable for obtaining highly reliable and accurate sensitivity coefficients.

The second factor which determines the quality of the structural and sensitivity analyses is the underlying finite element formulation. In the particular case of shells, it is well-known that standard displacement finite elements with Reissner-Mindlin kinematics suffer from so-called locking phenomena, leading to a severe overestimation of bending stiffness, i.e. an underestimation of displacements, and thus a wrong modeling of the load carrying behavior of thin shells (see e.g. Bathe (1996) and Zienkiewicz and Taylor (2000b)). As a consequence, information about the objective function and constraints forwarded

to the optimization algorithm is altered. Consequently, the optimization algorithm will solve a different optimization problem than the intended one, and the optimized design will, in general, be different than the *real* optimum. Moreover, it may occur that the optimum obtained is not even in the real feasible domain. That is, the solution obtained from the optimization procedure is not even in the group of admissible solutions.

It should be remarked that this effect is independent of the technique used for sensitivity analysis. If the underlying finite element formulation suffers from locking phenomena, sensitivity coefficients are no longer reliable.

In the present chapter, the significance of a reliable finite element formulation in the optimization process is discussed. Particularly, the effects of locking on shape optimization of shells are studied through numerical experiments. Optimization results of a standard displacement shell formulation are compared with those obtained with DSG shell elements (Bletzinger et al., 2000), avoiding transverse shear locking. The shell element formulations used herein are explained in detail in Chapter 3. The sensitivity analysis by the analytical approach is explained in Chapter 5 for both formulations. It is shown that locking phenomena may affect the optimum not only quantitatively, but also qualitatively.

## 6.2   Shell of revolution with parabolic generatrix

The following example illustrates the differences between standard displacement method and DSG formulation in an optimization process, where displacements are to be minimized. The structure considered is a thin shell of revolution with parabolic generatrix and a hole at the top, as shown in Fig. 6.1. It is clamped at the lower boundary, subjected to a crown load and it is discretized by 187 bilinear elements. The objective is to minimize the vertical displacement at the crown. The height of the structure is taken as the only design variable, while top and bottom radii remain constant.

For the case of displacement elements, the optimal design has a height of 133.8 cm and the crown displacement is $-5.55 \times 10^{-5}$ cm. However, for the case of DSG elements, the height of the optimal design is 167.9 cm and the displacement is $-6.47 \times 10^{-5}$ cm. In Figure 6.2, the optimal designs obtained with both formulations are depicted. Figure 6.1 shows the vertical displacement
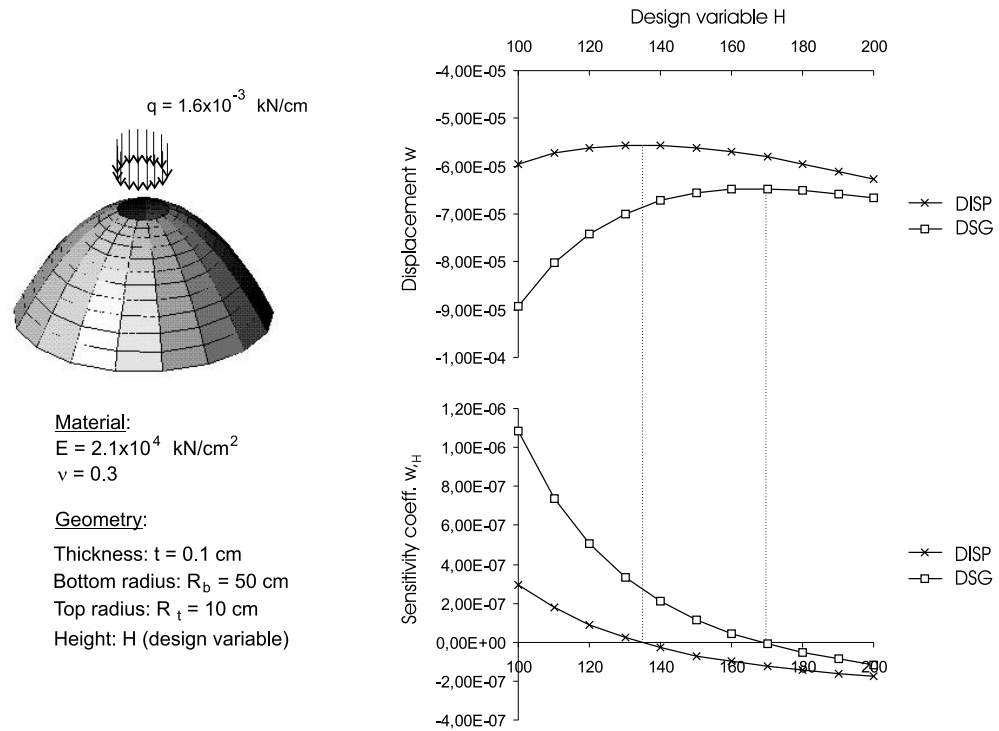
Figure 6.1: Paraboloidal shell, problem data. Vertical displacement $w$ and sensitivity coefficient $w,_H$ versus design variable $H$

and its sensitivity coefficients at the crown for different heights of the structure, computed with both standard displacement elements and with DSG elements. Due to locking, sensitivity coefficients obtained with the standard displacement formulation provide false information for the optimization algorithm. It is remarkable that in the domain between the two optimal solutions, the sensitivities have different signs.

For a relatively shallow cupola, structural behavior is dominated by bending, while for a relatively high cupola, it is dominated by membrane action. Due to transverse shear locking, standard displacement elements significantly overestimate bending action. As a result, the optimization process interpretes bending to be favorable. It is therefore no surprise that the 'optimal' design obtained in this case involves more bending action than the result when applying DSG elements, alleviating locking effects. We may conclude that standard displacement formulation misinterpretes the structural behaviour and, therefore, the optimization process yields wrong optima.

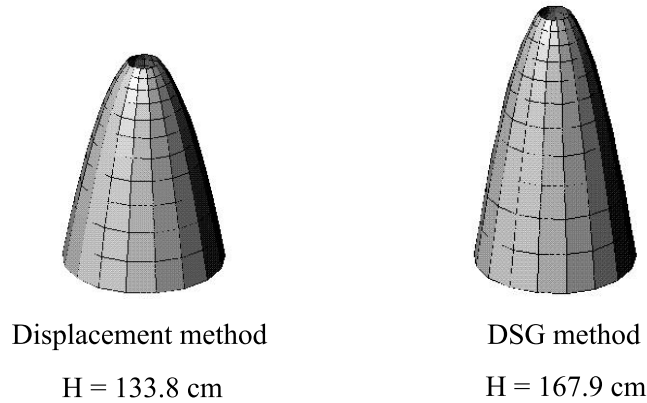It can be anticipated that for more complex problems this simple and obvious

Displacement method               DSG method

H = 133.8 cm                      H = 167.9 cm

Figure 6.2: Optimal results obtained with both formulations.

mechanism will lead to unidentifiable mistakes in results.

## 6.3 Roof shell with two parabolic generatrices

This example is used to demonstrate the influence of finite element technology on the evaluation of objective functions and stress constraints, and its consequences for the final design. The considered structure is a roof with rectangular plan and uniform constant thickness $t = 0.1$ m. With its slenderness of approx. 100, it can be considered that the shell is relatively thin. Its geometry is taken from Ramm et al. (1993) and it is reproduced in Fig. 6.3. The shell has double symmetry with respect to $xz$- and $yz$-coordinate planes. Edges at $y = 3$ m and $y = -3$ m are free, while edges at $x = 6$ m and $x = -6$ m are supported by diaphragms. These diaphragms prevent movements in their plane, but offer no resistance to movements normal to this plane ($x$-direction) or to rotations.

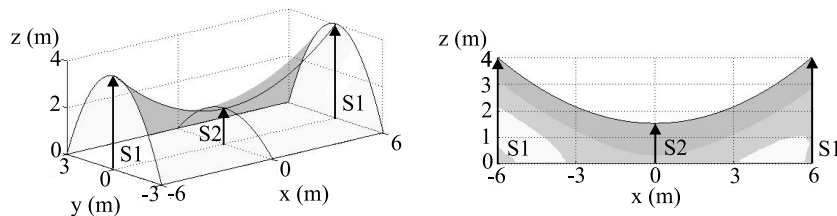Material properties are $E = 30000$ MPa, $\nu = 0.2$ and $\gamma = 24$ kN/m$^3$.



Figure 6.3: Roof shell, problem data.

96

Two design variables are considered: the height at the center of the edges $x = 6$ m and $x = -6$ m ($S1$) and the height at the center point of the structure ($S2$). Thickness remains constant. It should be remarked that double symmetry is preserved in the optimization process. The fact that only two design variables are considered allows us to represent the objective function graphically as a response surface. This is very instructive, since a comparison between the objective functions obtained with both formulations can be easily made and optimal designs obtained can be better understood (see Myers and Montgomery (2001)). A lower bound is imposed for both design variables, which have to be greater than zero. No upper bound is considered.

The structure is subjected to self-weight. This is a design dependent load because variations on design in the optimization process yield variations on the volume of the structure, and thus on the load. Therefore, derivatives of the load with respect to the design variables must be taken into account in the pseudo-load vector of sensitivity analysis. It should be remarked that this load case is different than the one considered by Ramm et al. (1993).

The structure is discretized with a mesh of 576 linear triangular (T1) elements and 325 nodes. When linear triangular elements are used, standard displacement formulation does not suffer from membrane locking but from transverse shear locking. Full integration has been used for standard displacement elements. It should be noted that reduced integration for T1 displacement elements, although frequently used, does not remove transverse shear locking completely.

### 6.3.1 Minimization of strain energy

First, strain energy is chosen as objective function. No stress constraints are considered, assuming that the structure is sufficiently reinforced. Fig. 6.4 represents a contour plot of the approximate response surface as a function of design variables $S1$ and $S2$, for the standard displacement formulation and for the DSG formulation. Each point of the contour plot represents the strain energy for a certain geometry of the structure. As the analytical expression of the strain energy is not avaliable as a function of the design variables, this response surface is approximated by computing the value of the strain energy for many different designs and by interpolating a surface with these values. Though being just an approximation, this response surface gives a fairly good picture of the structural stiffness for different designs.

STANDARD DISPLACEMENT FORMULATION                    DSG FORMULATION

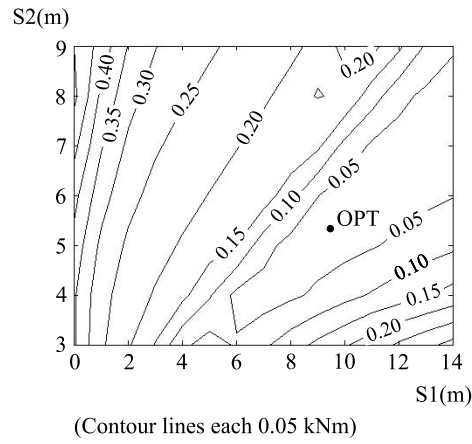(Contour lines each 0.01 kNm)                    (Contour lines each 0.05 kNm)
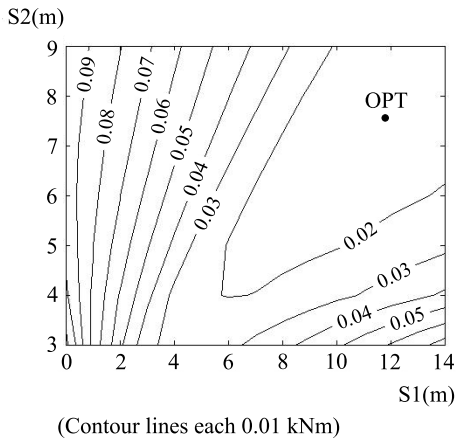
Figure 6.4: Contour plots of the strain energy (kNm) as a function of the design variables $S1$ and $S2$, computed with standard displacement elements and DSG elements.

As mentioned before, the standard displacement formulation suffers from transverse shear locking and this results in an overestimation of the bending stiffness of the structure. Thus, the computed strain energy is significantly underestimated, particularly for those designs involving more bending action. As a result, the standard displacement formulation yields an objective function significantly different from the one of a locking free formulation. Thus, the optimization problem is been altered because the finite element analysis and the sensitivity analysis are providing wrong information to the optimization algorithm.

Fig. 6.5 represents the longitudinal cross section of the corresponding optimal designs. Both are anticlastic surfaces and the values of design variables for each case are given in Table 6.1. Regardless of significant differences between objective functions produced by both formulations, it can be observed that the principal types of design of the optima are similar. The reason why both formulations yield similar results is that these optimal designs are working principally in a membrane state. Due to the non-existence of a vertical tangent at the free edges, there is always going to be some bending action at the boundaries. But for these optimal designs, membrane forces are significantly more important. As a consequence, the shear locking phenomenon does not significantly alter stiffness of the structure.

However, it should be remarked that the consideration of additional constraints, like limitations in volume or stresses, may accentuate differences between both optimal designs.
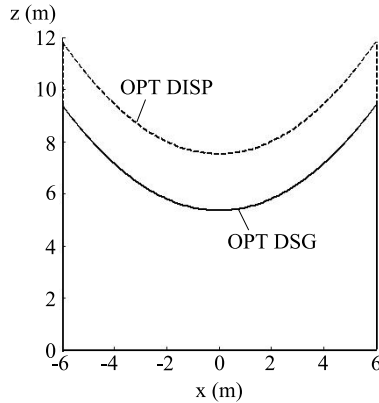
Figure 6.5: Optimal designs with respect to minimization of strain energy, computed with standard displacement elements (DISP) and DSG elements.

Table 6.1: Convergence of optimal designs

| Number of elements | STANDARD DISP | | | DSG | | |
|---|---|---|---|---|---|---|
| | S1 (m) | S2 (m) | Strain energy (kNm) | S1 (m) | S2 (m) | Strain energy (kNm) |
| 576 | 11.86 | 7.52 | 0.0159 | 9.43 | 5.35 | 0.0228 |
| 1600 | 11.41 | 6.87 | 0.0182 | 8.98 | 5.19 | 0.0238 |
| 6400 | 10.21 | 6.04 | 0.0209 | 8.80 | 5.14 | 0.0245 |
| 14400 | 9.97 | 5.70 | 0.0221 | 8.79 | 5.14 | 0.0246 |

In Table 6.1, convergence of optimal designs computed with both formulations and different meshes are shown. By refining the mesh, slenderness of the elements is reduced and, therefore, shear locking decreases. As a consequence, the optimal design obtained with displacement elements will tend to the one obtained with the DSG formulation. Reduction of the shear locking effect for finer meshes can also be noticed in the computed strain energy. Overestimation of bending stiffness by the standard displacement formulation is no longer so dramatic. As a consequence, deformations converge to those obtained by a locking free formulation, and so does the computed strain energy.

It should be remarked that convergence is very slow and mesh refinement is not a solution to the locking problem.

Even though this may seem as a simple example, there are a few interesting factors, which play an important role in determination of the optimal design and help understanding the strain energy plot of the DSG formulation, alleviating

99

transverse shear locking.

First, in a barrel vault under a vertical load and with the above considered boundary conditions some bending action is going to appear at the free edges (see Flügge (1973)). The optimal load-carrying behaviour of a shell structure is membrane action, since material is optimally utilized in this case. Thus, presence of bending reduces the stiffness of the structure.

It is known that, if the intersection of the shell surface with a plana parallel to $yz$-coordinate plane has a vertical tangent at these free edges, the bending action at these edges is reduced. The cross section of the considered structure is a parabola, whose height depends on the design variables. The higher the structure is, the more the tangent at the free edges tends to be vertical and, therefore, the smaller these bending moments are going to be. For that reason, higher values of design variables lead to a structural behaviour at free edges more suitable to membrane theory.

Second, the fact that the structure is subjected to self-weight will make design variables decrease. Obviously, smaller values of the design variables yield designs with less volume and, therefore, less weight. Thus, the load acting on the structure will be smaller.

Third factor of major importance is structural stiffness. This is related to dimensions and amount of material. It is important to remark that this factor essentially differs from the aforementioned first factor. Here we are not refering to the relation between membrane stresses and bending action, but to those geometrical properties that have an influence on structural stiffness.
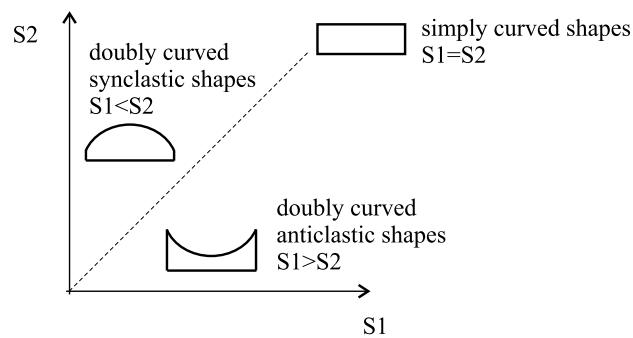


Figure 6.6: Principal types of designs depending on the values of the design variables

However, not only the amount of material determines structural stiffness. The principal type of design is decisive. Fig. 6.6 qualitatively represents different

100

types of shapes obtained for different values of the design variables. When both design variables are equal, simply curved structures are obtained. When they are not equal, doubly curved structures are obtained. These can be anticlastic designs, in the case that $S1 > S2$, or synclastic designs, if $S1 < S2$.

The type of curvature of the surface has a direct influence on load carrying behaviour of the structure. In order to explain the differences between the load carrying behaviour of the different principal types, we consider three different principal types of structures. These three different structures are chosen such a way, that their weight is the same. Thus, they are carrying the same load, but in a different way.

Fig. 6.7 presents the initial configuration of the structures and the deformed configuration. In order to avoid the effect of shear locking, the analysis has been performed with DSG elements.

The synclastic and the simply curved structure are significantly more flexible than the anticlastic design. In both cases, the lower edges, which are free, show high tensile stresses and large deformations.

In the synclastic design, most part of the volume and, therefore, of the acting load, is located at the center of the structure, far away from the supports at the curved edges. In addition, these edges are smaller than for the other two designs, so the supporting area is also smaller. As a consequence, corner areas suffer also from high bending moments. This can be noticed in the figure, where the edges are significantly deformed.

In addition to high tensile stresses at the lower edges, the simply curved design suffers from high bending moments at this area and also at the top of the structure. In this case, deformations at the lower edges are slightly smaller than in the synclastic shape.

In the anticlastic design membrane tensile stresses at the lower edges are significantly reduced as compared to synclastic and simply curved designs. Moreover, bending moments are also smaller. It can be noticed that displacements of the structure are one order of magnitude smaller than in the preceding cases. Thus, the anticlastic shape is the stiffest design for the given boundary conditions and load case. Different factors contribute to this fact. A good part of the volume of the structure is located close to the diaphragms, and the supporting edges are longer than in the other two cases. Furthermore, the opposite curvatures optimize traction and compression trajectories, minimizing bending action.

It can be recognized, that the underlying mechanics behind the problem are crucial for understanding the optimal design.
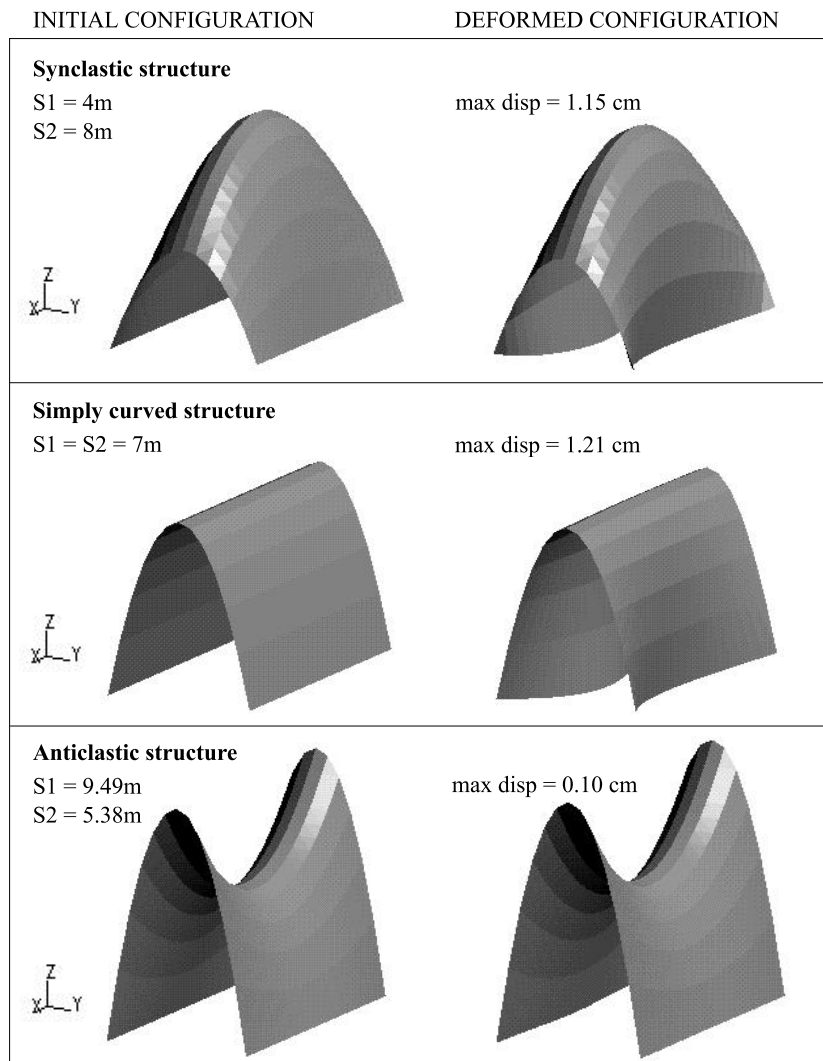
INITIAL CONFIGURATION          DEFORMED CONFIGURATION

**Synclastic structure**
S1 = 4m
S2 = 8m                        max disp = 1.15 cm

**Simply curved structure**
S1 = S2 = 7m                   max disp = 1.21 cm

**Anticlastic structure**
S1 = 9.49m
S2 = 5.38m                     max disp = 0.10 cm

Figure 6.7: Initial configuration and deformed configuration of different principal designs of identical weight, computed with DSG elements.

## 6.3.2 Minimization of weight

In this case, minimization of structural weight is studied. Fig. 6.8 represents the contour plot of weight as a function of the design variables $S1$ and $S2$. Weight of the structure does not depend on the finite element formulation used, because stiffness does not play any role. If no stress constraint were imposed, the optimal design would be trivially for $S1 = 0$ and $S2 = 0$, that is, a plate.

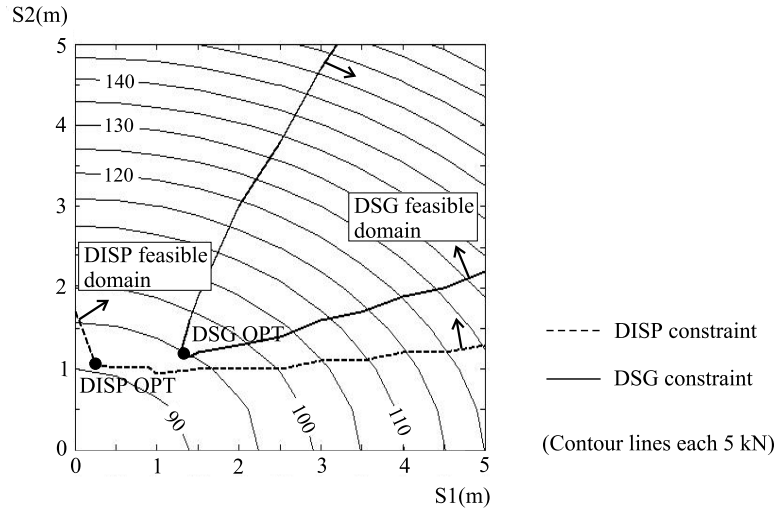However, as in engineering applications stresses are usually limited by material

Figure 6.8: Contour plots of weight (kN) as a function of design variables $S1$ and $S2$, and stress constraints computed with standard displacement elements (DISP) and DSG elements.

properties, it is interesting to study the effect of the finite element formulation on the evaluation of stress constraints. In this example, the stress constraint considered limits tensile stresses, since concrete has a low tensile resistance. A typical value for tensile resistance of concrete has been used. Thus,

$$\sigma_1 \leq 3000 \text{ kN/m}^2 \tag{6.1}$$

at upper and lower layers of the shell, where $\sigma_1$ is the primary principal stress. Stresses at upper and lower layers have been computed considering membrane stresses and stresses due to bending at these points. No shear stresses have been considered, since according to the shell theory they vanish at upper and lower layers.

In Fig. 6.8, the constraints for the standard displacement formulation and for the DSG formulation are represented as dashed and solid lines respectively. Arrows point towards the feasible domain, that is, the domain where the maximum tensile stress at any point of the structure is smaller than the prescribed value. Again, we do not have the analytical expression of the constraint curves, but we approximate them by analyzing many structures, studying the maximal value of the traction stress, and determining whether it would be a feasible design or not.

It is easy to notice that feasible domains for both formulations are significantly

103

different. Analogously to the case of strain energy response surface, when the mesh is refined, the feasible domain obtained from the computation with the standard displacement formulation, tends to the one computed with the DSG formulation.

Fig. 6.9 represents the longitudinal sections of optimal designs obtained for both formulations. The difference between these designs is not only quantitative but also qualitative. Moreover, the principal type of design in the case of the standard displacement formulation is wrong. For the DSG formulation, the optimal design is an anticlastic shape, while for the standard displacement formulation it is a synclastic surface, almost a cylinder.
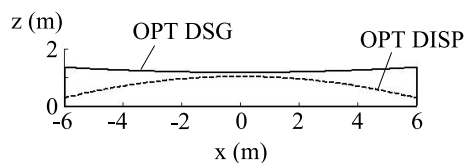


Figure 6.9: Optimal designs with respect to minimization of weight with stress constraints, computed with standard displacement elements (DISP) and DSG elements.

Some important remarks should be made with respect to the optimal designs obtained.

It should be noted that the optimal design obtained with the standard displacement formulation is not even contained in the feasible domain provided by DSG elements, removing the influence of transverse shear locking. As a consequence, in some area of this design the stresses will violate the given constraints. This area is located at lower fibers of the free edges, which exhibit high tensile stresses due to bending. The reason is that the displacement formulation, due to the locking, behaves too stiffly and the computed displacements are underestimated. As a consequence, bending moments are also underestimated and principal stresses are also lower than for a locking-free formulation. Thus, the standard displacement formulation identifies it as a feasible design, while actually it is not.

In this case, the dramatic consequences of locking phenomena on stress constraints can be recognized. It is known that the standard displacement formulation underestimates displacements and leads to errors in stresses, but, in general, no a priori statement can be made about the stresses being lower or higher than those of a locking-free formulation. Particularly, shear stresses suf-

104

fer from strong oscillations. This fact leads to unidentifiable errors in optimal designs.

It is important to remark that, if quadratic elements are chosen, reliable results for stresses are not guaranteed, even though satisfactory results may be obtained for displacements.

# Chapter 7

# Shape Description and Control

## 7.1 Introduction

Structural optimization is a part of a more global design process. Apart from the mechanical requirements inherent to structural optimization, in this global process the designer wants the structure to also fulfill certain shape requirements due to esthetic, utilization or any other reasons. Therefore, when submitting an initial design to an optimization process, the best solution for a designer may not be the design which minimizes the objective function satisfying the constraints, but that which, in addition, satisfies some shape requirements.

At this point, we may perceive a duality in the treatment of designs during a shape optimization process: they are improved based on their mechanical behavior and on the deliberate control of their shape.

In the preceeding chapters, a shell finite element and its sensitivity analysis were studied. This is a tool used to study the mechanical behavior of shell structures and to predict its changes, when the design is modified. In the present chapter the shell structure 'looses' its mechanical properties and is studied from the geometrical point of view, that is, as a surface.

From this geometrical point of view, there are two main factors, which determine the shape of the design: its parametrization and the control of its shape during the optimization process.

In the context of shape optimization, design parametrization means the definition of a design as a function of a set of design variables, which may change during the optimization process yielding modified designs. Design parametrization determines the shape of the optimal design, insofar as it determines the set

of admissible designs. This statement can be illustrated with a simple example. A cylinder with circular cross section is considered, and its radius is defined as the only design variable. As a result of an optimization process one may obtain a cylinder with a different radius, but still with circular cross section. One will not get a cylinder with an elliptic cross section, because the chosen parametrization does not allow it. At this point it may seem intuitive that parametrizations with few design variables may strongly restrict the set of admisible designs, while considering more design variables increases it. However, an advantage of using few design variables is that computational cost of the optimization process is not so high. In the end, the chosen design parametrization is a designer's decision. But still, the designer should be aware that choosing a certain design parametrization, he is already conditioning the optimal design.

The two most common techniques of design parametrization are *CAD-based design parametrization* and *FE-based design parametrization*. In the first one, design variables are chosen among the parameters of an underlying CAD model. In the second one, design variables are related to the finite element mesh of the initial design.

Apart from the design parametrization used, there are other means for the designer to control the shape during the optimization process. The most common is the use of constraints related to geometry. Through these constraints restrictions on certain dimensions of the structure are imposed.

Variable linking is also another way to control design shape. The idea is to link two or more design variables, so that they are no longer independent from each other, but so that their value is related through certain linking coefficients. Typical reasons for the use of linking variables are to attain symmetry or antimetry, to enforce geometrical relations between them, or to restrict the movement of a node to a certain direction. It shoulb be noted that in the present chapter, when speaking about the movement of a node, no reference is made to the displacement due to the action of some loads, but to its movement in sequent iterations of the optimization process that leads to modified designs.

In the last five years, a new type of shape control method has been emerging in shape optimization. This method appears in the context of shape optimization with fluids using FE-based parametrization. The key of the approach is to control the smoothness of the design by controlling its curvature. Two important aspects are to be considered: the computation of a certain curvature measure and the way it is used to control the shape. The first point is not obvious, insofar as real geometries are usually discretized by meshes with $C^0$ continuity across element boundaries. As curvatures are related to second order deriva-

tives, their computation for a discretized geometry is not as easy as it would have been, when its analytical expression were available. Once these curvatures are available there are several ways to control the design shape through them. One method is the addition of a penalization term to the objective function, so that designs with a curvature function very different from the desired one are penalized. This approach is known as regularization, since it allows to get regular solutions to the optimization problem. Other shape control techniques by means of curvatures are: design parametrization choosing curvatures as design variables and the introduction of constraints in curvatures.

In the frame of the present work, shape description and control is focused in shape optimization of shells. In the present chapter, a brief review of the different design parametrization techniques used in shape optimization is presented. Special attention is paid to the comparison between CAD-based parametrization and FE-based parametrization.

A review of the shape control techniques is also presented focusing on regularization techniques used for FE-based parametrization. Shape control by curvature measures is extended to surfaces by a penalization or regularization term added to the original objective function. This regularization term is a function of a curvature measure of the surface. A new approach to compute different curvature measures of a surface discretized by a $C^0$ continuous finite element mesh is presented in detail. Analytical computation of sensitivities of these curvature measures is also explained. This shape control technique is not only applicable to shape optimization of shells, but also to other two-dimensional domains, like boundaries of a 3D solid structure or form finding of membranes.

Several numerical examples illustrate the most important aspects treated in the chapter. Good performance of the proposed method to compute curvature measures of a $C^0$ approximated surface is shown, and the effect of the regularizing term on surfaces is presented. Important differences between CAD and FE design parametrization are illustrated by further examples. Last, simple applications of shape control by regularization with mean curvatures are shown.

## 7.2 Parametrization of design surfaces for shape optimization

In shape optimization, design parametrization deals with selection of design variables and determination of their relation to the current design during the

optimization process. As aforementioned, parametrization of a certain design has significant consequences for the optimization process and result, since it determines the set of admissible designs and influences the cost of the whole optimization process.

There are two main design parametrization methods to be used in a general shape optimization problem: CAD-based parametrization and FE-based parametrization. There are also other parametrization techniques that can be used for solving certain concrete problems.

In the present section, after a brief review of these parametrization techniques, a study of their advantages and disadvantages is presented. This analysis will permit the designer to acknowledge of the implications that the selection of each parametrization approach has.

There are two important aspects to be discussed for each parametrization technique: its flexibility and its cost. Under the concept *flexibility* of a design parametrization technique, both the size of the allowed set of admissible designs and the possibilities of controlling the shape according to designer's desires, are understood. *Cost* of a design parametrization technique we refer to both modeling cost, which is to be "paid" by the designer and to the implications that this technique has in the computational cost of the whole optimization process.

### 7.2.1 CAD based design

In the CAD-based parametrization, design variables are chosen among parameters that determine the underlying CAD model (Bletzinger, 1990; Bletzinger et al., 1991).

The design element concept was introduced in shape optimization by Imam (1982), who applied it to shape optimization of three dimensional structures. Integration of the CAD method in shape optimization for two dimensional problems is done by Braibant and Fleury (1986).

In Computer Aided Geometric Design, a mathematical model of an engineering design or a real object is created through a set of computer applications. This mathematical model is created following a hierarchy of design elements, that is, of geometrical entities. The hierarchy levels, from the simplest one to the most complex one, are

- 0D - design nodes

- 1D - design edges

- 2D - design patches or surfaces

- 3D - design bricks

Design elements of a certain level are created based on those from lower levels. For instance, a design edge is created from two or more design nodes. The shape of each of the design elements can be described in terms of a mathematical function. Typical examples of 1D design elements are 1D Lagrange elements, Bézier-splines and B-splines. Splines are more sophisticated than Lagrange elements because they consider additional nodes to control tangents at beginning and end of the curve. Due to this possibility of controlling tangents locally, splines are especially interesting for shape optimization.

Another type of splines are the non-uniform rational B-splines, so called NURBS. Their advantage with respect to other types of splines is that they are able to represent both standard analytical shapes (e.g. conics) and free form shapes.

In 2D, the simplest element is the 2D Lagrange element, whose mathematical representation is, to this point, well known from the Finite Element method. More sophisticated elements are the Bézier element, which is an extension of the Bézier spline to 2D, and the Coons patch, which is defined univocally by arbitrary edges. One or more patches can be used to describe an initial design of a surface. Geometrical continuity between patches can be enforced by controlling tangents at edges. An introduction to computational geometry for curves and surfaces is given by Davies and Samuels (1996).

Because of the hierarchy of the CAD mathematical model, in CAD-based design optimization, design variables will be finally related to the position of design nodes. It should be noted that these design nodes may determine the position of a certain point of an edge, patch or brick or, in the case of control points in splines, they may determine a tangent.

Once the optimization algorithm provides new values of design variables for the next iteration step, update of the finite element mesh has to be performed. This problem was already reported by Imam (1982). A design element is actually a macroelement which is in turn discretized in finite elements. Associated to the design element is a local system and some shape functions. Coordinates of the finite element nodes can be expressed both in the global coordinate system and in the local coordinate system of the design element to which they belong. An update of design element's shape implies an update of the relation

between its local system and the global one. As this relation has changed and local coordinates of the finite element nodes remain constant, their updated global coordinates can be computed. Therefore, relation between design element and finite element mesh has to be considered as an intermediate step of the optimization loop. This is actually a special type of variable linking.

Nevertheless, it may occur that the current configuration of the design element differs so much from the initial one, that after update the mesh is very distorted. In these cases, remeshing or mesh smoothing is required.

## 7.2.2   FE-based design

In the FE based design, also called CAD-free parametrization, coordinates of finite element nodes are taken as design variables. Although usually the initial design is still defined by a CAD model, in the following iteration steps of the optimization process the relation to this model is lost and the design is determined only by the finite element mesh.

This method is very intuitive when using the Finite Element Method for structural analysis in an optimization process because the same parametrization is used for simulation and optimization. Optimal designs may be mesh-dependent, but this dependency can be controlled with shape control techniques.

In optimization of plane structures or 3D bodies, the position vectors of boundary nodes are generally chosen as design variables. In addition, mesh movement algorithms are used to attain mesh quality (see Bängtsson et al. (2003), for instance). In the case of shell structures, the position vectors of the FE nodes are defined as design variables. Nodal movements can be restricted to a certain direction. In this kind of parametrization, it is very common to restrict these movements to directions normal to boundary edges or surfaces of actual, or initial, design.

In the FE-based technique, the mesh does not need to be updated in each iteration step. However, as in the case of CAD-based optimization, to retain mesh quality in the optimization process is a very important task. One of the proposed approaches is the method of mesh adaptation by metric control (Mohammadi and Pironneau, 1999), which allows the use of meshes with variable connectivities.

The main characteristic of this method is the high number of design variables that are usually considered. This implies both advantages and disadvantages in

the optimization process, which are analyzed in Section 7.2.3. Advices to avoid the disadvantages are also given.

## 7.2.3 Comparison between CAD- and FE-based design parametrization

Nowadays, CAD-based shape optimization is probably the most commonly used design parametrization technique in shape optimization. This parametrization technique allows to describe a design shape as a function of few design variables. The set of admissible designs determined by this parametrization is relatively reduced. Modeling of complex structures can be a problem because of this lack of flexibility. Although multiple design elements can be used, continuity requirements and smooth transitions between adjacent patches can be very difficult or even impossible to achieve. Moreover, the user should know in advance how the final form will approximately look like, in order to use a design patch that has a suitable approximation order. An important advantage in application of the CAD- based optimization is its suitability to produce shapes adequate for manufacturing.

Contrary to the CAD-based, the FE-based parametrization determines a wider set of admissible designs because more design variables are considered. This provides the possibility of finding a 'better' optimum, since the space, where it is looked for, is larger. This is the main advantage of this approach.

The parametrization technique has a direct influence on computational cost, since, in principle, the less design variables are considered to solve a certain optimization problem, the lower is its computational cost. For this reason, the use of a FE based parametrization implies a higher computational cost than the CAD one. Paradoxically, the main advantage of this approach is simultaneously its drawback. This is the reason why very quickly CAD based parametrization captured almost all attention in practical applications of shape optimization. Nevertheless, nowadays the increment of computational power and the use of parallelization techniques have reduced significantly computational time. In addition, the use of adjoint sensitivity analysis is highly recommended to also reduce computational time. As explained in Section 4.3.2, adjoint sensitivity analysis is more efficient than discrete one when the number of active constrains is smaller than the number of design variables. In general this is the case of FE based design.

However, as it was already mentioned, the cost of the parametrization technique

should not be restricted to study its influence on the computational cost of the optimization process. Another important cost that has to be considered is the modeling cost, paid by the designer. This cost is not to be underestimated, especially in designs with complex shapes.

For a simple problem, where the rough shape of the optimal design searched is known, CAD based optimization may be the right choice. However, for more complicated problems, where no previous fixed idea of the aimed optimal design exists, important difficulties arise with defining the underlying CAD model. As aforementioned, in CAD parametrization, the CAD model strongly determines the set of admissible designs and consequently, the optimum. Therefore, selection of a certain underlying CAD model implies very important restrictions for the optimum design, the scope of which is actually unknown. As a consequence, it may occur that more than one CAD model has to be tried to achieve the desired optimum shape. The different CAD models considered may vary in the number of design patches considered, the type of these patches or continuity conditions imposed among patches. Considering a new underlying CAD model implies not only further computational time, since optimization has to be performed again, but, most importantly, modeling time. The designer has to start over the process of designing a new model, taking decisions about design patches and variable linking. This may involve a significant modeling effort.

These difficulties related to modeling can be circumvented using the FE based design parametrization technique. The selection of this parametrization does not imply the inexistence of an underlying CAD model of the initial design considered, since this is the usual model technique used by optimization and structural analysis programs. However, only the initial design is related to the CAD model. After meshing is performed, design variables are related to the finite element mesh. Consequently, designs of subsequent iteration steps of optimization process and, optimum design are dissociated from the underlying CAD model of initial design.

Thus, if FE parametrization is used, the designer needs to create only CAD model for the initial design. Moreover, this CAD model does not need to be as complicated as in the case when CAD parametrization is used. There is no need to use complex patch configurations or to adjust their continuity, as long as their nodes can freely move in the optimization process. To this point, it can be concluded that in general FE design parametrization requires a higher computational cost but a lower modeling cost. This lower modeling cost makes the approach specially suitable for obtaining preliminary designs.

Shape freedom is the main advantage of FE design parametrization because it

114

allows to search for the optimum in a wider set of designs and it is free from the implicit shape constraints of the underlying CAD model. However, this advantage is associated to an effect that may be not desirable: the presence of local optima.

It is known that an optimum obtained from an optimization process may be a local or a global optimum. Unfortunately, there is no immediate way to determine the type of optimum, except by finding a better design. However, the optimization algorithm may get fixed at this local optimum and deliver it as optimal result. This is not a question of the design parametrization technique used, but of the difficulties inherent to mathematical programming in distinguishing local and global optima.

Nevertheless, the selection of a design parametrization technique may have consequences in the presence of more or less local optima. In principle, the more design variables are considered, the more local optima can be expected. The reason for this is that a higher number of design variables may increase the nonconvexity of the objective function and constraints. As FE design parametrization involves more design variables than CAD design parametrization, a higher number of local optimal is to be expected.

The main problem of the FE-based design is that some of these local optima can be wiggly shapes. Moreover, these waves may be mesh-dependent and it is not desirable that the optimum design depends on the coarseness of the mesh used.

This is the main reason why FE-based design parametrization is actually not as widely used. Usually these wiggly shapes are not desired as optimum designs, even though they may have a lower objective function than other smoother shapes, and may satisfy the considered constraints. They are not desired because they are not regular, that is, they are not 'smooth enough' according to designer's preconception. It is legitimated to discard those wiggly designs due to manufacturability, utilization or purely esthetical reasons. But there is an additional problem related to these wiggly shapes, which should not to be underestimated: the mesh distortion. It is well known that mesh distortion may significantly harm the quality of structural and sensitivity analysis. To minimize these consequences, a reliable finite element formulation should be used. This topic is studied in Chapter 6. The issue of retaining mesh quality during the optimization process is very important in both parametrization approaches. The control of the mesh distortion is crucial for obtaining reliable results.

Methods to control regularity of optimum solutions in shape optimization have

been developed, especially in the recent years. Although these methods are intended to get smooth shapes in FE-based design optimization, they can also be applied to control the shape in CAD-based optimization.

In conclusion, the main disadvantages of FE-based parametrization are its high computational cost and the wiggly shapes obtained. In recent years, computational power has significantly increased and shape control methods have been successfully developed. Further, the wide set of admissible designs that this parametrization offers is highly appreciated. Consequently, there has been a return to this kind of parametrization, started by Mohammadi (1997). As most recent research in shape optimization has been done for systems of fluid mechanics, it is also here where this parametrization became more prominent. Successful applications both in 2D and 3D are given by Jameson et al. (1998), Gunzburger et al. (2000), Mohammadi and Pironneau (2001) and Bängtsson et al. (2003).

| PARAMETRIZATION TECHNIQUE | |
|---|---|
| CAD based | FE based |
| • Lower number of design variables | • Higher number of design variables |
| • Restricted set of admissible designs | • Larger set of admissible designs |
| • Mesh update required | • More presence of local optima |
| • Control of mesh quality required | • Control of mesh quality required |
| • High modelling cost payable by designer | • Higher computational cost |
| • Shape control: impose continuity between design patches → may be difficult for complex designs. | • Shape control: needed to avoid wiggly shapes → regularization techniques |
| • Good for manufacture | • Good for free formed shapes → preliminary design |

Figure 7.1: Scheme of the comparison between CAD based parametrizationand FE based parametrization techniques in shape structural optimization.

A scheme of the aspects treated in this comparison of CAD- and FE-based parametrization techniques is provided in Figure 7.1. It can be concluded that none of these parametrization techniques are ideal. Both have advantages and disadvantages and selection of one or the other should be made by the designer considering the circumstances of the optimization process at hand.

### 7.2.4 Other parametrization techniques

A survey of different shape parametrization techniques for multidisciplinary optimization is given by Samareh (1999). In addition, a comparison of the suitability of the different techniques for optimization of complex geometries is offered.

Some of these techniques are the domain element approach, the basis vector approach and the free deformation approach.

Among the alternative parametrizations to CAD and FE based designs, it is important to emphasize the partial differential equation parametrization (PDE) method. The reason is that this method has an inherent control of smoothness. This parametrization was introduced in the field of computer-aided geometric design for blend generation (Bloor and Wilson, 1989, 1990; Vida et al., 1994). Ugail and Wilson (2003) applied it for the definition and parametrization of surfaces in shape optimization by introducing it into the loop of an automatic design optimization process.

In the PDE method, admissible surface designs are chosen satisfying a partial differential equation and certain boundary conditions. During the optimization process, the shape of these PDE surfaces is controlled by the chosen boundary conditions, so that changes on boundary conditions will produce changes on the resulting surface.

An important characteristic of this approach is the fact that the surfaces obtained are smooth in a global sense, even though the mesh may only be $C^0$ continuous. The reason for this is that the PDE operator represents a smoothing process. In addition, more than one surface patch can be considered and the control of the smoothness of the transition between patches is relatively easy. The control of smoothness is a clear advantage of the PDE approach with respect to the CAD based method. Nevertheless, in this approach the group of admissible designs is significantly reduced with respect to the FE based parametrization. Moreover, this technique is time consuming.

## 7.3 Shape control

Shape control was introduced in shape optimization in order to obtain a design satisfactory not only from the mechanical, but also from the geometrical point

of view. A satisfactory shape is determined by the designer, using shape control techniques as tools.

There are several techniques of shape control. The most common ones are the use of geometry constraints and variable linking. However, in recent years and in the frame of FE-based design optimization, a new type of shape control techniques, aimed to control design smoothness of surfaces and curves, have emerged.

As explained in Section 7.2.3, FE-based parametrization may yield wiggly shapes. There are two main reason why these wiggly shapes are to be avoided. First, these oscillations in the design geometry cause a significant mesh distortion. As a consequence the element quality is affected and the results of structural and sensitivity analysis may no longer be reliable. Furthermore, high mesh distortions may even cause the failure of the optimization process. A second reason to avoid these wiggly shapes is that, in general, smooth, regular, mesh independent shapes are preferred.

The need to smooth designs obtained with FE-based parametrization was already noted by Mohammadi (1997), who proposed a smoothing operator over the shape. Other smoothing techniques have been proposed based on the control of curvatures. In these techniques, a distinction between two aspects should be made: the approach used to compute the selected curvature measure and how design shape is controlled by means of this curvature. A common curvature control method in shape optimization of fluids is regularization. This approach consists on penalizing the objective function with a certain term, which is the integral of the square of a certain curvature measure over the shape domain. This way, wiggly designs are penalized and smooth designs favored.

In the present section, after a brief review of the variable linking concept, attention is focused on shape control by regularization methods. After a brief overview of the application fields of regularization methods, this concept is extended to smoothing designs in shape optimization of shells. A regularization term, which is function of a curvature measure of the shell, is proposed and its sensitivity analysis is performed.

## 7.3.1    Variable linking

Variable linking is a very common way to control design shape during the optimization process. It is a way to introduce geometrical constraints: it can

introduce geometrical relations of variables or it can force continuity requirements of curves (Ramm et al., 1993).

Strictly speaking, Bletzinger (1990) distinguishes between three levels of variables in the optimization problem: optimization variables, design variables and structural variables. The optimization variables are the independent variables which take part in the optimization process. The design variables are the independent optimization variables and the dependent variables linked to those. Structural variables are those related to the structural analysis of the structure, for instance the FE nodal coordinates. The most common linking strategy establishes a linear relation between optimization variables and design variables, and a second linear relation between design variables and structural variables (Bletzinger, 1990). In the particular case of FE based designs, the design variables are the same as the structural variables. Nonlinear links can also be considered but they are not commonly used due to their complexity.

There are several reasons for linking variables. Some of them are: the need to impose certain symmetry or antimetry conditions, the need to prescribe interactions between variables (describing the movement of a certain variable as a linear combination of other variables), and the need to prescribe a certain direction in which a node is allowed to move.

In the mathematical and numerical formulation of the optimization problem, variable linking is imposed through linking matrices. It should be remarked that in linear linking these matrices remain constant during the optimization process, and therefore they do not have to be derived in sensitivity analysis.

### 7.3.2 Regularization

In some engineering problems, it may occur that the solution to a problem is difficult to handle because of its discontinuities or singularities. Tikhonov and Arsenin (1977) studied ill-posed mathematical problems and regularization methods to overcome this ill-posedness. They propose the so called Tikhonov regularization. Nowadays, regularization is applied to engineering and mathematical problems in order to obtaining smooth and regularized solutions without undesirable noise (Belytschko et al., 2000).

Some examples of applications of regularization to engineering problems are von Neumann's regularization in fluids, regularization through the penalty method in contact-impact problems, the Curnier-Mroz friction model and regularization of material instabilities (Belytschko et al., 2000).

Von Neumann regularization is applied to the Euler fluid equation to smooth oscillations in the solution produced by shocks. In this case, regularization is achieved through the addition of an artificial viscosity.

In contact-impact problems, the penalty method is also a regularization method. At the contact interface, velocities are discontinuous at the time of impact. The velocity field is smoothed through the addition of a penalty term.

An important issue in regularization is the selection of the regularizing parameter. Often, in engineering problems, regularization has a mathematical basis but lacks physical interpretation. This fact makes it difficult to determine the value of the parameter. Many studies have been performed to obtain the values of regularization parameters for different problems.

Regularization methods solve, instead of the original problem, a sequence of regularized problems obtained by adding to the original functional a penalization term. In optimization problems, regularization consists of penalizing the objective function with an adequate term which favors smooth designs.

In the recent years, some interesting applications of regularization techniques in shape optimization for fluids have been presented. Jameson et al. (1998), for instance, considered smoothing of gradients in optimization for aerodynamic shape design.

Gunzburger et al. (2000), Mohammadi and Pironneau (2001) and Bängtsson et al. (2003) used FE design parametrization for shape optimization for fluids. They realized the necessity of using a smoothing technique to avoid noise in shape designs. Therefore, the addition of a regularization term to the objective function is considered. This term is the integral of the square of a certain curvature measure of the design over a certain reference domain. This curvature measure is the second derivative of a function which defines the modified designs, taking into account that only normal movements to the initial design are allowed. Relation between the curvature measure and this function is established by means of the Poisson equation. Therefore, this curvature is a relative measure with respect to the initial, or reference, design.

Bängtsson et al. (2003) considered also an additional smoothing approach in shape optimization of a curve describing the section of an acoustic horn. This control approach is inherent to the computation of the curvature. Such computation is done by discretizing the Poisson problem and using a $C^0$ approximation for both geometry function and curvature function. If the curvatures at the nodes are considered as unknowns, and the geometry is given, curvatures can be computed from the geometry by solving the Poisson problem. In the

formulation of the optimization problem, a change of variables is done, and curvatures at FE nodes are considered now as design variables. After that an iteration on the optimization process is performed, the optimization algorithm yield new values of the curvatures. In order to obtain the modified geometry which corresponds to these curvatures, the inverse process is carried out: In the solution of the Poisson problem, the nodal positions of the FE mesh are now considered as unknowns, and the curvatures as given data.

### 7.3.3 Regularization (Smoothing) in shape optimization of shells

Regularization will be applied to structural shape optimization of shells, in a similar manner as it is done in shape optimization for fluids. The aim is to avoid wiggly shapes obtained with FE based parametrization. This regularization of designs is achieved by adding a regularizing or penalizing term to the objective function.

In order to penalize excessive oscillations, this term is chosen to be of the form

$$\frac{\beta}{2} \int_{\Omega} (\kappa - \bar{\kappa})^2 d\Omega \tag{7.1}$$

where $\beta$ is a certain control or regularization parameter, $\kappa$ is a certain measure of the curvature of the design and $\bar{\kappa}$ is a certain prescribed function of this curvature measure.

If this penalizing term is considered, the modified objective function is now given by

$$F_\beta = F + \frac{\beta}{2} \int_{\Omega} (\kappa - \bar{\kappa})^2 d\Omega \tag{7.2}$$

where $F$ is the original objective function, that is, strain energy or weight, for instance.

The effect of this regularization term over a design is very intuitive. For designs with a curvature function $\kappa$ equal to the prescribed $\bar{\kappa}$, this term vanishes. In this case, the modified objective function is equal to the original objective function. For designs with a curvature function different from the prescribed one, the regularization term does not vanish and its contribution has to be added to the original function. The more the actual curvature function approximates to the prescribed curvature function, the smaller is the contribution of regularization

term to the modified objective function. Therefore, the consideration of this regularization term favors obtaining designs with a curvature function close to the prescribed one. It should be noted that the regularization term will not, in general, vanish for the optimal design, since the contribution of the original objective function is also considered. The sum of both original objective function and regularization term, is to be minimized in the optimization problem, not the individual contributions.

The regularization parameter $\beta$ tunes the influence of the penalization term in the modified problem. It is a tool to control design shape: Using higher values, optimum designs will have a curvature approximated to the prescribed one, and using lower values optimum designs may have a curvature which differs from the prescribed one, but they may have a lower original objective function. Numerical examples of tuning of this parameter are shown in Section 7.7.4.

At his point, a new vision of the optimization problem is introduced. Until now, the problem was only loocked at from a mechanical point of view, since all considerations were based on the structural behavior of the shell. However, now the penalizing term is exclusively based on the design geometry and not on its mechanics. Therefore a pure geometrical vision of the structure is needed. The design is actually observed from two different points of view:

1. The mechanical vision, considering the design as a shell, which is necessary because optimization is done based on the structural behavior.

2. The geometrical vision, considering the design as a surface (with no thickness), which is treated in the present chapter and is necessary to control the design shape during the optimization process.

It is important to achieve harmony between the two visions. For the structural analysis, a geometrical description of the structure is also needed, so now shape control should be performed on the basis of this description. This implies that the computation of the selected curvature measure should be based on the data related to the finite element mesh (i.e. connectivities, nodal positions, director vectors).

Another important point is the selection of the curvature measure introduced to the penalization term. For curves, there exists only one definition of curvature, that is the magnitude of the second derivative of the curve function with respect to the parameter considered. However, in a surface, different curvature measures can be defined and, therefore, different penalization terms can

be considered. In Section 7.4, a brief review of differential geometry of surfaces is given and different curvature measures and their interpretation are outlined. In Section 7.5, a procedure to compute these curvature measures for a surface approximated by a $C^0$ mesh (as usually in finite element analysis) is proposed.

These curvature measures will be computed at each node of the mesh and interpolated with the shape functions associated to the finite elements at hand. Thus, curvature $\kappa$ at a certain element is approximated by

$$\kappa = \sum_{a=1}^{n_{en}} N_a \kappa_a \tag{7.3}$$

where $N_a$ are the shape functions related to this element (the same as for the finite element formulation at hand), $\kappa_a$ are the nodal curvature values ans $n_{en}$ is the number of element nodes.

The prescribed curvature function is also given as

$$\bar{\kappa} = \sum_{a=1}^{n_{en}} N_a \bar{\kappa}_a \tag{7.4}$$

where $\bar{\kappa}_a$ are prescribed nodal curvature values.

Once nodal curvatures are obtained, regularization term (7.1) can be computed for the discrete problem as the sum of the elemental contributions. Hence,

$$\frac{\beta}{2} \int_\Omega (\kappa - \bar{\kappa})^2 d\Omega = \beta \sum_e \int_{\Omega_e} \left( \sum_a N_a \kappa_a - \sum_b N_b \bar{\kappa}_b \right)^2 d\Omega_e \tag{7.5}$$

Surface integrals have to be performed over the element area. It is desirable to express the differential of area $d\Omega_e$ in the natural coordinate system, because it facilitates integration. In the present case, integration is considered in the surface, which is the mid-plane of the shell element, that is, when $\zeta = 0$. Therefore, the element of area can be written as (Belytschko et al., 2000; Hughes, 2000)

$$d\Omega_e = J_s \Big|_{\zeta=0} d\xi d\eta \tag{7.6}$$

where $J_s$ is the surface Jacobian given by

$$J_s = \|\mathbf{x},_\xi \times \mathbf{x},_\eta\| \tag{7.7}$$

Here, $\mathbf{x},_\xi$ and $\mathbf{x},_\eta$ are partial derivatives of the position vector with respect to natural coordinates at the point where the Jacobian is to be evaluated (see equations (3.22) and (3.23)).

Considering (7.6), the elemental contribution to regularization term can be computed as

$$\frac{\beta}{2} \int_{\Omega_e} (\kappa - \bar{\kappa})^2 d\Omega_e = \frac{\beta}{2} \int_{-1}^{1} \int_{-1}^{1} \left( \sum_a N_a \kappa_a - \sum_b N_b \bar{\kappa}_b \right)^2 J_s d\xi d\eta \qquad (7.8)$$

The considered modified objective function is the sum of the original one and the regularization term (see (7.2)). Therefore, its sensitivity with respect to a design variable $s$ is given by

$$F_{\beta,s} = F_{,s} + \frac{\beta}{2} \left( \int_{\Omega} (\kappa - \bar{\kappa})^2 d\Omega \right)_{,s} \qquad (7.9)$$

The sensitivity of regularization term can be computed as

$$\beta \int_{\Omega_e} (\kappa - \bar{\kappa}) \kappa_{,s} \, d\Omega_e = \beta \int_{-1}^{1} \int_{-1}^{1} \left( \sum_a N_a \kappa_a - \sum_b N_b \bar{\kappa}_b \right) \left( \sum_a N_a \kappa_{a,s} \right) J_s d\xi d\eta$$
$$+ \frac{\beta}{2} \int_{-1}^{1} \int_{-1}^{1} \left( \sum_a N_a \kappa_a - \sum_b N_b \bar{\kappa}_b \right)^2 J_{s,s} \, d\xi d\eta$$

$$(7.10)$$

Computation of derivatives of different nodal curvature measures with respect to design variable $s$ is explained in Section (7.6).

## 7.4 Differential geometry of surfaces

In the present section, a review of some concepts of differential geometry of surfaces is presented. This is not intended to be a detailed introduction, but just a review of some concepts necessary to understand the procedure used to compute the curvature of a surface approximated by a $C^0$ mesh, which is explained in Section 7.5. A deep introduction to differential geometry of curves and surfaces is given by do Carmo (1976) or Dubrovin et al. (1992).

First, some basic concepts of differential geometry of surfaces are reviewed. The surfaces considered are supposed to be regular surfaces defined in an Euclidean space. A rough definition of a regular surface is a surface that is smooth enough, with no sharp points or edges, so that a tangent plane can be defined at every point of it. A detailed study of regularity of surfaces is given by do Carmo

(1976). In an Euclidean space, two quadratic fundamental forms of the surface can be defined. These fundamental forms will permit to deduce some invariants and metric properties of the surface. Attention is focused on principal curvatures, Gaussian curvature and mean curvature. It is said that these properties are invariants because they are independent of the coordinate system used and, therefore, they are intrinsic properties of the surface.

## 7.4.1 Basic concepts

A surface in a three dimensional Cartesian space can be represented mathematically in three ways:

- explicit representation: $z = f(x, y)$

- implicit representation: $F(x, y, z) = 0$

- and parametric representation: $\mathbf{x} = \mathbf{x}(\theta^1, \theta^2)$

Before the concept of curvature of a surface is introduced, it is convenient to review some basic concepts related to differential geometry of spatial curves. Let $\mathbf{x}(r)$ be a spatial curve parametrized by the arc length $r$. The tangent vector to this curve is given by

$$\mathbf{t}(r) = \frac{d\mathbf{x}(r)}{dr} = \dot{\mathbf{x}}(r) \tag{7.11}$$

where $(\dot{\bullet}) = d(\bullet)/dr$.

The normal to a curve is given by

$$\mathbf{n}(r) = \frac{\ddot{\mathbf{x}}(r)}{|\ddot{\mathbf{x}}(r)|} \tag{7.12}$$

where $(\ddot{\bullet}) = d^2(\bullet)/dr^2$. Note that $\mathbf{n}(r)$ is an unitary vector and $\mathbf{n}(r) \perp \mathbf{t}(r)$. The curvature of a curve is defined as

$$\kappa(r) = |\ddot{\mathbf{x}}(r)| \tag{7.13}$$

so that

$$\ddot{\mathbf{x}}(r) = \kappa(r)\mathbf{n}(r) \tag{7.14}$$

Consider now a surface given in parametric representation $\mathbf{x} = \mathbf{x}(\theta^1, \theta^2)$. The vectors $\mathbf{x}_{,\theta^1}$ and $\mathbf{x}_{,\theta^2}$ are tangent to the surface and to parameter lines $\theta^1$ and $\theta^2$, respectively. At a point $P$ of the surface, these two vectors define a plane tangent to the surface.

In addition, at any point $P$ of a regular surface, a unit normal vector can be defined as

$$\mathbf{N}_P = \left. \frac{\mathbf{x}_{,\theta^1} \times \mathbf{x}_{,\theta^2}}{\left| \mathbf{x}_{,\theta^1} \times \mathbf{x}_{,\theta^2} \right|} \right|_P \tag{7.15}$$

This vector is normal to the tangent plane at $P$. It is said that a surface is orientable if it admits a differentiable field of unit normal vectors defined on the whole surface. The choice of this vector field determines the orientation of the surface. It should be remarked that not every regular surface is orientable. A typical example of non-orientable regular surface is the Möbius strip (see do Carmo (1976), for instance).
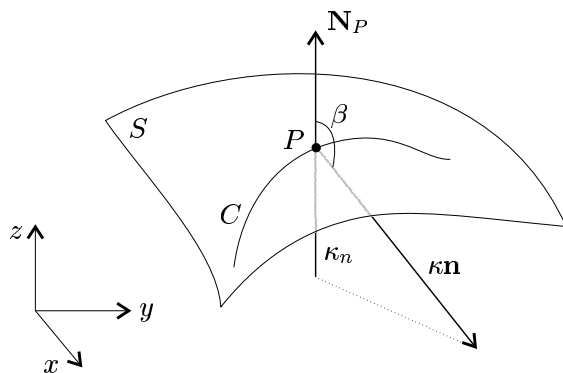


Figure 7.2: Definition of normal curvature

Consider now a curve $C$ lying in a surface $S$, as depicted in Figure 7.2. At a point $P$ of the curve, $\mathbf{n}$ is the normal vector to the curve and $\kappa$ the curvature. At this same point, $\mathbf{N}_P$ is the normal vector to the surface. Let us denote $\beta$ the angle between vectors $\mathbf{n}$ and $\mathbf{N}_P$. The length of the projection of the vector $\kappa\mathbf{n}$ on the normal to the surface $\mathbf{N}_P$ is called *normal curvature* of curve $C$ at surface $S$, and it is usually denoted as $\kappa_n$. Hence,

$$\kappa_n = \kappa \cos \alpha \tag{7.16}$$

A proposition due to Meusnier states that all curves lying on this surface $S$ and having at point $P$ the same tangent line, have also the same normal curvature. As a consequence, this curvature is usually referred to as *directional curvature*,

126

since it is associated with a certain direction. This directional curvature does not depend on the orientation of curve $C$, but on the orientation of surface $S$.

The curvature at a point $P$ gives an idea of how the surface pulls away from the tangent plane at $P$. This is equivalent to saying that curvature at $P$ gives an idea of how the normal vector at $P$ changes in its proximity.

### 7.4.2 First fundamental form

Let us suppose that the length of a curve $\mathbf{x}(r) = (x(r), y(r), z(r)) = \mathbf{x}\left(\theta^1(r), \theta^2(r)\right)$ laying on a certain surface is to be measured. If the differential or element arch length of the curve is denoted $ds$, then

$$ds^2 = E\left(d\theta^1\right)^2 + 2F\left(d\theta^1 \ d\theta^2\right) + G\left(d\theta^2\right)^2 \tag{7.17}$$

where

$$
\begin{aligned}
E &= x_{,\theta^1} \ x_{,\theta^1} + y_{,\theta^1} \ y_{,\theta^1} + z_{,\theta^1} \ z_{,\theta^1} \\
F &= x_{,\theta^1} \ x_{,\theta^2} + y_{,\theta^1} \ y_{,\theta^2} + z_{,\theta^1} \ z_{,\theta^2} \\
G &= x_{,\theta^2} \ x_{,\theta^2} + y_{,\theta^2} \ y_{,\theta^2} + z_{,\theta^2} \ z_{,\theta^2}
\end{aligned}
\tag{7.18}
$$

Now, the arch length of the curve can be written as

$$\left(\frac{ds}{dr}\right)^2 = \sqrt{E\left(\dot{\theta}^1\right)^2 + 2F\left(\dot{\theta}^1 \ \dot{\theta}^2\right) + G\left(\dot{\theta}^2\right)^2} \tag{7.19}$$

The quadratic form,

$$\mathbf{I}_P = E\left(d\theta^1\right)^2 + 2F\left(d\theta^1 \ d\theta^2\right) + G\left(d\theta^2\right)^2 \tag{7.20}$$

is called the *first fundamental form of the surface*. The matrix

$$\begin{pmatrix} E & F \\ F & G \end{pmatrix} \tag{7.21}$$

is called *matrix of the first fundamental form.*

If the surface is given in its explicit form, the metric of the first fundamental form is given by

$$\begin{pmatrix} E & F \\ F & G \end{pmatrix} = \begin{pmatrix} 1 + f_{,x}^2 & f_{,x} \ f_{,y} \\ f_{,x} \ f_{,y} & 1 + f_{,y}^2 \end{pmatrix} \tag{7.22}$$

From this fundamental form, the area of a region $\Omega$ of the surface can be computed as:

$$A = \iint_\Omega \sqrt{\det \begin{pmatrix} E & F \\ F & G \end{pmatrix}} \, d\theta^1 d\theta^2 \tag{7.23}$$

### 7.4.3   Second fundamental form

Considering again a surface $\mathbf{x}(\theta^1, \theta^2)$ and a curve on this surface given as $\mathbf{x}(r) = (x(r), y(r), z(r)) = \mathbf{x}\left(\theta^1(r), \theta^2(r)\right)$, it can be written

$$\dot{\mathbf{x}} = \mathbf{x}_{,\theta^1}\, \dot{\theta^1} + \mathbf{x}_{,\theta^2}\, \dot{\theta^2} \tag{7.24}$$

$$\ddot{\mathbf{x}} = \left( \mathbf{x}_{,\theta^1\theta^1} \left(\dot{\theta^1}\right)^2 + 2\mathbf{x}_{,\theta^1\theta^2}\, \dot{\theta^1}\dot{\theta^2} + \mathbf{x}_{,\theta^2\theta^2} \left(\dot{\theta^2}\right)^2 \right) + \left( \mathbf{x}_{,\theta^1}\, \ddot{\theta^1} + \mathbf{x}_{,\theta^2}\, \ddot{\theta^2} \right) \tag{7.25}$$

Taking into account that $\mathbf{N} \perp \mathbf{x}_{,\theta^1}$ and $\mathbf{N} \perp \mathbf{x}_{,\theta^2}$, we have

$$\begin{aligned} \mathbf{N} \cdot \ddot{\mathbf{x}} &= \mathbf{N} \cdot \mathbf{x}_{,\theta^1\theta^1} \left(\dot{\theta^2}\right)^2 + 2\mathbf{N} \cdot \mathbf{x}_{,\theta^1\theta^2}\, \dot{\theta^1}\dot{\theta^2} + \mathbf{N} \cdot \mathbf{x}_{,\theta^2\theta^2} \left(\dot{\theta^2}\right)^2 \\ &= L \left(\dot{\theta^1}\right)^2 + 2M \left(\dot{\theta^1}\, \dot{\theta^2}\right) + N \left(\dot{\theta^2}\right)^2 \end{aligned} \tag{7.26}$$

The quadratic form

$$\mathbf{II}_P = L \left(d\theta^1\right)^2 + 2M \left(d\theta^1\, d\theta^2\right) + N \left(d\theta^2\right)^2 \tag{7.27}$$

is called *second fundamental form of the surface*. It should be noted that coefficients $L$, $M$ and $N$ are independent of the curve $\mathbf{x} = \mathbf{x}\left(\theta^1(r), \theta^2(r)\right)$ and depend only on the surface itself. The matrix

$$\begin{pmatrix} L & M \\ M & N \end{pmatrix} \tag{7.28}$$

is called *matrix of the second fundamental form.*

### 7.4.4 Invariants of the fundamental forms of a surface: principal curvatures, Gaussian curvature and mean curvature

In the preceding sections, we have seen that to each point of a regular surface in an Euclidean three dimensional space, a pair of fundamental forms are associated. From these two quadratic forms, a set of invariants of the surface can be defined. Since these properties are invariants, they do not depend on the coordinate system used and, therefore, they are intrinsic properties of the surface.

Let us consider the equation

$$\det \left( \begin{pmatrix} L & M \\ M & N \end{pmatrix} - \lambda \begin{pmatrix} E & F \\ F & G \end{pmatrix} \right) = 0 \tag{7.29}$$

The roots $\lambda_1$ and $\lambda_2$ of this equation are the eigenvalues of the pair of quadratic forms. These are also called *principal curvatures* of the surface and they are usually denoted by $\kappa_1$ and $\kappa_2$. These are the maximum and minimum curvatures of the surface at the point considered. Associated to these eigenvalues are two eigenvectors, which are called principal directions. If eigenvalues $\lambda_1$ and $\lambda_2$ are different, then principal directions are orthogonal.

The *Gaussian curvature* is defined as the product of principal curvatures, that is

$$K = \kappa_1 \kappa_2 \tag{7.30}$$

And *mean curvature* is defined as the arithmetic mean of principal curvatures, that is

$$H = \frac{\kappa_1 + \kappa_2}{2} \tag{7.31}$$

Gaussian curvature can be also written as the ratio of the determinants of second and first fundamental forms. That is,

$$K = \frac{\det \begin{pmatrix} L & M \\ M & N \end{pmatrix}}{\det \begin{pmatrix} E & F \\ F & G \end{pmatrix}} = \frac{LN - M^2}{EF - G^2} \tag{7.32}$$

The sign of Gaussian curvature has a geometrical meaning. If $K > 0$ at a point $P$ on surface $S$, then in a certain proximity of this point the surface lies on

one side of the tangent plane at $P$. An example of a surface with $K > 0$ at all points is a sphere. If $K < 0$ at a point $P$ on surface $S$, then the tangent plane intersects the surface close to point $P$. A typical example of this case is a hyperbolic paraboloid. A surface with $K = 0$ is said to be developable. It can be a plane or a surface generated by a straight line moving along two generators.

A surface given in explicit form as $z = f(x, y)$ will be now considered, with a point $P(x_P, y_P, z_P)$ on it, and $f_{,x} = 0$ and $f_{,y} = 0$, that is the $z$-coordinate axis is normal to the tangent plane of the surface at $P$. In this particular case, the matrices of first and second fundamental forms at $P$ are given respectively by

$$\begin{pmatrix} E & F \\ F & G \end{pmatrix} = \begin{pmatrix} 1 & 0 \\ 0 & 1 \end{pmatrix} \tag{7.33}$$

$$\begin{pmatrix} L & M \\ M & N \end{pmatrix} = \begin{pmatrix} f_{,xx} & f_{,xy} \\ f_{,xy} & f_{,yy} \end{pmatrix} \tag{7.34}$$

The last matrix is also called *Hessian* of $f$. In this particular case, its components are the components of the *curvature tensor* at $P$ expressed in the basis $\{\mathbf{e}_x, \mathbf{e}_y\}$ of the Cartesian system. Now, Gaussian curvature of the surface at $P$ is given by the determinant of this Hessian, that is

$$K = f_{,xx}\, f_{,yy} - (f_{,xy})^2 \tag{7.35}$$

and the mean curvature by the half of its trace, that is

$$H = \frac{f_{,xx} + f_{,yy}}{2} \tag{7.36}$$

It is easy to see here that both Gaussian curvature and mean curvature are invariants. Therefore, it does not matter which orientation $x$ and $y$ coordinate axes have (as long as they are contained in the tangent plane at $P$, for this particular case). In a case where the $x$ and $y$ coordinate lines at $P$ coincide with principal directions, the components of the curvature tensor are

$$\begin{pmatrix} \kappa_1 & 0 \\ 0 & \kappa_2 \end{pmatrix} \tag{7.37}$$

The case in which the $z$-coordinate is perpendicular to the tangent plane at $P$ may seem a rather particular case. However, it will be very useful for computation of curvatures of surfaces approximated by a $C^0$ mesh by the method

explained in Section 7.5. The reason is that at each node of the mesh a local Cartesian coordinate system is defined. The two first base vectors of this system are contained in the tangent plane to the approximated surface at the node, and the third base vector is normal to the surface at this node. Therefore, at each node the components of curvature tensor in this local Cartesian system can be computed and from these, Gaussian, mean, and principal curvatures can be calculated.

## 7.5 Computation of the curvature of a surface approximated by a $C^0$ continuous mesh

Both Finite Element analysis and Computer Aided Visualization require approximation of geometries. Surfaces are approximated by a mesh of facets, or elements, usually with $C^0$ continuity across its boundaries. As a consequence, smoothness of the original surface is lost and computation of its curvature is not obvious. However, often curvature of the original surface is required and for this reason, different approaches have been proposed to compute it.

Within the past ten years a lot of research has been done aimed to compute intrinsic surface properties. This research has been pursued mainly in the field of Computer Aided Visualization. However, the increase of the number of degrees of freedom considered in shape optimization problems and the need to control smoothness of resulting shapes has caused interest in these issues in the field of shape optimization to grow.

Numerous approaches have been proposed to estimate curvature measures of a surface approximated by a mesh. These curvature measures can be mean curvature, Gaussian curvature, principal curvatures, Weingarten curvature matrix or other quantities related to second order derivatives of the surface function. Gatzke and Grimm (2003) presented a systematic review to several approaches to estimate different curvature measures of a surface represented by a triangular mesh. Moreover, a comparison of accuracy and efficiency of different approaches is done. Taubin (1995) proposed a method to estimate principal curvatures and principal directions at a point of a faceted surface. The main advantage of this method is its simplicity. An approach to compute a curvature measure based on the discrete Laplacian, by means of the umbrella operator, was presented by Kobbelt et al. (1998). They apply this measure to smooth surfaces in Computer Aided Visualization. Estimation of principal directions

and of Weingarten curvature matrix is studied in Goldfeather (2001). A study of the relation between errors in surface approximation and errors in principal directions approximations is also presented.

In Gunzburger et al. (2000), Mohammadi and Pironneau (2001) and Bängtsson et al. (2003), a measure of the curvature of a curve with respect to a fixed reference is computed by means of the Poisson equation. The computed curvatures are used in shape optimization problems related to fluids, to penalize the objective function and obtain smoother shapes.

In the present section, a method to estimate the curvature tensor, mean curvature and Gaussian curvature at the nodes of a surface approximated by facets or elements is explained. The proposed method for computation of the curvature tensor of a piecewise defined surface is organized in two steps. First, an approximation of the directional curvature at a node of the surface is computed based on the approach proposed by Taubin (1995). Second, with the known directional curvatures in three different directions, a system of equations is built, and the components of the curvature tensor, in an arbitrary system contained in the tangent plane, are computed. Once these components are available, mean curvature, principal curvatures and Gaussian curvatures can be computed. Numerical examples presented in Section 7.7.2 confirm the good performance of the method.

### 7.5.1   Approximation of the directional curvature

Considering a smooth space curve $S$ parametrized by an arch length $r$, the function $\mathbf{x}(r)$ denotes the position vectors of the points belonging to the curve. The expansion in Taylor series of the function $\mathbf{x}(r)$ about the point $r = 0$ up to second order yields

$$\mathbf{x}(r) = \mathbf{x}(0) + r\frac{d\mathbf{x}}{dr}\Big|_{r=0} + \frac{r^2}{2!}\frac{d^2\mathbf{x}}{dr^2}\Big|_{r=0} + O(r^3) \tag{7.38}$$

It is known that $\frac{d\mathbf{x}}{dr}\big|_{r=0}$ is the tangent vector at point $\mathbf{x}(0)$ and that

$$\frac{d^2\mathbf{x}}{dr^2}\Big|_{r=0} = \kappa\mathbf{n} \tag{7.39}$$

where $\mathbf{n}$ is the normal vector at point $\mathbf{x}(0)$ and $\kappa$ is the curvature at the same point. All vectors are defined as column vectors.

Neglecting higher order errors in (7.38), the curvature can be computed as

$$\kappa \approx \frac{2\mathbf{n} \cdot \left(\mathbf{x}(r) - \mathbf{x}(0) - r\frac{d\mathbf{x}}{dr}\big|_{r=0}\right)}{r^2} \tag{7.40}$$
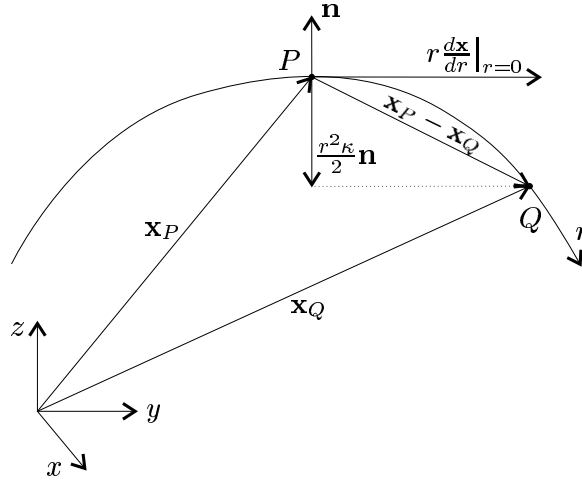


Figure 7.3: Vectors related to the computation of the curvature of a spatial curve at point $P$.

The geometrical interpretation of this equation is shown in Figure 7.3. At point $P$, $r = 0$, so that $\mathbf{x}(0) = \mathbf{x}_P$ and $Q$ is a generic point with parameter $r$, so that $\mathbf{x}(r) = \mathbf{x}_Q$.

This idea can be extended to compute the directional curvature of a faceted surface at a point. Let us consider that a real smooth surface is approximated by a mesh of elements with continuity $C^0$ across element boundaries. Typical examples, where this kind of discretization is used, are Finite Element analysis and Computer Aided Visualization. The mesh information at hand is the nodal positions and the approximated normal to the surface at the nodes. The position vector of node $P$ is denoted $\mathbf{x}_P$, and the unit vector normal to the surface at this node is denoted $\mathbf{A3}_P$. The vector $\mathbf{A3}_P$ is computed as the normalized average of the normals to the adjacent elements to $P$, as explained in Section 3.4.

Let us now consider the patch of bilinear elements shown in Figure 7.4. It is desired to compute the curvature at point $P$ in the direction $PQ_1$. The position vector of points $P$ and $Q_1$, as well as the unit normal vector $\mathbf{A3}_P$, are known. Let us denote

$$\mathbf{r}_1 = \mathbf{x}_{Q_1} - \mathbf{x}_P \tag{7.41}$$

133
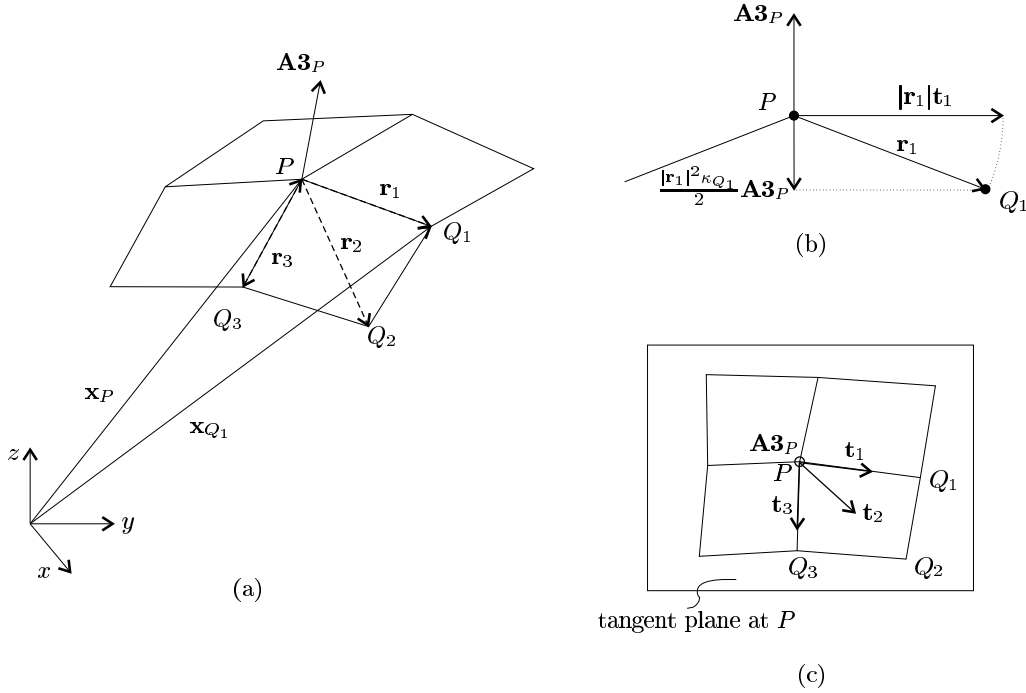
Figure 7.4: Patch of elements where the vectors required for computation of the directional curvature at the center node are shown. (a) Perspective, (b) section and (c) top view.

and $\mathbf{t}_1$ the unit vector resulting from the projection of vector $\mathbf{r}_1$ in the tangent plane at $P$. The tangent plane to the approximated surface at point $P$ can be defined as the plane perpendicular to $\mathbf{A3}_P$ and containing point $P$. The unit tangent vector can be computed as

$$\mathbf{t}_1 = \frac{\mathbf{r}_1 - \mathbf{A3}_P(\mathbf{A3}_P \cdot \mathbf{r}_1)}{|\mathbf{r}_1 - \mathbf{A3}_P(\mathbf{A3}_P \cdot \mathbf{r}_1)|} = \frac{(\mathbf{I} - \mathbf{A3}_P\mathbf{A3}_P^T) \cdot \mathbf{r}_1}{|(\mathbf{I} - \mathbf{A3}_P\mathbf{A3}_P^T) \cdot \mathbf{r}_1|} \tag{7.42}$$

As only a $C^0$ approximation to the original surface is known, a curve laying on the original surface and which contains $P$ and $Q$ and with tangent $\mathbf{t}_1$ at $P$ is unknown. Therefore, the arch length $r$ is also unknown and an approximation to it has to be considered in (7.40). Depending on how the arch length $r$ is approximated, the directional curvature computed will be different, since the curve related to it will be also different. If $r$ is taken to be the length of the secant $\mathbf{r}_1$, then the directional curvature $\kappa$ computed is the curvature of a circle. If $r$ is the length of the projection of the secant $\mathbf{r}_1$ in the direction of $\mathbf{t}_1$, then $\kappa$ is the curvature of a parabola. Both the aforementioned circle and parabola,

134

contain $P$ and $Q$ and their tangent at $P$ is $\mathbf{t}_1$. A sketch of both options is given in Figure 7.5. In the present work, $r$ is taken to be the length of the secant $\mathbf{r}_1$.

(a) Circle

$$r = |\mathbf{r}_1|$$

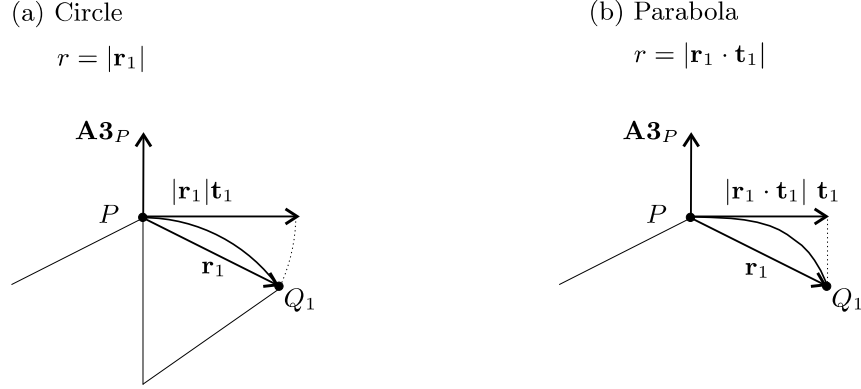(b) Parabola

$$r = |\mathbf{r}_1 \cdot \mathbf{t}_1|$$



Figure 7.5: Different approximations of the arch length $r$ and curves related to them.

Taking into account (7.41), (7.42) and (7.40), the curvature at $P$ in direction $PQ_1$ can be computed as

$$\kappa_{Q_1} = \frac{2\mathbf{A3}_P \cdot (\mathbf{r}_1 - |\mathbf{r}_1|\mathbf{t}_1)}{|\mathbf{r}_1|^2} \tag{7.43}$$

Considering that the vectors $\mathbf{A3}_P$ and $\mathbf{t}_1$ are perpendicular, it is possible to simplify (7.43). Thus,

$$\kappa_{Q_1} = \frac{2\mathbf{A3}_P \cdot \mathbf{r}_1}{|\mathbf{r}_1|^2} \tag{7.44}$$

## 7.5.2 Relation between curvature tensor and directional curvature

In Section 7.5.1, the directional curvature at a point of a surface discretizated by a faceted mesh has been approximated with help of the Taylor series expansion. In the present section, the relation between the directional curvature and the curvature tensor of the surface at a point will be established.

$\{\mathbf{A1}_P, \mathbf{A2}_P, \mathbf{A3}_P\}$ is a local Cartesian system at node $P$, where $\mathbf{A3}_P$ is a unit vector approximately normal to the surface at node $P$ and $\mathbf{A1}_P$ and $\mathbf{A2}_P$ are unit vectors that lay on the tangent plane to the surface at $P$, as depicted in

Figure 7.6. Notice that this local Cartesian system is the same one required for the formulation of the shell finite element explained in Chapter 3. Now, the tangent vector $\mathbf{t}_1$ defined in equation (7.42), can be expressed in this local Cartesian system as

$$\mathbf{t}_1 = a_1 \mathbf{A1}_P + b_1 \mathbf{A2}_P + 0\mathbf{A3}_P \tag{7.45}$$

It should be noted that the component in $\mathbf{A3}_P$ direction vanishes, because $\mathbf{t}_1$ is by definition perpendicular to $\mathbf{A3}_P$.
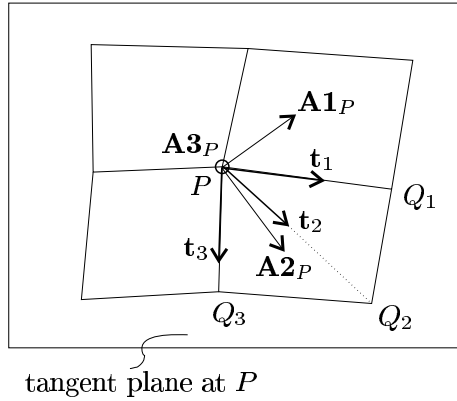


Figure 7.6: View of the patch of elements perpendicular to the tangent plane showing tangent vectors and local Cartesian system.

The directional curvature at point $P$ in direction $PQ_1$ can now be expressed as

$$\kappa_{Q_1} = \begin{pmatrix} a_1 & b_1 \end{pmatrix} \begin{pmatrix} \kappa_{11} & \kappa_{12} \\ \kappa_{21} & \kappa_{22} \end{pmatrix} \begin{Bmatrix} a_1 \\ b_1 \end{Bmatrix} \tag{7.46}$$

where

$$\{\kappa_{\alpha\beta}\} = \begin{pmatrix} \kappa_{11} & \kappa_{12} \\ \kappa_{21} & \kappa_{22} \end{pmatrix} \tag{7.47}$$

is the matrix containing the components of the curvature tensor at point $P$ in the local Cartesian basis $\{\mathbf{A1}_P, \mathbf{A2}_P\}$ that defines the tangent plane at $P$. Component $\kappa_{11}$ is the curvature in direction $\mathbf{A1}_P$, $\kappa_{22}$ is the curvature in direction $\mathbf{A2}_P$, and $\kappa_{12} = \kappa_{21}$. Note that Greek indices $\alpha$ and $\beta$ run from 1 to 2. From equation (7.46), we obtain

$$\kappa_{Q_1} = a_1^2 \kappa_{11} + 2a_1 b_1 \kappa_{12} + b_1^2 \kappa_{22} \tag{7.48}$$

136

In this equation, it can be observed that there are three unknowns, which are the components of the curvature tensor in the local Cartesian basis. Therefore, two more equations are needed. These are obtained establishing the same relation between directional curvature and curvature tensor components at node $P$ for directions $PQ_2$ and $PQ_3$. Note that $P$, $Q_1$, $Q_2$ and $Q_3$ are all nodes of the same element $e$. Thus, the system of equations obtained is

$$\begin{pmatrix} a_1^2 & 2a_1b_1 & b_1^2 \\ a_2^2 & 2a_2b_2 & b_2^2 \\ a_3^2 & 2a_3b_3 & b_3^2 \end{pmatrix} \begin{Bmatrix} \kappa_{11}^e \\ \kappa_{12}^e \\ \kappa_{22}^e \end{Bmatrix} = \begin{Bmatrix} \kappa_{Q_1} \\ \kappa_{Q_2} \\ \kappa_{Q_3} \end{Bmatrix} \tag{7.49}$$

Solving this system, the components $\kappa_{11}^e$, $\kappa_{12}^e$ and $\kappa_{22}^e$ are obtained, which are an approximation to the components of the curvature tensor obtained considering element $e$. Now, the components of the curvature tensor at each node in the local Cartesian system $\{\mathbf{A1}_P, \mathbf{A2}_P\}$ can be obtained at each node as the average of the elemental contributions weighted by the relative element area. That is,

$$\{\kappa_{\alpha\beta}\} = \frac{\sum\limits_{e=1}^{\mathrm{nae}} \{\kappa_{\alpha\beta}^e\} A^e}{\sum\limits_{e=1}^{\mathrm{nae}} A^e} \tag{7.50}$$

where $nae$ is the number of adjacent elements and $A^e$ is the area of element $e$. As the local Cartesian system is unique for each node, the different contributions of the components of the curvature tensor involved in this formula are all expressed in the same basis.

## 7.5.3 Approximation of mean curvature, Gaussian curvature and principal curvatures

Once the components of curvature tensor are obtained at each node, different curvature measures explained in Section 7.4 can be computed.

Mean and Gaussian curvature at a node $P$ can be approximated by

$$H = \frac{\mathrm{trace}\{\kappa_{\alpha\beta}\}}{2} \tag{7.51}$$

and

$$K = \det\{\kappa_{\alpha\beta}\} \tag{7.52}$$

137

respectively, where $\{\kappa_{\alpha\beta}\}$ are the components of the curvature tensor at this node expressed in the local Cartesian basis.

Principal curvatures can also be computed. They are the eigenvalues of matrix $\{\kappa_{\alpha\beta}\}$. Therefore, they can be computed from equation

$$\det\left(\{\kappa_{\alpha\beta}\} - \lambda\{\delta_{\alpha\beta}\}\right) = 0 \tag{7.53}$$

Hence,

$$\lambda = \frac{(\kappa_{11} + \kappa_{22}) \pm \sqrt{(\kappa_{11} + \kappa_{22})^2 - 4(\kappa_{11}\kappa_{22} - \kappa_{12}^2)}}{2} = H \pm \sqrt{H^2 - K} \tag{7.54}$$

### 7.5.4 Further remarks

It should be remarked that curvatures computed by this method are not curvatures of the elements, but of the surface approximated by the finite element mesh or facets. So, even though elements used to approximate the surface are plane (e.g. linear or bilinear), the curvature computed at a node may not be zero. At this point, it is clear that nodal director vectors provide the crucial information. It should be recalled that director vectors are approximately normal to the surface but not necessarily normal to the adjacent elements (see Section 3.4).

Nodes located at a boundary constitute a particular case. At these nodes the director vectors do not have information on how the surface goes on beyond the boundary, because actually it does not go beyond this boundary. Therefore, the presented method yields null curvatures at a node located at a boundary, in direction perpendicular to this boundary (outwards or inwards), because the director vector at a boundary node is perpendicular to this direction. As a consequence the approximations obtained for curvature measured at boundary nodes will not, in general, be accurate.

An important advantage of this method is that the information required (i.e. element topology, nodal positions, normal vectors at the nodes, etc.) is also required in finite element analysis of shells and membranes. Moreover, the local Cartesian system defined at each node is also involved in the formulation of the shell element explained in Chapter 3. Therefore, only little extra effort has to be made to compute curvatures.

The third base vector of the local Cartesian system at a point $P$, $\mathbf{A3}_P$, is determined by the surface approximated, since it is normal to it. However,

the two other base vectors that complete the system, $\mathbf{A1}_P$ and $\mathbf{A2}_P$, can be arbitrary as long as they complete a Cartesian coordinate system. Therefore, they are to be chosen among the perpendicular pairs of unit vectors contained in the tangent plane. An important key of the approach is the invariance of the curvature measures computed. That is, it does not matter which pair of vectors $\{\mathbf{A1}_P, \mathbf{A2}_P\}$ are chosen. However, once the base $\{\mathbf{A1}_P, \mathbf{A2}_P, \mathbf{A3}_P\}$ is chosen, this choice will be kept, since it is decisive for computing the average of the components of the curvature tensor at a node (see (7.50)).

Although the procedure to compute the components of the curvature tensor was explained for the case of a mesh of bilinear elements, the method can be easily extended to any other element type. In the case of a linear element, only two directions per element are, in principle, available to compute directional curvatures. However, in order to solve system (7.49) at element level, three directional curvatures are needed. In this case, a third directional curvature can be computed by selecting a direction between the considered node and an arbitrary point on the element. As the triangular linear element is plane, it does not matter which point it is, as long as it lies on the element plane.

Here, the curvature tensor is evaluated at element level and then the average of adjacent elements is computed. An alternative way, especially suitable for triangular linear elements, is to evaluate the curvature tensor at patch level, that is, to consider three directions pointing to nodes of the patch, which do not share the same element. The average of this curvature tensor may also be needed at patch level. A similar approach is used by Kobbelt et al. (1998) in surface smoothing applied to computer graphics and geometric modelling. A discrete Laplacian smoothing at a vertex of the mesh is computed by the so-called umbrella operator. This operator gets this name because it takes into account the first neighborhood of the considered vertex. This relation can be visualized as an umbrella, being the considered vertex its top point, and the vertices of its first neighborhood the points located at the low edge of the umbrella.

## 7.6 Sensitivity of the curvature of a surface approximated piecewise

As it has been shown in Section 7.3.3, in order to compute the sensitivity of the regularization term, derivatives of the curvature measure considered with

respect to design variables are required. In the present section, the procedure to obtain these derivatives is shown for the directional curvature, mean curvature, Gaussian curvature and principal curvatures computed by the method explained in Section 7.5.

Sensitivities of the mechanical problem are computed analytically (see Chapter 5). To attain coherence, sensitivities of these curvatures will also be computed with this technique. In the following section, only one design variable $s$ is considered.

As it will be shown, an important part of the information required to compute sensitivities of the curvature measures explained in Section 7.5, is also required for the sensitivity analysis of the shell element explained in Chapter 5. Particularly, derivatives of nodal position vectors and of nodal director vectors are required in both cases. This confirms once more the harmony between the mechanical vision and the geometrical vision of the problem.

## 7.6.1 Derivative of the approximation of the directional curvature

As explained in Section 7.6, the curvature at a node $P$ in direction $PQ_1$ depends on the position vector and director vector of this node $P$ and on the position vector of node $Q_1$. Therefore, changes on these vectors may affect directional curvature of point $P$. However, it should be noted that only a change on the director vector of node $Q_1$ does not produce a change on directional curvature at node $P$.

In order to obtain the derivative with respect to $s$ of the curvature at node $P$, in direction $PQ_1$, the product rule has to be applied to equation (7.44). Hence,

$$\kappa_{Q_1,s} = 2\left(\frac{\mathbf{A3}_P \cdot \mathbf{r}_1}{|\mathbf{r}_1|^2}\right)_{,s} = 2\left(\frac{\mathbf{A3}_{P,s} \cdot \mathbf{r}_1 + \mathbf{A3}_P \cdot \mathbf{r}_{1,s}}{|\mathbf{r}_1|^2} - \frac{(\mathbf{A3}_P \cdot \mathbf{r}_1)\,|\mathbf{r}_1|_{,s}}{|\mathbf{r}_1|^3}\right)$$
(7.55)

The geometrical interpretation of vectors appearing in this formula is shown in Figure 7.7. Superscript 'new' denotes entities related to the new modified design.

Computation of the derivative of the nodal director vectors was also required for the sensitivity analysis of the shell element and is explained in Chapter 5. Moreover,

$$\mathbf{r}_{1,s} = \mathbf{x}_{Q_1,s} - \mathbf{x}_{P,s}$$
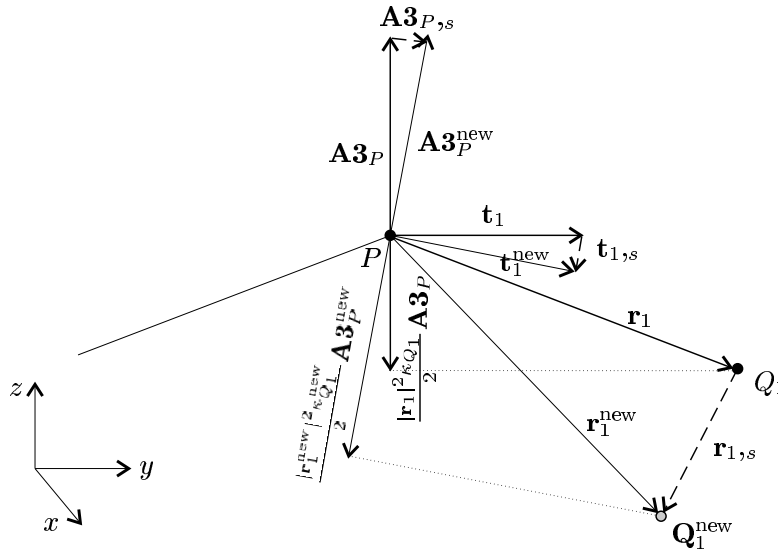(7.56)

Figure 7.7: Vectors related to the computation of the derivative of directional curvature of a faceted surface at point $P$.

where $\mathbf{x}_{Q_1}$ and $\mathbf{x}_P$ are the position vectors of nodes $Q_1$ and $P$ respectively. Their derivatives are also available from the sensitivity analysis of the shell element. It should be remarked that $\mathbf{r}_{1,s}$ will not vanish only if any of these position vectors are linked with design variable $s$.

## 7.6.2 Derivative of the approximation of the curvature tensor

In Section 7.5.2, the relation between directional curvatures and components of the curvature tensor was explained. Based on this relation and considering three directional curvatures, these components can be computed in a certain local Cartesian system by solving the $3 \times 3$ system of equations given in (7.49). Now, derivatives of the components of the curvature tensor can be obtained in the same manner, as derivatives of nodal degrees of freedom are obtained in the discrete sensitivity analysis (see (4.10) and (4.11)). Let us denote,

$$\mathbf{A} = \begin{pmatrix} a_1^2 & 2a_1b_1 & b_1^2 \\ a_2^2 & 2a_2b_2 & b_2^2 \\ a_3^2 & 2a_3b_3 & b_3^2 \end{pmatrix} \tag{7.57}$$

141

Deriving expression (7.49), we obtain

$$
\begin{Bmatrix} \kappa^e_{11,s} \\ \kappa^e_{12,s} \\ \kappa^e_{22,s} \end{Bmatrix} = \mathbf{A}^{-1} \cdot \left( \begin{Bmatrix} \kappa_{Q_1,s} \\ \kappa_{Q_2,s} \\ \kappa_{Q_3,s} \end{Bmatrix} - \mathbf{A}_{,s} \cdot \begin{Bmatrix} \kappa^e_{11} \\ \kappa^e_{12} \\ \kappa^e_{22} \end{Bmatrix} \right)
\tag{7.58}
$$

where

$$
\mathbf{A}_{,s} = \begin{pmatrix} 2a_1 a_{1,s} & 2(a_{1,s}\, b_1 + a_1 b_{1,s}) & 2b_1 b_{1,s} \\ 2a_2 a_{2,s} & 2(a_{2,s}\, b_2 + a_2 b_{2,s}) & 2b_2 b_{2,s} \\ 2a_3 a_{3,s} & 2(a_{3,s}\, b_3 + a_3 b_{3,s}) & 2b_3 b_{3,s} \end{pmatrix}
\tag{7.59}
$$

It is important to remember that $\{a_1, b_1, 0\}$ are the components of the tangent vector $\mathbf{t}_{,1}$ at node $P$ in the local Cartesian basis $\{\mathbf{A1}_P, \mathbf{A2}_P, \mathbf{A3}_P\}$. Vectors $\mathbf{A1}_P$ and $\mathbf{A2}_P$ define the tangent plane at $P$ and $\mathbf{A3}_P$ is normal to it. Thus, $\{a_{1,s}, b_{1,s}, 0\}$ are the derivatives of the components of $\mathbf{t}_{,1}$ in this local Cartesian basis. Note that the derivative of the third component vanishes. The reason for that is that, when a design is modified, the tangent plane at $P$ tilts to continue being tangential to the modified design during the shape optimization process. That is, $\mathbf{A1}_P$ and $\mathbf{A2}_P$ change to continue being tangential to the modified surface at $P$ and $\mathbf{A3}_P$ changes to continue being normal. To conclude, if we denote $c_1$ as the third component of vector $\mathbf{t}_{,1}$ in the local Cartesian basis, we have

$$
c_1 = \mathbf{t}_1 \cdot \mathbf{A3}_P = 0
\tag{7.60}
$$

and

$$
c_{1,s} = \mathbf{t}_{1,s} \cdot \mathbf{A3}_P + \mathbf{t}_1 \cdot \mathbf{A3}_{P,s} = 0
\tag{7.61}
$$

The derivative of the tangent vector $\mathbf{t}_1$ expressed in the global Cartesian system can be computed applying the product rule to equation (7.42). Let us denote,

$$
\mathbf{t}_1^* = (\mathbf{I} - \mathbf{A3}_P \mathbf{A3}_P^T) \cdot \mathbf{r}_1
\tag{7.62}
$$

Then,

$$
\mathbf{t}_1 = \frac{\mathbf{t}_1^*}{|\mathbf{t}_1^*|}
\tag{7.63}
$$

According to Appendix A.2, where the formula to compute the derivative of a normalized vector is given, the derivative of the tangent vector $\mathbf{t}_1$ can be computed as

$$
\mathbf{t}_{1,s} = \frac{\mathbf{t}_{1,s}^* |\mathbf{t}_1^*| - \mathbf{t}_1^* |\mathbf{t}_1^*|_{,s}}{|\mathbf{t}_1^*|^2}
\tag{7.64}
$$

where,

$$\mathbf{t}_{1,s}^{*} = (\mathbf{I} - \mathbf{A3}_P\mathbf{A3}_P^T) \cdot \mathbf{r}_{1,s} - 2(\mathbf{A3}_{P,s}\,\mathbf{A3}_P^T)\mathbf{r}_1 \qquad (7.65)$$

Note that all vectors needed to compute $\mathbf{t}_{1,s}^{*}$ are known to this point. The components of $\mathbf{t}_{1,s}$ in the local Cartesian system can be computed from those in the global Cartesian system with a change of basis.

Therefore, from expression (7.58) derivatives of the components of the curvature tensor in the local Cartesian basis, considering contributions of element $e$, can be obtained. Rearranging these derivatives in a matrix, it can be written,

$$\{\kappa_{\alpha\beta}\}_{,s}^{e} = \begin{pmatrix} \kappa_{11,s}^{e} & \kappa_{12,s}^{e} \\ \kappa_{21,s}^{e} & \kappa_{22,s}^{e} \end{pmatrix} \qquad (7.66)$$

### 7.6.3 Derivative of approximation of mean curvature, Gaussian curvature and principal curvatures

Once derivatives of the components of the curvature tensor are available, derivatives of the different curvature measures considered in Section 7.5 can be computed. Sensitivities of mean curvature and Gaussian curvature, respectively, are given by

$$H_{,s} = \frac{(\mathrm{trace}\{\kappa_{\alpha\beta}\})_{,s}}{2} \qquad (7.67)$$

$$K_{,s} = (\det \kappa_{\alpha\beta}) = \kappa_{11,s}\,\kappa_{22} + \kappa_{11}\kappa_{22,s} - 2\kappa_{12}\kappa_{12,s} \qquad (7.68)$$

Derivatives of principal curvatures can be computed from (7.54). Two different cases should be distinguished, depending on whether both principal curvatures are equal or not. That is,

$$
\begin{aligned}
\lambda_{,s} &= H_{,s} \pm \frac{2HH_{,s} - K_{,s}}{2\sqrt{H^2 - K}} \quad ; \quad \text{if} \quad H^2 - K > 0 \\
\lambda_{,s} &= H_{,s} \quad ; \qquad\qquad\qquad \text{if} \quad H^2 - K = 0
\end{aligned}
\qquad (7.69)
$$

## 7.7 Numerical experiments

In the present section, different aspects treated in this chapter are further analyzed with the help of some numerical experiments. Emphasis is made on the same example, on which different tests are performed. This way several factors can be studied in the same structure and their effects can be better understood.

This is important since it allows a better comprehension of the influence of shape description and control techniques in results obtained.

It should be noted that even though stress and displacement constraints are very common and neccesary in structural optimization, in numerical experiments presented here they are not considered. This is due to the fact that the consideration of additional constraints may conceal the real effects under study.

First, a simple numerical experiment shows the differences between the two parametrization techniques compared in Section 7.2: CAD-based and FE-based parametrization. Comparison is made on the basis of analysis of optimum results obtained for both techniques, with different initial designs in a problem where strain energy is minimized.

Curvatures of a certain surface are computed both analytically and numerically with the approach proposed in Section 7.5. Good performance of this numerical approach is shown. These curvatures are also used to control design shape in structural optimization problems by introducing a regularization term as explained in Section 7.3.3. To show how this regularization term influences designs, experiments of design optimization minimizing the regularization term alone are presented. Here, it will be observed how design shape can be controlled by means of curvatures. Finally, examples where regularization term is applied to a structural optimization problem of minimizing strain energy are given.

## 7.7.1 Comparison of CAD-based and FE-based parametrization

A shell structure is to be optimized with respect to strain energy using both a CAD and a FE based design parametrization.

The initial design, depicted in Figure 7.8, consists of a parabolic cupola, whose projection on the $xy$-coordinate plane is a square. The cupola is modeled by a 9-node Lagrange design element, where the $z$-coordinate of the central node is $s_1$ and the $z$-coordinate of the central nodes at the edges is $s_2$. Therefore, different initial designs can be considered giving different values to $s_1$ and $s_2$. Any vertical section containing the main axis of the structure will be a parabola. However, in general the design is not a paraboloid of revolution, since two of these arbitrary sections may produce parabolas of different characteristics. Material properties are also given in Figure 7.8. The load case considered is self-weight.

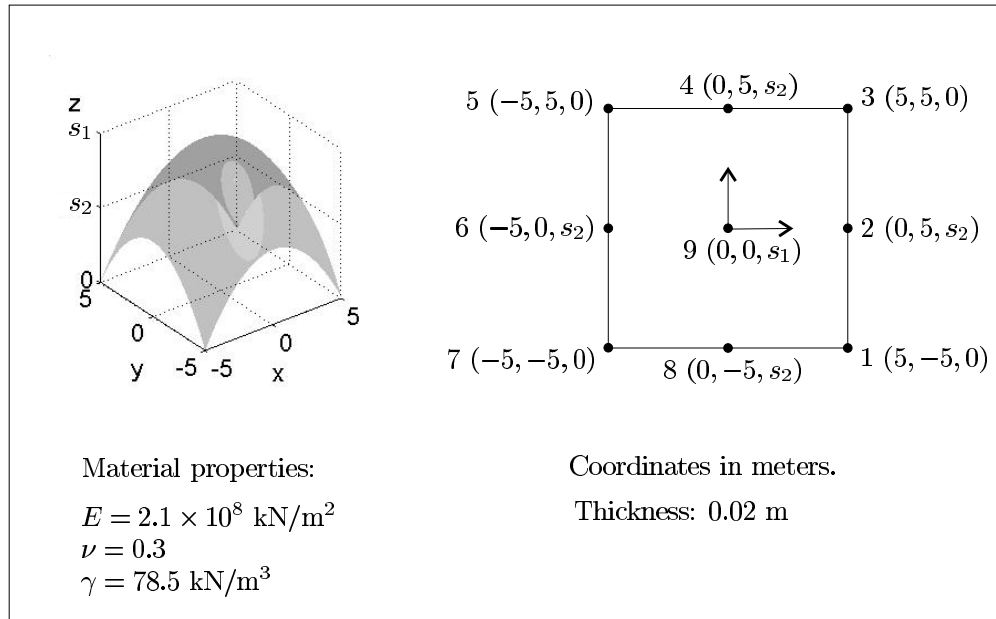The structure is discretized by a mesh of $7 \times 7$ bilinear elements. The DSG

Figure 7.8: Parabolic cupola. Initial design and material properties

method, explained in Section 3.12, is considered in order to prevent shear locking, because the structure is a thin shell. No modification is used to prevent membrane locking, since as elements are bilinear and the mesh is not highly distorted, no significant membrane locking is expected. The importance of a reliable finite element formulation and, in particular, the influence of locking in the optimization process, has been stated in Chapter 6.

The structure is pin-supported at its four corners. These supports are modelled preventing displacements of the four corner nodes. It is known that this technique is a source of singularities, that is, stresses at these nodes will not converge when the mesh is refined. However, as the mesh used is too coarse ($7 \times 7$ elements), there is no need to consider preventing displacements of adjacent nodes. That is, the real dimension of supports is very small in relation to the element side. Nevertheless, it should be remarked that in case the mesh is refined, displacements of the adjacent nodes have also to be prevented, up to a certain refinement level.

Shape optimization which minimizes strain energy of this initial design, is performed in two different ways. First, CAD design parametrization is used. The same variables used to produce different initial designs, $s_1$ and $s_2$, are now considered as design variables. Second, FE based design parametrization is used. Here, all FE nodes except those located at the corners are allowed to move in $z$-

direction to produce modified designs. Therefore, a total of 60 design variables are considered.

Figure 7.9 shows optimal designs obtained with both parametrizations, for different initial designs. All considered initial designs have the same value for $s_1$ but different values for $s_2$. Values of strain energy for initial and optimal designs are also given.

The obtained results show the significance of the influence of the initial design on the final optimal designs. In a shape optimization process, optimal designs obtained by the optimization algotithm may be local or global optima. Obtaining one or the other is difficult to predict and control because the objective function is usually highly nonconvex and its trend is difficult to forecast. The more design variables are considered, the more probable is the presence of local optima.

In Figure 7.9, it can be observed that even for CAD parametrization, where only two design variables are considered, two different optima are obtained. For initial designs with $s_2 = 3.0$ m and $s_2 = 5.0$ m (examples (c) and (d)), a local optimum design is obtained which is a significantly higher structure. However, initial designs with $s_2 = 0.0$ m and $s_2 = 1.5$ m (examples (a) and (b)) yield a different optimal design, more shallow than the previous one and with a strain energy almost 50% lower. All of them are optimal designs in the sense that their strain energy represent a minimum. However, final design of (a) and (b) are a 'better' optimum.

In FE-based parametrization, as more design variables are considered, the presence of more local optima is expected. For this reason, different results are obtained for each initial design. It can be seen that FE parametrization is more flexible than CAD-based parametrization because it allows a wider set of admissible designs. None of the final designs obtained with FE parametrization could be obtained with the CAD parametrization chosen. It is important to note that these designs are more optimal than those obtained for CAD parametrization because their strain energy is lower in all cases. Of course, it may be argued that in this example the underlying CAD model is very simple. A more complex one with multiple spline based patches could have been chosen. However, as explained in Section 7.2.3, this would imply a higher modelling effort to be made by the designer.

A significant characteristic of FE parametrization is that it can yield to nonsmooth solutions. These can be seen especially in optimal designs obtained for the initial design with $s_2 = 0.0$ m and $s_2 = 5.0$ m. These designs are actually
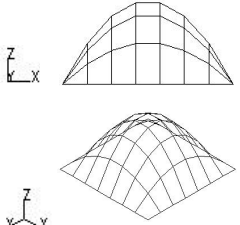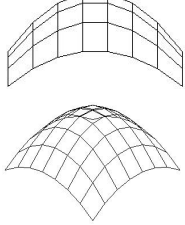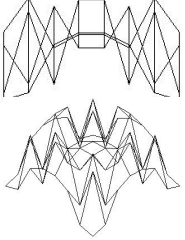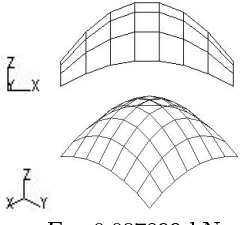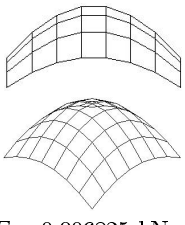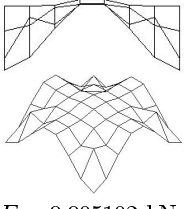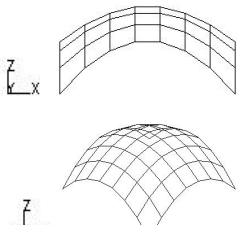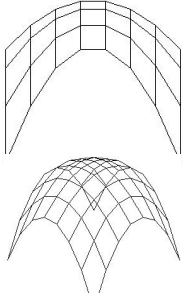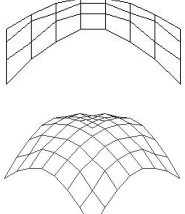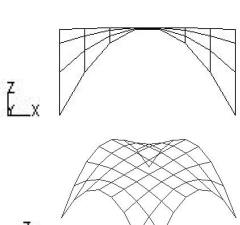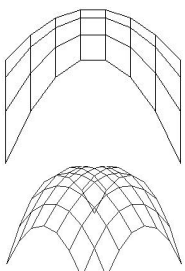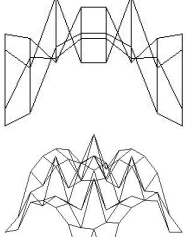
| INITIAL DESIGN | CAD BASED PARAMETRIZATION | FE BASED PARAMETRIZATION |
|---|---|---|

(a) $s_1 = 5.0$ m and $s_2 = 0.0$ m



$F = 0.050481$ kN m     $F = 0.006815$ kN m     $F = 0.005933$ kN m

(b) $s_1 = 5.0$ m and $s_2 = 1.5$ m



$F = 0.007899$ kN m     $F = 0.006825$ kN m     $F = 0.005102$ kN m

(c) $s_1 = 5.0$ m and $s_2 = 3.0$ m



$F = 0.029245$ kN m     $F = 0.013362$ kN m     $F = 0.005218$ kN m

(d) $s_1 = 5.0$ m and $s_2 = 5.0$ m



$F = 0.155494$ kN m     $F = 0.013351$ kN m     $F = 0.005872$ kN m

Figure 7.9: Optimal designs obtained by minimization of strain energy for different initial designs and parametrization techniques.

147

solutions to the optimization problem, but usually smooth shapes are prefered. Moreover, because of the waves, resulting meshes may be too distorted and yield unreliable results in the structural and sensitivity analyses. They may even cause the abort of the optimization process, due to high distortion of individual elements. This is the case of examples (a) and (d) in Figure 7.9. They are not converged designs and the optimization process was aborted due to the high level of mesh distortion. As shown in Chapter 6, the quality of structural and sensitivity analyses is crucial in the optimization process.

For these reasons, regularization and smoothing techniques are required to control design smoothness.

## 7.7.2   Computation of mean and Gaussian curvature of a discretized surface

This section presents some examples, where mean and Gaussian curvatures of surfaces approximated by a $C^0$ continuous mesh are computed by the approach proposed in Section 7.5. These examples will show the good approximation obtained by this method.
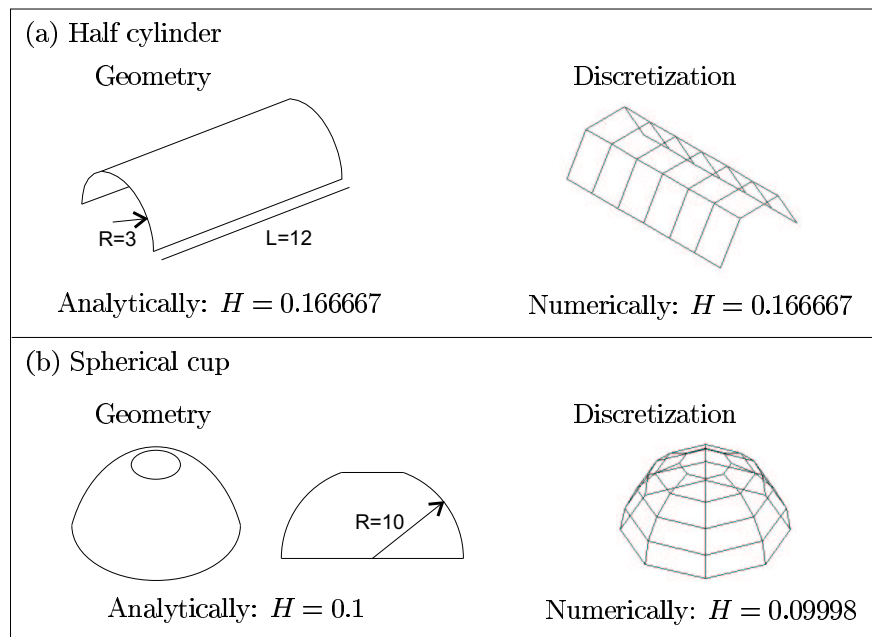


Figure 7.10: Examples of computation of the mean curvature numerically

The first example is a cylinder depicted in Figure 7.10.a. It is known that the

principal curvatures at any point of the cylinder are $\kappa_1 = \frac{1}{3}$, since $R = 3$ is the cylinder radius and $\kappa_2 = 0$, because a cylinder is a developable surface. Therefore, the mean curvature at any point of the cylinder is

$$H = \frac{\kappa_1 + \kappa_2}{2} = \frac{1}{6} \tag{7.70}$$

The surface is discretized with a very coarse mesh and its mean curvature is computed numerically. The numerical curvature computed at the interior nodes coincides with the exact value. For nodes located at the boundary meridians, the computed curvature differs from the exact value, due to limitations of this approach explained in Section 7.5.4.

In the second example, depicted in Figure 7.10.b, the mean curvature of a semisphere with a hole at the top is computed. The radius of the sphere is $R = 10$, and therefore, the principal curvatures are $\kappa_1 = \kappa_2 = \frac{1}{10}$. The analytical mean curvature is $H = 0.1$. The surface has been also discretized with a coarse mesh. The numerical mean curvature, obtained with this mesh for the interior nodes, is $H = 0.09998$, which is again a very good approximation.

A paraboloid of revolution is now considered. The general explicit equation of a paraboloid of revolution, whose axis of revolution is coincident with the $z$ coordinate axis, is given by

$$z(x, y) = a(x^2 + y^2) + h \tag{7.71}$$

$a$ and $h$ being two parameters. The paraboloid of revolution has parabolic cross sections in planes parallel to the axis of revolution and circular cross sections in planes normal to the axis of revolution. The analytical expresion which gives the mean curvature of this paraboloid at any point $P(x, y, z)$ of its surface, reads

$$H(x, y) = \frac{2(a + 2a^3(x^2 + y^2))}{(1 + 4a^2(x^2 + y^2))^{(3/2)}} \tag{7.72}$$

And the expression for the Gaussian curvature is

$$K(x, y) = \frac{4a^2}{(1 + 4a^2(x^2 + y^2))^2} \tag{7.73}$$

In Figure 7.11, mean curvature function and Gaussian curvature function for a paraboloid of revolution are shown. Analytically, they are computed according to formulae 7.72 and 7.73. Numerically, they are computed at nodes using a
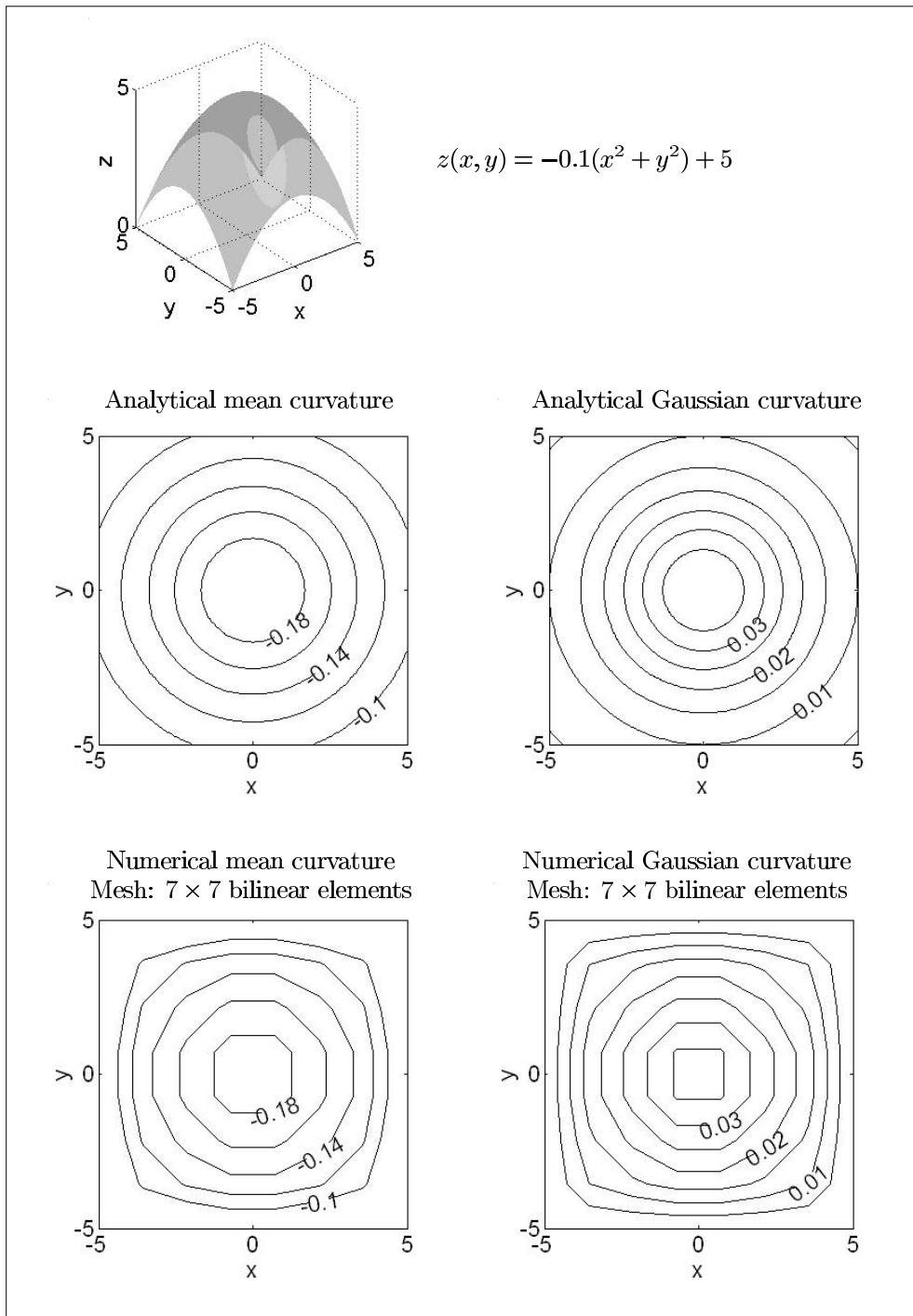
Figure 7.11: Paraboloid of revolution and its mean curvature function and Gaussian curvature function, computed both analytically and numerically

150

mesh of $7 \times 7$ bilinear elements. In order to obtain the curvature functions, nodal curvatures have been interpolated using shape functions. It should be noted that in the plots of the numerical curvatures two approximation factors are mixed: the numerical computation of curvature at nodes and the numerical interpolation of these values.

It can be concluded that the present method approximates very well the curvature of surfaces discretized by a $C^0$-continuous mesh of elements, even for rough discretizations.

### 7.7.3 Interpretation of the regularization term

Before applying the proposed regularization term to strain minimization problems, it is very interesting to see its effects, when used alone as objective function in a shape optimization process. For this reason, the shape optimization of a surface has been considered, minimizing an objective function of the form

$$\int_{\Omega} (H(x,y) - \bar{H})^2 d\Omega \tag{7.74}$$

This expression is obtained considering the mean curvature in regularization term (7.1).

The initial geometrical data considered is the same as in Figure 7.8 with $s_1 = 3.0$ m and $s_2 = 0.0$ m. Of course, in this case no material properties or load need to be considered, because here design optimization is based only on geometrical properties and not on the structural behaviour. FE-based design parametrization is used. As in Section 7.7.1, all FE nodes except those located at the corners are allowed to move in $z$-direction to produce modified designs. It should be noted that, in this case, objective function (7.74) converges to zero during the optimization process.

In Figure 7.12, optimal designs obtained for three different constant values of $\bar{H}$ over all domain are presented. In these experiments, only contributions of inner elements to objective function (7.74) are considered. Contributions of elements at boundaries are not considered, due to limitations of the approach used to compute curvatures at boundary nodes (see Section 7.5.4).

In Figure 7.12.a, the prescribed curvature is $\bar{H} = 0.0$ m$^{-1}$. Intuitively, it can be interpreted that, in this particular case, minimizing (7.74) implies that a search for a surface, whose mean curvature approximately vanishes, is undertaken. The
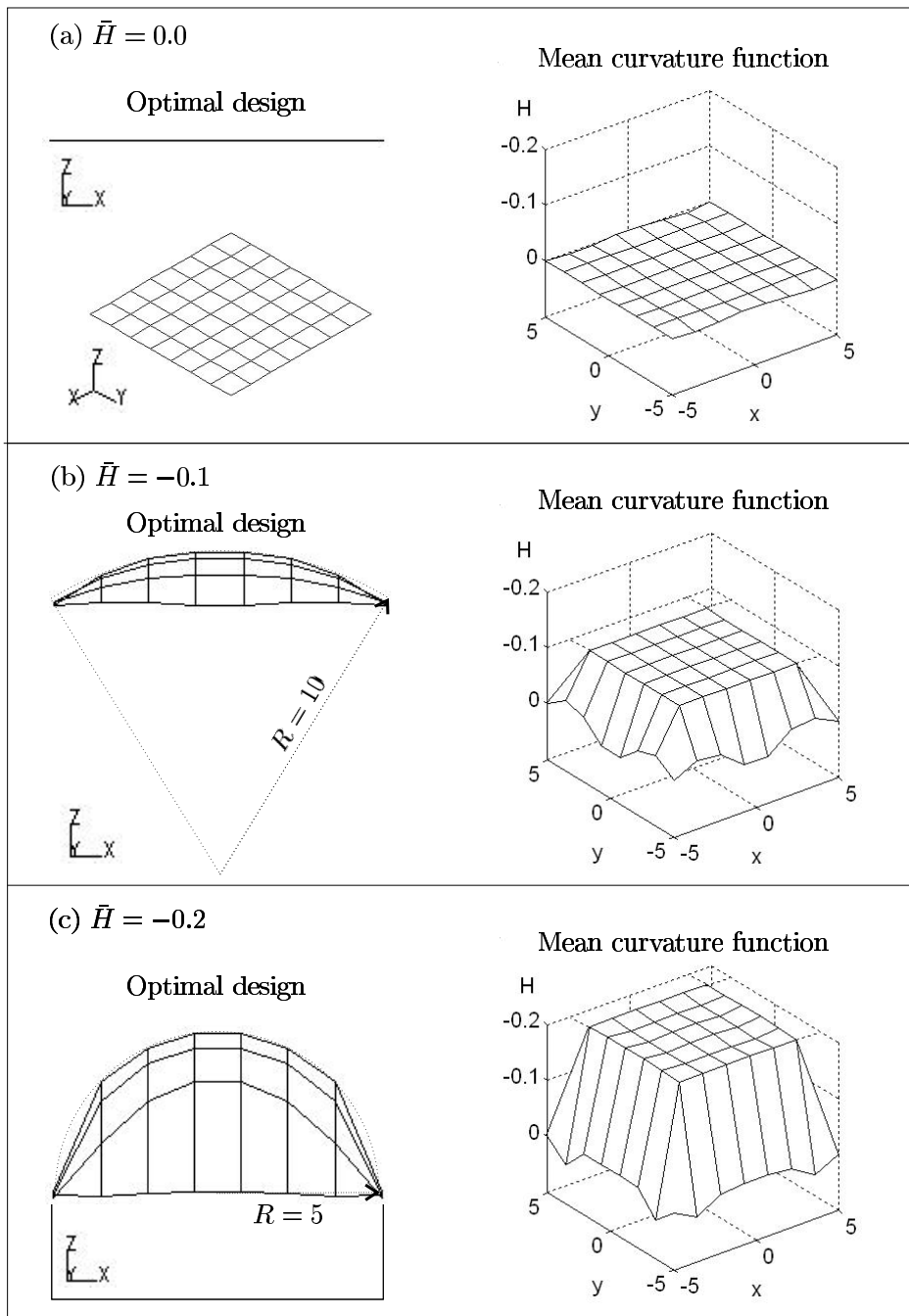
Figure 7.12: Minimization of the regularization term for different values of prescribed mean curvature: optimal designs obtained and its mean curvature function.

optimal design obtained, a plane, and its mean curvature function confirms this fact.

In Figure 7.12.b, the optimal design obtained for a prescribed mean curvature $\bar{H} = -0.1 \text{ m}^{-1}$ is depicted. The negative sign is due to the surface orientation and definition of the normal vectors to the surface at the FE nodes, which, in the present case, point outwards. This prescribed curvature is actually the mean curvature of a sphere of diameter 20 m. Notice that the length of the side of the plan of the designs in the $xy$-coordinate plane is 10 m. Therefore, as a result we can expect 'a kind of' a part of a sphere of diameter 20 m. It will be only 'a kind of' because the plan is a square, and not a circle. An arc of a circle of diameter 20 m has been ploted in dashed line. It can be seen how this arc matches with the section of the optimal design obtained. The plot of the mean curvature function of the optimal design also shows a good approximation to the prescribed function. It is important to note that as contributions of boundary elements to the regularization term are not considered, no value has been prescribed for curvatures of boundary nodes.

Figure 7.12.c shows results obtained for the case of $\bar{H} = -0.2 \text{ m}^{-1}$. This is the mean curvature of a sphere with a diameter of 10 m. Analogous to the previous case, an arc of a circle 10 m in diameter has been ploted. It can also be seen that it matches with the section of the optimal design. Mean curvatures at interior nodes are also very well approximated to the prescribed one. Consequently, the optimal design obtained is a kind of hemisphere.

In these numerical experiments, it has been shown how the regularization term alone controls design shape. Design is modified to obtain a curvature function approximated to the prescribed one at the nodes where regularization is considered. Here, a constant prescribed mean curvature function has been considered and contributions of all inner elements have been taken into account. More sophisticated applications of the regularization term can also be considered. Instead of a constant function for the prescribed curvature, another kind of function can be chosen. Moreover, contributions of only certain selected elements can be considered, permiting arbitrary curvatures at nodes, which are not sharing these elements.

### 7.7.4   Regularization of FE-based optimization

In Section 7.7.3,the effects of minimizing only the regularization term over surface designs have been shown. This regularization term is used to smooth de-

signs in a structural shape optimization problem, which minimizes strain energy and uses FE-based parametrization.

In Section 7.7.1 a parabolic cupola was optimized with respect to strain energy, using both CAD- and FE-based parametrization. Designs obtained for FE design parametrization were wiggly shapes. The same optimization problem is considered in this section but, in addition to the original objective function, a regularization term based on mean curvatures is considered. Therefore, the modified objective function reads,

$$F_\beta = F + R_\beta \tag{7.75}$$

where

$$F = \frac{1}{2} \int_V \bar{\sigma} \bar{\varepsilon} dV \tag{7.76}$$

$$R_\beta = \frac{\beta}{2} \int_\Omega (H - \bar{H})^2 d\Omega \tag{7.77}$$

It is important to note that, as

$$\frac{1}{2} \int_\Omega (H - \bar{H})^2 d\Omega = \frac{R_\beta}{\beta} \tag{7.78}$$

is dimensionless, the regularization parameter $\beta$ has the units of strain energy to perform summation in equation (7.75).

The initial geometry considered is again the same as in Figure 7.8 with $s_1 = 5.0$ m and $s_2 = 0.0$ m. Material properties are also the same and the load considered is again self weight as in Section 7.7.1. Pin supports are again considered at the four corners. Also a mesh of $7 \times 7$ is used and the DSG method is considered to prevent shear locking. FE based design parametrization is used and design variables are $z$-coordinates of all nodes except those located at the corners.

As in Figure 7.12.c, a prescribed mean curvature $\bar{H} = -0.2$ m$^{-1}$ is considered and only contributions of inner elements are taken into account.

Different values of the regularization parameter have been considered. The regularization parameter tunes the significance of the regularization term in the optimization process. Consequently, it can be used as a control tool of the shape design. This effect can be observed in the final designs obtained and their mean curvature functions shown in Figure 7.13, as well as by analyzing Tables 7.1 and 7.2.

Analysis of Table 7.1 shows values of the objective function for the initial design considering different regularization parameters. As in all cases, the initial

design is the same, the strain energy and $\frac{R_\beta}{\beta}$ is also the same. However, as the regularization parameter is different for each case, $R_\beta$ and, consequently, $F_\beta$ are also different. Therefore, for identical optimization problems, the larger the regularization parameter is, the larger is the contribution of the regularization term in the initial modified objective function $F_\beta$.

Table 7.1: Initial values for strain minimization with regularization.

| $\beta$ | $F_\beta$ | Strain energy | $R_\beta$ | $\frac{R_\beta}{\beta}$ |
|---------|-----------|---------------|-----------|-------------------------|
| (kN m)  | (kN m)    | (kN m)        | (kN m)    |                         |
| 0.001   | 0.050583  | 0.050481      | 0.000103  | 0.103                   |
| 0.005   | 0.050994  | 0.050481      | 0.000513  | 0.103                   |
| 0.01    | 0.051507  | 0.050481      | 0.001026  | 0.103                   |
| 0.05    | 0.055611  | 0.050481      | 0.005130  | 0.103                   |

Table 7.2: Final values for strain minimization with regularization.

| $\beta$ | $F_\beta$ | Strain energy | $R_\beta$ | $\frac{R_\beta}{\beta}$ |
|---------|-----------|---------------|-----------|-------------------------|
| (kN m)  | (kN m)    | (kN m)        | (kN m)    |                         |
| 0.001   | 0.007159  | 0.006460      | 0.000699  | 0.699000                |
| 0.005   | 0.006738  | 0.005912      | 0.000826  | 0.165200                |
| 0.01    | 0.007289  | 0.006264      | 0.001025  | 0.102500                |
| 0.05    | 0.009732  | 0.009531      | 0.000201  | 0.001930                |

The use of a larger regularization parameter implies a stronger control of the shape design through the regularization term. Therefore, it can be expected that the design moves tending to the prescribed curvature function during the optimization process, even to the point of sacrificing in part the strain energy criteria. Lower values of the regularization parameter, on the contrary, imply a not so severe control of the design shape. In these cases, design will be influenced mostly by the strain energy minimization criteria.

In Figure 7.13 it can be observed that tests done with a larger regularization parameter yield smoother designs and their mean curvature function is closer to the prescribed value $\bar{H} = -0.2$ m$^{-1}$. On the other hand, the lower this parameter is chosen, the less significance the regularization term has and the less smooth is the final design obtained. Its mean curvature function differs also each time more from the prescribed constant value and it is very noisy, because of the wiggles present in the optimal design.
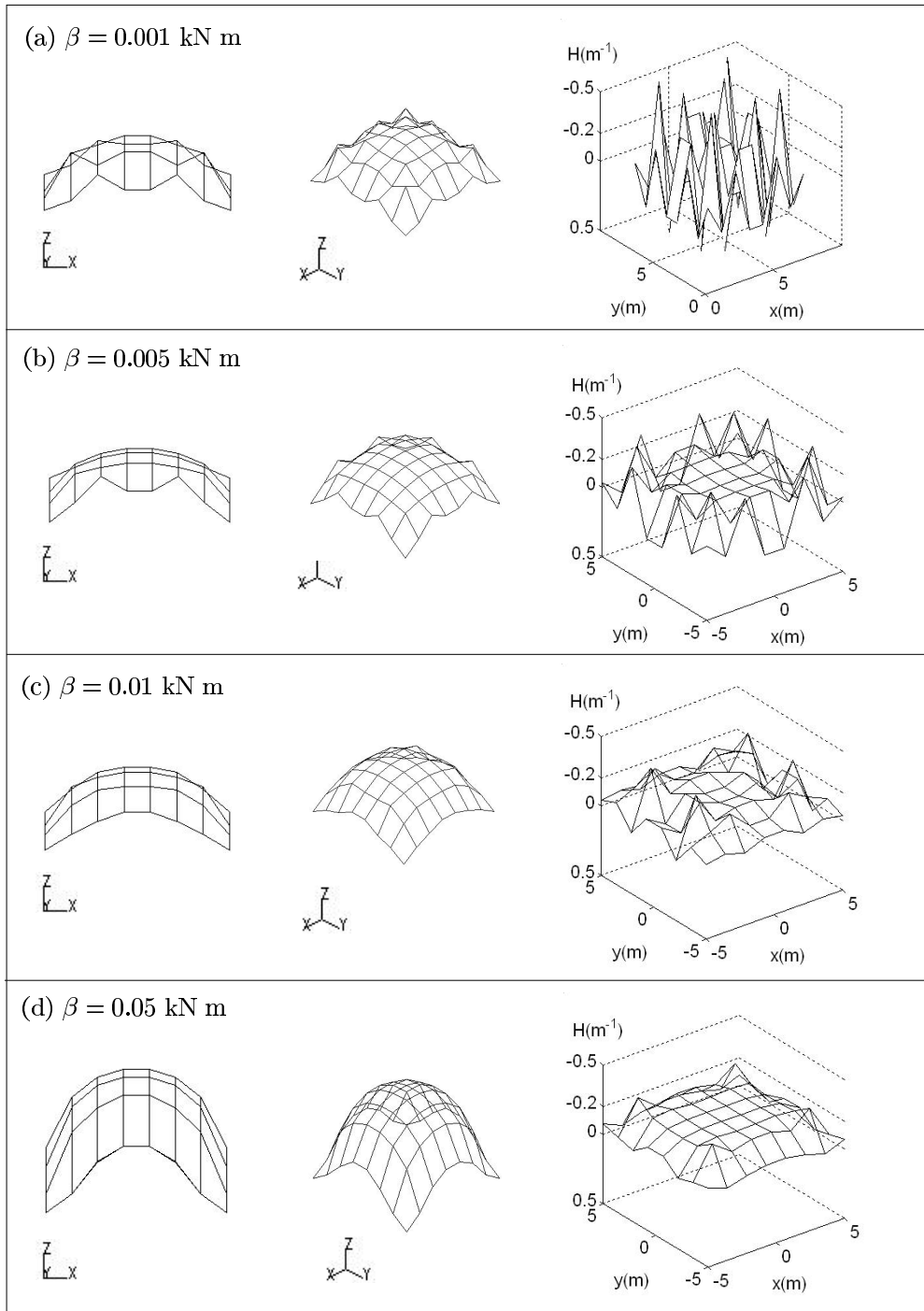
Figure 7.13: Final designs and their mean curvature function considering strain minimization and a regularization term for different regularization parameters.

156

The optima obtained are most probably not the only possible results to the optimization problem. That is, we can not affirm that they are global optima. The penalization of the original objective function with a regularization term does not ensure the elimination of alternative local optima. It is important to note that the set of admissible designs is not modified by the consideration of this regularization term but it only favours obtaining designs with a curvature close to the prescribed one.

In Table 7.2 the final values for the modified objective function and the single contribution of strain energy and regularization term are given. A larger regularization parameter implies that the adaptation of the design to the prescribed curvature function has more influence on the search for an optimal design. Therefore, it can be expected that, for larger regularization parameters, the term $\frac{R_\beta}{\beta}$ for the final design is lower. This can be confirmed in Table 7.2 and is interpreted as a better approximation of the curvature's design to the prescribed curvature function.

On the other hand, a lower regularization parameter implies that shape control through regularization is relaxed and the strain energy criteria gains more relevance in the optimization process. In principle, the more relaxed this shape control is, the lower the values for the strain energy can be expected. This is the general trend that can be observed in Table 7.2. However, due to the presence of multiple local optima, nothing assures this and final designs may have a larger strain energy even though they are less smooth (see the case of $\beta = 0.001$ kN m).

Let us now consider the same shape optimization problem (Figure 7.8) but using a different prescribed curvature function in the regularization term. The structure is discretized now with a mesh of 18x18 elements, that is, a finer mesh as before. The $z$-coordinates of all finite element nodes, except those located at the corners, are taken as design variables.
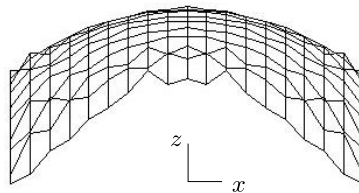


Figure 7.14: Final design obtained with minimization of strain energy when no regularization is considered.

Figure 7.14 shows the final result obtained if no regularization is used. As in

the case of the coarser mesh, a wiggly shape is obtained. The waves appearing are mesh depending, since FE-parametrization is used.

(a) Prescribed mean curvature H ($m^{-1}$)        b) Design with the curvature function given in (a)
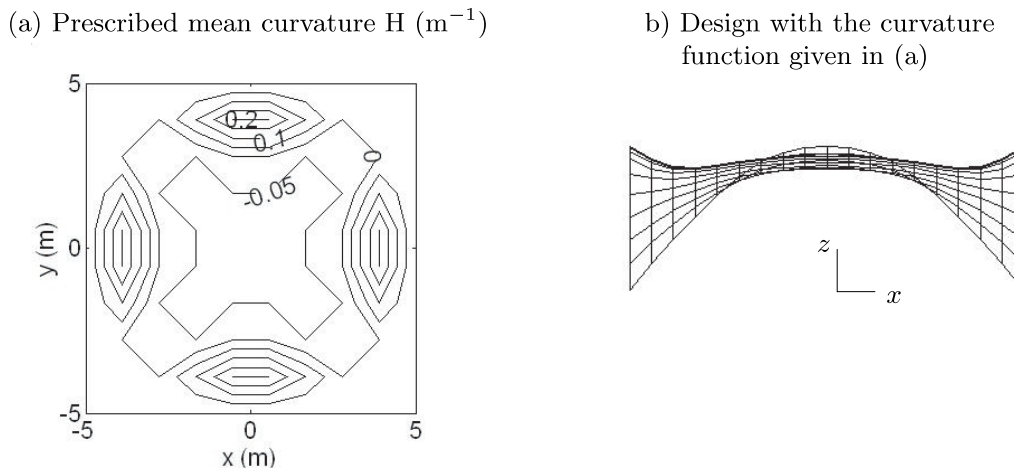


Figure 7.15: Prescribed curvature function and design related to it.

In Figure 7.15.a the contour plot of the prescribed curvature function considered now is depicted. It is important to note that in this case the prescribed curvature function is not constant over the domain. The curvature function depicted in Figure 7.15.a is that of the design shown in Figure 7.15.b. As in the previous case, regularization is only applied in the inner elements. The regularization parameter is chosen to be $\beta = 0.05$kNm.
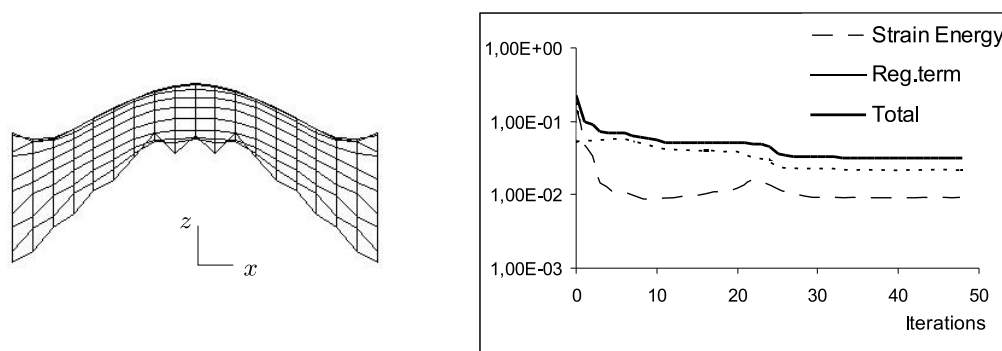


Figure 7.16: Final design obtained considering regularization and evolution of the terms of the objective function in the optimization process.

Figure 7.16 shows the final design obtained considering minimization of the strain energy and the aforementioned regularization. As it can be observed, the

158

final design obtained is a compromise between the one obtained without considering regularization and the one related to the curvature function prescribed. The graphic given shows the evolution of the strain energy, regularization term and the sum of both (modified objective function) during the optimization process.

An important point not to be overlooked is that now minimization is performed on the sum of strain energy and regularization terms, and not on these terms separately. For this reason special attention should be paid to the value of the original function for the initial and final design. If the prescribed curvature function describes a totally inappropiate design shape in relation to the original objective function considered (here, the strain energy) and/or the regularization parameter is too high, it may occur that the value for the original objective function obtained is even larger than that for the initial design. The designer has to assess these cases based on his engineering experience.

Moreover, in minimization of the modified objective function, nothing assures that the value of the original energy function is lower than that of an optimization problem without regularization term. Designs with a lower original objective function may be sacrificed in favoring other designs with a higher original objective function but a curvature closer to the desired one.

Here, we come again to the question of what is an optimal design. In shape optimization not only structural criteria are considered, but also geometrical criteria. This is inherent to shape optimization and can not be circumvented, because the key is to modify the geometry of an initial design. The designer has to balance the significance of both structural and geometrical criteria in each particular case.

FE-based parametrization combined with regularization by means of curvatures is a good alternative to CAD parametrization especially for preliminary design. The flexibility of this approach is the key of its suitability. This flexibility is based on two important aspects:

- FE parametrization allows a wider set of admissible designs

- Performing experiments with different prescribed curvatures, different regularization parameters or different regularization areas does not require much effort from the designer. Only some parameters in the input data have to be changed.

In the case of CAD parametrization, in order to obtain such a flexibility, the underlying CAD model must be changed followed by subsequent modelling cost

for the designer. Consequently, FE parametrization with regularization is more interactive and user friendly when design flexibility is needed.

# Chapter 8

# Conclusions and Further Lines of Research

Optimum structural design is systematized as a group of several disciplines organized in modules, which interact in the optimization loop. A factor that may affect any of the modules in the optimization loop may spread throughout it and influence the final optimization result. Therefore, it is necessary to ensure that all modules provide reliable results and that the designer is aware of the consequences of his decisions regarding the formulation of the problem.

In shape optimization, the influence of the structure typology is extended in the optimization loop to the design module, structural analysis and sensitivity analysis. This is not that influential in the mathematical programming module, since there the optimization problem is considered in its most abstract form.

In the present work, special aspects of shape optimization of shells regarding the structural and geometrical vision of these structures have been studied.

In finite element analysis and sensitivity analysis, the structural behavior of the shell is studied for the actual design and predicted for potential design modifications. The information yielded by these analyses is used in the mathematical programming module by gradient based optimization algorithms, as basis for taking decisions about improving the actual design. Therefore, the quality of this information is most important for the optimization result.

The effects of shear locking phenomena on shape optimization of shells have been demonstrated both from the point of view of structural analysis and sensitivity analysis. Accuracy errors related to standard displacement finite elements will not only affect structural analysis but also sensitivity analysis.

The DSG method, a simple but efficient formulation to avoid locking, is considered as an alternative. The simplicity of the method, its good performance, its efficiency, and its uniform formulation for both triangular and quadrilateral elements make it particularly attractive. Analytic computation of sensitivity coefficients with DSG elements turns out to be as simple as for standard displacement elements, coming along with no additional computational cost. Consequently, the use of DSG elements in shape optimization appears to be very advantageous.

Numerical experiments confirm that a reliable analysis method is crucial not only for the accuracy of the optimum, but also for the principal type of design. In the optimization process, locking phenomena lead to a systematic error, which is difficult to detect and may have severe consequences. These consequences can be especially dramatic in the case of stress and displacement constraints. It has been demonstrated that in these cases, it may occur that the optimal design obtained is not even in the 'real' feasible domain, that is, the considered displacement or stress will violate the given constraint. Consequently, the solution obtained from the optimization procedure is not even in the group of admissible solutions. It should be remarked that the use of quadratic, instead of linear, standard displacement elements does not guarantee reliable results for stresses, even though displacements may converge rapidly.

Another important point regarding the quality of the information transferred to the optimization algorithm is the sensitivity analysis technique used. The need for more accurate results legitimates the use of the analytical approach, which involves higher mathematical complexity and requires profound knowledge of the finite element formulation at hand. The kind of sensitivity analysis is also decisive in the overall computational cost of the optimization process. If a high number of design variables are involved, adjoint techniques are highly recommended to attain a reasonable computational cost.

However, in an optimization process not only the computational cost has to be taken into account. The modeling cost is also a crucial factor, especially if it is considered that it is paid by the designer. This modeling cost is the effort, the designer invests in the formulation of the optimization problem, that is, the formulation of objective function and constraints and the definition of the design model.

Regarding the design model, two tasks are to be carried out: shape description and shape control of the design. These two tasks determine to a large extent the optimization result.

The parametrization of the design shape determines the set of admissible designs. The CAD-based parametrization constrains the admissible designs to a CAD model. This may be interesting, if the designer has a preconceived idea about the rough final shape, because of manufacture reasons, esthetics or previous optimization experiments. Shape control is attained by the underlying CAD model.

However, on occasions, the designer may have no previous idea about the final shape or the CAD definition may turn very complex because of the multitude of design patches and continuity requirements across them. For these cases, FE based design parametrization seems more suitable. This technique considers a larger number of design variables and, therefore, provides more freedom to the potential designs. This fact makes it very suitable for free formed shells. However, the larger the number of design variables, the more increases the probability of existence of local optima. The initial design considered may have special influence in obtaining the one or the other local optima. This is especially relevant when numerous local optima are present in the feasible domain.

A significant characteristic of the FE based parametrization is that wiggly shapes may appear. For instance, in the case of strain energy minimization, there is a tendency for these wiggly forms to appear, since they are prone to have a low strain energy. The problem of wiggly shapes is that the finite element reliability can be affected due to the high mesh distortion. Also, usually wiggly optimal designs are not desired because smooth shapes are preferred. For these reasons, shape control by regularization techniques is used.

Shape control by regularization techniques with consideration of intrinsic curvature properties has proved to be a very efficient method for obtaining smooth surfaces in shape optimization of shells. This approach is defined by the addition of a regularization term to the objective function. This term has the form of the integral of the square of the difference between an intrinsic curvature measure of the surface and a prescribed function. The consideration of this regularization term favors designs whose curvature function approximates the prescribed one. As the considered curvatures are intrinsic surface properties, this smoothing technique does not depend on underlying reference surfaces, as do other regularization approaches, used in shape optimization for fluids. The designer can control the smoothness of the final design through the reference curvature and the regularization parameter defined in the input data. The modeling cost of an optimization problem, using FE-based parametrization together with the smoothing techniques studied, is significantly low. On the contrary, achieving a similar versatility with a CAD-based parametrization technique would require a

change of the underlying CAD model, which may be very expensive, especially if multiple patches are considered, and continuity conditions across them are required.

An important point of the considered regularization techniques is the computation of curvature measures of a surface approximated by a polygonal mesh. The key aspect of the proposed approach lies on the information contained by the averaged director vectors defined at the nodes of the mesh. These vectors are computed as the average of the normals to the adjacent elements at the considered point. As a consequence, they are an approximation to the normals of the original surface at the nodes. The tensor of curvatures at each node is computed and from this, other curvatures such as mean, Gaussian and principal curvatures can be computed. Numerical examples showed the good performance of this method. An important advantage of the approach is its coherence with the geometrical definition of the finite element mesh, which means that all geometrical and topological data is already available. Moreover, sensitivities of the different curvature measures can be computed analytically, which is important for the derivation of the regularization term.

The consideration of this kind of regularization modifies the objective function and, as a consequence, the original mathematical formulation of the optimization problem. The designer has to assess the influence of this shape control by analyzing the objective function values and adjusting the regularization parameter as well as prescribed curvatures, in order to find the optimal design. Probably, the most difficult task in optimization is to determine what is an optimum. When a certain design is said to be optimal, it is meant that it is optimal with respect to certain criteria. From the criteria that the designer may want to consider, only those which are possible to be translated into a mathematical expression, can be considered in the formal definition of the optimization problem. Other more subjective criteria, like esthetics, are considered in the design module and shape control. Therefore, shape control is also a module of decision, not based on the value of a certain function, but on the subjective criteria of the designer. Also, he can control the weighting of this subjective factor by tuning the parameters of shape control.

In the present work, this smooth control approach is explained in the frame of shape optimization of shells. However, these control techniques can also be applied to smooth control of membranes or boundaries of 3D bodies. Moreover, they can be used in combination with CAD-based parametrization, although here, its effectivity is constrained by the underlying CAD model.

In shape optimization with FE-based design parametrization, questions regard-

ing shape control require solving, especially in case of surfaces. An important aspect is the determination of the most advantageous way to define the nodal movements in the optimization process. In the case of surfaces and curves, it should be noted that if the position of a node changes, such as its new position is also contained in the previous design, the finite element mesh is modified, but not the design shape. This fact has important consequences because it may cause high mesh distortion, which affects the results of the structural analysis and, hence, the final result of the optimization process. For this reason, it is neccesary to study different alternatives to avoid this phenomenon, such as allowing movements only in the normal direction to the surface or curve.

Further lines of research in the design module should be directed to provide flexibility to the optimization process. The aim is to develop more tools, which can be used by the designer to control the design geometry, while still attaining a low modeling cost. Some of these tools may be used to control design shape wavelength or to filter high frequency shape waves on surfaces and curvatures. Providing the designer with a high versatile set of design and control tools allows him to tackle a larger variety of shape optimization problems, especially of free formed surfaces. The search of this generality points the way towards a new concept of shape optimization and fits in the evolution tendency of structural optimization.

# Appendix A

## A.1 Two dimensional shape functions

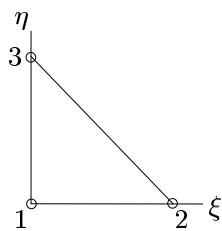The shape functions for the linear and bilinear elements are given by

Bilinear element (Q1)
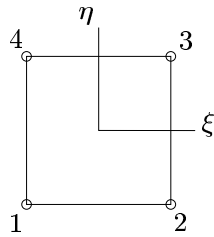


$$N_1 = \tfrac{1}{4}(1-\xi)(1-\eta) \; ; \qquad N_2 = \tfrac{1}{4}(1+\xi)(1-\eta) \; ;$$

$$N_3 = \tfrac{1}{4}(1+\xi)(1+\eta) \; ; \qquad N_4 = \tfrac{1}{4}(1-\xi)(1+\eta) \; ;$$

Linear element (T1)



$$N_1 = 1-\xi-\eta$$

$$N_2 = \xi$$

$$N_3 = \eta$$

## A.2 Derivative of a normalized vector

Consider a vector

$$\mathbf{v} = \mathbf{v}^*/|\mathbf{v}^*| \tag{A.1}$$

Its partial derivative with respect to a variable $s$ is given by

$$\mathbf{v}_{,s} = \frac{\mathbf{v}^*_{,s} |\mathbf{v}^*| - \mathbf{v}^* |\mathbf{v}^*|_{,s}}{|\mathbf{v}^*|^2} \tag{A.2}$$

where

$$|\mathbf{v}^*|_{,s} = \frac{\mathbf{v}^* \cdot \mathbf{v}^*_{,s}}{|\mathbf{v}^*|} \tag{A.3}$$

## A.3  Derivative of the magnitude of a vector

Consider a vector $\mathbf{v}^*$. The magnitude of $\mathbf{v}^*$ is given by

$$|\mathbf{v}^*| = \sqrt{\mathbf{v}^* \cdot \mathbf{v}^*} \tag{A.4}$$

and the derivative of this magnitude with respect to $s$ is given by

$$|\mathbf{v}^*|_{,s} = \frac{\mathbf{v}^* \cdot \mathbf{v}^*_{,s}}{|\mathbf{v}^*|} \tag{A.5}$$

## A.4  Derivative of a cross product

If we consider two vectors $\mathbf{a}(s)$ and $\mathbf{b}(s)$ in $\mathcal{R}^3$, the cross product $\mathbf{a} \times \mathbf{b}$ is given by

$$\mathbf{a} \times \mathbf{b} = \begin{pmatrix} a_2 b_3 - a_3 b_2 \\ a_3 b_1 - a_1 b_3 \\ a_1 b_2 - a_2 b_1 \end{pmatrix} \tag{A.6}$$

where $a_i$ and $b_i$ are the $i^{th}$ component of the vectors $\mathbf{a}$ and $\mathbf{b}$ respectively.

The derivative of the cross product with respect to the variable $s$ is obtained as

$$
\begin{aligned}
(\mathbf{a} \times \mathbf{b})_{,s} &= \begin{pmatrix} (a_2)_{,s}\, b_3 - (a_3)_{,s}\, b_2 + a_2 (b_3)_{,s} - a_3 (b_2)_{,s} \\ (a_3)_{,s}\, b_1 - (a_1)_{,s}\, b_3 + a_3 (b_1)_{,s} - a_1 (b_3)_{,s} \\ (a_1)_{,s}\, b_2 - (a_2)_{,s}\, b_1 + a_1 (b_2)_{,s} - a_2 (b_1)_{,s} \end{pmatrix} \\
&= \begin{pmatrix} (a_2)_{,s}\, b_3 - (a_3)_{,s}\, b_2 \\ (a_3)_{,s}\, b_1 - (a_1)_{,s}\, b_3 \\ (a_1)_{,s}\, b_2 - (a_2)_{,s}\, b_1 \end{pmatrix} + \begin{pmatrix} a_2 (b_3)_{,s} - a_3 (b_2)_{,s} \\ a_3 (b_1)_{,s} - a_1 (b_3)_{,s} \\ a_1 (b_2)_{,s} - a_2 (b_1)_{,s} \end{pmatrix} \\
&= (\mathbf{a}_{,s} \times \mathbf{b}) + (\mathbf{a} \times \mathbf{b}_{,s})
\end{aligned} \tag{A.7}
$$

In (A.7) it can be seen that the product rule applies for the cross product.

# Bibliography

Adelman, H. M. and Haftka, R. T. (1986). Sensitivity analysis of discrete structural systems. *AIAA Journal*, 24(5):823–832.

Ahmad, S. (1969). *Curved Finite Elements in the Analysis of Solids, Shells and Plate Structures*. PhD thesis, Department of Civil Engineering, University of Wales, Swansea.

Arora, J. S. (1993). An exposition of the material deirvative approach for structural shape sensitivity analysis. *Computer Methods in Applied Mechanics and Engineering*, 105:41–62.

Arora, J. S., Lee, T. H., and Cardoso, J. B. (1992). Structural shape sensitivity analysis: Relationship between material derivative and control volume approaches. *AIAA Journal*, 30(6):1638–1648.

Bängtsson, E., Noreland, D., and Berggren, M. (2003). Shape optimization of an acoustic horn. *Computer Methods in Applied Mechanics and Engineering*, 192:1533–1571.

Barthelemy, B., Chon, C. T., and Haftka, R. T. (1988). Accuracy problems associated with semi-analytical derivatives of static response. *Finite Elements in Analysis and Design*, 4:249–265.

Barthelemy, B. and Haftka, R. T. (1988). Aiaa paper 88-2284. In *Proc. AIA/ASME/ASCE/ASC 29th Structures, Structural Dynamics and Material Conf. Part 1*, pages 572–581, Williamsburg, VA. Also as: Accuracy analysis of the semi-analytical method for shape sensitivity. Mech. Struct. Mach., 18, 407-432 (1990).

Barthelemy, B., Haftka, R. T., and Cohen, G. A. (1989). Physically based sensitivity derivatives for structural analysis problems. *Computational Mechanics*, 4:465–476.

Bathe, K.-J. (1996). *Finite Element Procedures.* Prentice Hall, New Jersey.

Becker, E. B., Carey, G. F., and Oden, J. T. (1981). *Finite Elements. Vol I: An Introduction.* Prentice Hall, New Jersey.

Belytschko, T., Liu, W. K., and Moran, B. (2000). *Nonlinear Finite Elements for Continua and Structures.* Wiley.

Benbenuto, E. (1991). *An Introduction to the History of Structural Mechanics. Part II: Vaulted Structures and Elastic Systems.* Springer.

Bendsoe, M. P. (1989). Optimal shape design as a material distribution problem. *Structural Optimization*, 1:193–202.

Bischoff, M. (1999). *Theorie und Numerik einer dreidimensionalen Schalenformulierung.* PhD thesis, Institut für Baustatik, Universität Stuttgart.

Bischoff, M. and Bletzinger, K.-U. (2001). Stabilized dsg plate and shell elements. In *Trends in Computational Structural Mechanics.*, Barcelona. CIMNE.

Bischoff, M., Wall, W. A., Bletzinger, K.-U., and Ramm, E. (2004). Models and finite elements for thin-walled structures. In *Encyclopedia of Computational Mechanics*. John Wiley & Sons. To appear.

Bletzinger, K.-U. (1990). *Formoptimierung von Flächentragwerken.* PhD thesis, Institut für Baustatik, Universität Stuttgart.

Bletzinger, K.-U. (1998). Form finding and optimization of membranes and minimal surfaces. Technical Report Report No. S 81, Lecture notes for the Ph.D.-course / Advanced school on Advanced Topics in Structural Optimization. Danish Center for Applied Mathematics and Mechanics,Technical University of Denmark.

Bletzinger, K.-U., Bischoff, M., and Ramm, E. (2000). A unified approach for shear-locking free triangular and rectangular shell finite elements. *Computers and Structures*, 75:321–334.

Bletzinger, K.-U., Kimmich, S., and Ramm., E. (1991). Efficient modelling in shape optimal design. *Computing Systems in Engineering*, 2(5/6):483–495.

Bletzinger, K.-U., Reitinger, R., Kimmich, S., and Ramm, E. (1993). Shape optimization with program carat. *International Series of Numerical Mathematics*, 110.

Bletzinger, K.-U., Wüchner, R., and Daoud, F. (2002). Stress controlled modification of minimal surface membrane design. In Mang, H. A., Rammerstorfer, F. G., and Eberhardsteiner, J., editors, *Proceedings of the Fifth World Congress on Computational Mechanics (http://wccm.tuwien.ac.at)*, Austria. Vienna University of Technology.

Bloor, M. I. G. and Wilson, M. J. (1989). Generating blend surfaces using partial differential equations. *Computer-Aided Design*, 21:165–171.

Bloor, M. I. G. and Wilson, M. J. (1990). Using partial differential equations to generate freeform surfaces. *Computer-Aided Design*, 22:202–212.

Braibant, V. and Fleury, C. (1986). Shape optimal design and cad oriented formulation. *Engineering with Computers*, 1:193–204.

Brockman, R. A. (1987). Geometric sensitivity analysis with isoparametric finite elements. *Communications in Applied Numerical Methods*, 3:495–499.

Brockman, R. A. and Lung, F. Y. (1988). Sensitivity analysis with plate and shell finite elements. *Int. J. Num. Meth. Engrg.*, 26:1129–1143.

Büchter, N. (1992). *Zusammanführung von Degenerationskonzept und Schalentheorie bei endlichen Rotationen*. PhD thesis, Institut für Baustatik der Universität Stuttgart, Stuttgart, Germany.

Cardoso, J. E. B. and Arora, J. S. (1988). Design sensitivity analysis of nonlinear structural response. *AIAA Journal*, 26(5):595–603.

Carey, G. F. and Oden, J. T. (1983). *Finite Elements. Vol II: A Second Course*. Prentice Hall, New Jersey.

Cheng, G., Gu, Y., and Zhou, Y. (1989). Accuracy of semi-analytic sensitivity analysis. *Finite Elements Anal. Des.*, 6:113–128.

Cheng, G. and Olhoff, N. (1991). New method of error analysis and detection in semi-analytical sensitivity analysis. In Rozvany, G. I. N., editor, *Lecture notes, NATO/DFG ASI, "Optimization of large structural systems" Vol 1*, pages 234–267, Berchtesgaden.

Cheng, G. and Olhoff, N. (1993). Rigid body motion test against error in semi-analytical sensitivity analysis. *Structural Optimization*, 46:515–527.

Choi, K. K. and Haug, E. J. (1983). Shape design sensitivity analysis of elastic structures. *Journal of Structural Mechanics*, 11(2):231–269.

171

Davies, A. and Samuels, P. (1996). *An Introduction to Computational Geometry for Curves and Surfaces.* Oxford Applied Mathematics and Computing Science Series. Oxford University Press, Oxford.

de Boer, H. and van Keulen, F. (2000). Refined semi-analytical design sensitivities. *International Journal for Solids and Structures*, 37:6961–6980.

de Boer, H., van Keulen, F., and Vervenne, K. (2002). Refined second order semi-analytical design sensitivities. *Int. J. Numer. Meth. Engng.*, 55:1033–1052.

Dems, K. and Mróz, Z. (1983). Variational approach by means of adjoint systems to structural optimization and sensitivity analysis - i. variation of material parameters with fixed domain. *International Journal of Solids and Structures*, 19(8):677–692.

Dems, K. and Mróz, Z. (1984). Variational approach by means of adjoint systems to structural optimization and sensitivity analysis - ii. structure shape variation. *International Journal of Solids and Structures*, 20(6):527–552.

do Carmo, M. P. (1976). *Differential Geometry of Curves and Surfaces.* Prentice-Hall, New Jersey.

Dubrovin, B. A., Fomenko, A. T., and Novikov, S. P. (1992). *Modern Geometry - Methods and Applications. Part I. The Geometry of Surfaces, Transformation groups and Fields.*, volume 93 of *Graduate Texts in Mathematics.* Springer-Verlag, New York.

Fenyes, P. and Lust, R. V. (1991). Error analysis of semi-analytic displacement derivatives for shape and sizing variables. *AAIA J.*, 29:271–279.

Flügge, W. (1973). *Stresses in Shells.* Springer- Verlag, Berlin.

Galilei, G. (1638). *Discorsi e Dimostrazioni matematiche, intorno á due nuove scienze Attenenti alla Mecanica et i Movimenti Locali.* Leida Appresso gli Elsevirii.

Gatzke, T. and Grimm, C. (2003). Improved curvature estimation on triangular meshes. In Kobbelt, L., Schröder, P., and Hoppe, H., editors, *Proceedings of the Eurographics Symposium on Geometriy Processing*, Aire-la-Ville, Switzerland. Eurographics Association.

Goldfeather, J. (2001). Understanding errors in approximating principal direction vectors. Technical report number 01-006, University of Minnesota, Minnesota.

Gunzburger, M. D., Kim, H., and Manservisi, S. (2000). On a shape control problem for the stationary navier-stokes equations. *Mathematical Modelling and Numerical Analysis*, 34(6):1233–1258.

Haftka, R. T. and Adelman, H. M. (1989). Recent developments in structural sensitivity analysis. *Structural Optimization*, 1:137–151.

Haftka, R. T. and Gürdal, Z. (1999). *Elements of Structural Optimization*. Kluwer Academic Publishers.

Haug, E. J. and Céa, J., editors (1981). *Optimization of distributed parameter structures*, volume 1 and 2. Sijthoff & Nordhoff, Alphen aan den Rijn, The Netherlands.

Haug, E. J., Choi, K. K., and Komkov, V. (1986). *Design Sensitivity Analysis of Structural Systems*, volume 177 of *Mathematics in Science and Engineering*. Academic Press.

Haug, E. J., Choi, K. K., and Yoo, Y. M. (1984). A variational method for shape optimal design of elastic structures. In Atrek, A., Gallagher, R. H., Ragsdell, K. M., and Zienkiewicz, O. C., editors, *New Directions in Optimum Structural Design*, chapter 5, pages 105–137. John Wiley and Sons, Chichester.

Hughes, T. J. R. (2000). *The Finite Element Method. Linear Static and Dynamic Finite Element Analysis.* Dover Publications, New York.

Hughes, T. R. J., Taylor, R. L., and Kanoknukulchai, W. (1977). A simple and efficient finite element for plate bending. *International Journal for Numerical Methods in Engineering*, 11:1529–1543.

Imam, M. H. (1982). Three-dimensional shape optimization. *International Journal for Numerical Methods in Engineering*, 18:661–673.

Jameson, A., Alonso, J. J., Reuther, J., Martinelli, L., and Vassberg, J. C. (1998). Aerodynamic shape optimization techniques based on control theory. Technical Report paper 98-2538, AIAA.

Kemmler, R. (2004). *Stabilität und große Verschiebungen in der Topologie- und Formoptimierung*. PhD thesis, Institut für Baustatik, Universität Stuttgart, Germany.

Kimmich, S. (1990). *Strukturoptimierung und Sensibilitätsanalyse mit finiten Elementen*. PhD thesis, Institut für Baustatik, Universität Stuttgart.

Kirchhoff, G. (1850). Über das gleichgewicht und die bewegung einer elastischen scheibe. *J. Reine und Angewandte Mathematik*, 40:51–88.

Kirsch, U. (1998). *Structural Optimization: Fundamentals and Applications*. Springer, Berlin.

Klein, B. (1955). Direct use of extremal principles in solving certain optimization problems involving inequalities. *J. ORSA*, 3:168–175.

Kobbelt, L., Campagna, S., Vorsatz, J., and Seidel, H. P. (1998). Interactive multi-resolution modeling on arbitrary meshes. In *Proceedings of the 25th International Conference on Computer Graphics and Interactive Techniques*, New York. ACM Press.

Koschnick, F., Bischoff, M., and Bletzinger, K.-U. (2002). Avoiding membrane locking with the dsg method. In Mang, H. A., Rammerstorfer, F. G., and Eberhardsteiner, J., editors, *Proceedings of the Fifth World Congress on Computational Mechanics (http://wccm.tuwien.ac.at)*, Austria. Vienna University of Technology.

Koschnick, F., Bischoff, M., Camprubí, N., and Bletzinger, K.-U. (2004). The discrete strain gap method and membrane locking. *Computer Methods in Applied Mechanics and Engineering*, Accepted for publication.

Lagrange, J. L. (1770). *Sur la figure des colonnes*. Miscellanea Taurinensia.

Liu, W. K., Belytschko, T., and Mani, A. (1986). Probabilistic finite elements for nonlinear structural dynamics. *Computer Methods in Applied Mechanics in Engineering*, 56:61–81.

Love, A. E. H. (1888). On the small vibrations and deformations of thin elastic shells. *Philosophical Transactions of the Royal Society*, 179:491 ff.

Malvern, L. E. (1969). *Introduction to the Mechanics of a Continuous Medium*. Prentice Hall, London.

Marsden, J. E. and Hughes, T. R. J. (1983). *Mathematical Fpundations of Elasticity*. Prentice Hall, London.

Maute, K. and Raulli, M. (2004). An interactive method for the selection of design criteria and the formulation of optimization problems in computer aided optimal design. *Computers and Structures*, 82:71–79.

Maxwell, J. C. (1890). *Scientific Papers*, 11:175.

Michell, A. G. M. (1904). The limit of economy of material in frame structures. *Philosophical Magazine*, 8:589–597.

Mindlin, R. D. (1951). Influence of rotatory inertia and shear in flexural motions of isotropic elastic plates. *Journal of Applied Mechanics*, 18:31–38.

Mlejnek, H. P. (1992). Accuracy of semi-analytical sensitivities and its improvement by the 'natural method'. *Struct. Optim.*, 4:128–131.

Mohammadi, B. (1997). A new optimal shape design procedure for inviscid and viscous turbulent flows. *International Journal for Numerical Methods in Fluids*, 25:183–203.

Mohammadi, B. and Pironneau, O. (1999). Mesh adaption and automatic differentiation in a cad-free framework for optimal shape design. *International Journal for Numerical Methods in Fluids*, 30:127–136.

Mohammadi, B. and Pironneau, O. (2001). *Applied Shape Optimization for Fluids*. Oxford University Press, Oxford.

Myers, R. H. and Montgomery, D. C. (2001). *Response Surface Methodology. Process and product optimization using designed experiments.* John Wiley and Sons, New York.

Naghdi, P. M. (1972). The theory of shells. In Flügge, S., editor, *Handbuch der Physik*, volume VI/2. Springer, Berlin.

Navarrina, F. (1987). *Una metodología general para optimización estructural en diseño asistido por ordenador.* PhD thesis, Escola Técnica Superior d'Enginyers de Camins, Canals i Ports de Barcelona, Universitat Politécnica de Catalunya.

Olhoff, N. and Rassmunsen, J. (1991). Study of inaccuracy of in semi-analytical sensitivity analysis - a model problem. *Struct. Optim.,*, 3:203–213.

Olhoff, N., Rassmunsen, J., and Lund, E. (1993). A method of "exact" numerical differentiation for error elimination in finite-element-based semi-analytical shape sensitivity analyses. *Mech. Struct. Mach.*, 21:1–66.

Otto, F. and Rasch, B. (1995). *Gestalt finden.* Edition Axel Menges, Fellbach, Germany.

Papalambros, Y. and Wilde, D. J. (2000). *Principles of Optimal Design.* Cambridge University Press, Cambridge, MA.

Parente, E. J. and Vaz, L. E. (2001). Improvement of semi-analytical design sensitivities of non-linear structures using equilibrium relations. *Int. J. Numer. Meth. Engng.*, 50:2127–2142.

Pearson, C. W. (1958). Structural design by high speed computing machines. In *Proceedings of the First ASCE Conference on Electronic Computation*, pages 417–436, New York.

Pedersen, P., Cheng, G., and Rassmunsen, J. (1989). On accuracy problems for semi-analytical sensitivity analyses. *Mech. Struct. Math.*, 17:373–384.

Phelan, D. G. and Haber, R. B. (1989). Sensitivity analysis of linear elastic systems using domain parametrization and a mixed mutual energy principle. *Computer Methods in Applied Mechanics and Engineering*, 77(1-2):31–59.

Ramm, E., Bischoff, M., and Braun, M. (1994). Higher order nonlinear shell formulation - a step back into three dimensions. In Bell, K., editor, *From Finite Elements to the Troll Platform, Ivar Holland 70th Anniversary*, pages 65–88. Norwegian Institute of Technology, Trondheim.

Ramm, E., Bletzinger, K.-U., and Reitinger, R. (1993). Shape optimization of shell structures. *IASS Bulletin of the International Association for Shell and Spatial Structures*, 34:103–121. Also in: Revue européene des éléments finis, 2, 377-398, (1993).

Ramm, E., Braun, M., and Bischoff, M. (1995). Higher order nonlinear shell formulations: Theroy and application. *Bulletin of the IASS*, 36:145–152.

Ramm, E. and Schunk, E. (1986). *Heinz Isler Schalen.* Karl Krämer Verlag, Stuttgart, Germany.

Reissner, E. (1945). The effect of transverse shear deformation on the bending of elastic plates. *Journal of Applied Mechanics*, 12:69–76.

Reitinger, R. (1994). *Stabilität und Optimierung imperfektionsempfindlicher-Tragwerke.* PhD thesis, Institut für Baustatik, Universität Stuttgart.

Saltelli, A., Chan, K., and Scott, E. M., editors (2000). *Sensitivity analysis.*, volume New York. J. Wiley.

Samareh, J. A. (1999). A survey of shape parameterization techniques. In *CEAS/AIAA/ICASE/NASA Langley International Forum on Aeroelasticity and Structural Dynamics*, pages 333–343, Williamsburg, VA.

Schmit, L. A. (1960). Structural design by systematic synthesis. In *Proceedings of the Second ASCE Conference on Electronic Computation*, pages 105–122, Pittsburg, Pennsylvania.

Schmit, L. A. (1981). Structural syntesys - its genesys and development. *AIAA Journal*, 19:1249–1263.

Schmit, L. A. (1986). Symposium summary and concluding remarks. In Bennet, J. A. and Botkin., M. E., editors, *The Optimum Shape*. Plenum Press, New York.

Taubin, G. (1995). Estimating the tensor of curvature of a surface from a polyedral approximation. In *Proceedings of Fifth International Conference on Computer Vision*, pages 902–907, Cambridge, Massachusetts.

Tikhonov, A. N. and Arsenin, V. Y. (1977). *Solutions of ill-posed problems.* John Wiley, Washington.

Tsay, J. J. and Arora, J. S. (1990). Nonlinear structural design sensitivity analysis for path dependent problems. part 1: General theory. *Computer Methods in Applied Mechanics and Engineering*, 81:183–208.

Tsay, J. J., Cardoso, J. E. B., and Arora, J. S. (1990). Nonlinear structural design sensitivity analysis for path dependent problems. part 2: Analytical examples. *Computer Methods in Applied Mechanics and Engineering*, 81:209–228.

Ugail, H. and Wilson, M. J. (2003). Efficient shape parametrisation for automatic design optimisation using a partial differential equation formulation. *Computers and Structures*, 81(28-29):2601–2609.

van Keulen, F. and de Boer, H. (1998a). Refined semi-analytical design sensitivities for bucking. In *In 7th AIAA/USAF/NASA/ISSMO Symposium on Multidisciplinary Analysis and Optimization. Part 2, 2-4*, pages 420–429, St Louis, MI.

van Keulen, F. and de Boer, H. (1998b). Rigorous improvement of semi-analytical design sensitivities by exact differentiation of rigid body motions. *Int. J. Numer. Meth. Engng.*, 42:71–91.

Vida, J., Martin, R. R., and Varady, T. (1994). A survey of blending methods that use parametric surfaces. *Computer-Aided Design*, 26:341–365.

Wang, S.-Y., Sun, Y., and Gallagher, R. H. (1985). Sensitivity analysis in shape optimization of continuum structures. *Computers and Structures*, 20:885–867.

Yamazaki, K. and Vanderplaats, G. N. (1993). Design sensitivity analysis with isoparametric shell elements. *Struct. Optim.*, 5:152–158.

Yang, R. J. and Botkin, M. E. (1986). Comparison between the variational and implicit differentiation approaches to shape design sensitivities. *AIAA Journal*, 24(6):1027–1032.

Zienkiewicz, O. C. and Campbell, J. S. (1973). Shape optimization and linear programming. In Gallagher, R. H. and Zienkiewicz, O. C., editors, *Optimum Structural Design*, pages 109–126. Wiley and Sons, London.

Zienkiewicz, O. C. and Taylor, R. L. (2000a). *The finite element method. Volume 1. The Basis.* Butterworth and Heinemann.

Zienkiewicz, O. C. and Taylor, R. L. (2000b). *The finite element method. Volume 2. Solid Mechanics.* Butterworth and Heinemann.

Zienkiewicz, O. C., Too, J., and Taylor, R. L. (1971). Reduced integration technique in general analysis of plates and shells. *International Journal for Numerical Methods in Engineering*, 3:275–290.

Zolesio, J. P. (1981). The material derivative (or speed) method for shape optimization. In Haug, E. J. and Céa, J., editors, *Optimization of Distributed Parameter Structures.* Sijthoff & Noordhoff, Aalphen aan den Rijn, The Netherlands.